Trabajo Fin de Grado
Grado en Ingeniería Aeroespacial

# Design of Optimal Gravity-Assist Trajectories for Electric Solar Wind Sails

Autor: Juan José López García

Tutores: Rafael Vázquez Valenzuela, Guillermo Pacheco Ramos

**Dpto. Ingeniería Aeroespacial y Mecánica de Fluidos**
**Escuela Técnica Superior de Ingeniería**
**Universidad de Sevilla**

Sevilla, 2023

Trabajo Fin de Grado
Grado en Ingeniería Aeroespacial

# Design of Optimal Gravity-Assist Trajectories for Electric Solar Wind Sails

Autor:
Juan José López García

Tutores:
Guillermo Pacheco Ramos, Rafael Vázquez Valenzuela
Profesor Sustituto Interino, Catedrático de Universidad

Dpto. Ingeniería Aeroespacial y Mecánica de Fluidos
Escuela Técnica Superior de Ingeniería
Universidad de Sevilla

Sevilla, 2023

Trabajo Fin de Grado: Design of Optimal Gravity-Assist Trajectories for Electric Solar Wind Sails

Autor: Juan José López García
Tutores: Rafael Vázquez Valenzuela, Guillermo Pacheco Ramos

El tribunal nombrado para juzgar el trabajo arriba indicado, compuesto por los siguientes profesores:

Presidente:

Vocal/es:

Secretario:

acuerdan otorgarle la calificación de:

El Secretario del Tribunal

Fecha:

# Agradecimientos

A mis padres, Luis y Ana María, por haberme dado siempre lo que he necesitado y más. Por inculcarme los valores que a día de hoy me hacen ser la persona que soy, y hacerme sentir orgulloso de lo conseguido en estos últimos años. Sin ellos y su entrega incondicional, habría sido muy difícil llegar hasta aquí.

A mi hermana Alba, por ser mi ejemplo a seguir. Por enseñarme el camino y demostrarme que con esfuerzo todo es posible.

A mis amigos y compañeros, esa familia que tenemos la suerte de elegir. Por hacerme sentir como en casa y hacer de esta etapa algo inolvidable.

Por último, a mis profesores, y en especial a mis tutores, Rafa y Guillermo, por la atención y el interés mostrado en todo momento. Por la confianza depositada en mí durante la realización de este proyecto. Ha sido todo un honor.

*Juan José López García*
*Sevilla, 2023*

# Resumen

## Título

Diseño de Trayectorias Óptimas con Asistencia Gravitatorias para Velas Solares Eléctricas.

## Resumen del trabajo

Las Velas Solares Eléctricas son una alternativa interesante a los sistemas de propulsión tradicionales, un nuevo tipo de propulsión espacial sin combustible que obtiene la energía de los protones del viento solar, obteniendo unos niveles de aceleración que las hace potencialmente útiles para misiones interplanetarias. Pese a que estos sistemas surgen como una alternativa para alcanzar objetos lejanos sin depender de maniobras asistidas por gravedad, la combinación de ambos puede ser muy prometedora. El primer objetivo de este proyecto es analizar diferentes trayectorias con asistencia gravitatora para Velas Solares Eléctricas. Tras esto, estas trayectorias han de ser optimizadas con el fin de reducir el tiempo de vuelo. Existen múltiples alternativas de optimización disponibles, y de entre estas opciones, se han elegido específicamente los algoritmos genéticos. Los algoritmos genéticos, un algoritmo evolutivo que ha experimentado un crecimiento significativo en el campo de estudio en la última década debido a los avances computacionales, proporcionan excelentes resultados; no obstante, implican un costo computacional sustancial. Distintas variaciones en los parámetros de control y las operaciones son llevadas a cabo, dando lugar a resultados comparables con un tiempo computacional reducido.

## Palabras clave

Velas Solares Eléctricas, Maniobras Asistidas por Gravedad, Programación No Lineal, Algoritmo Genético, Elitismo, Selección, Mutación, Cruce.

## Conclusiones

El uso de Velas Solares Eléctricas en trayectorias con asistencia gravitatoria es una opción muy favorable que permite viajes interplanetarios eficientes. Se ha implementado un código para el estudio mediante Programación No Lineal de órbitas óptimas. Tras esto, se plantean diversas misiones interplanetarias, destacando entre ellas las que tienen por destino Saturno, realizando una maniobra asistida por gravedad en diferentes planetas, y se verifica la importancia de la configuración en fase de los planetas para el tiempo de vuelo de la misión. El caso más favorable corresponde a realizar la maniobra en Venus. Cada uno de estos casos es optimizado mediante el algoritmo

genético, analizando diferentes variaciones en las operaciones y parámetros de control. Se concluye que la solución mejora para un mayor tamaño de la población base, a coste de un aumento del tiempo de computación, siendo este la principal limitación del proceso. Se prueban modificaciones tanto en la población inicial como en la mutación, siendo en ambos casos nula o despreciable la mejora del tiempo de vuelo, pero favorable para el coste computacional.

# Abstract

Electric Solar Wind Sails are an interesting alternative to traditional propulsion systems, a new type of spacecraft propellantless propulsion system that gets its energy from solar wind protons, making them potentially useful for interplanetary missions. Despite the fact that these systems emerge as an alternative to reach far away objects without depending on gravity assist maneuvers, the combination of both can be very promising. The first goal of this project is to analyze different gravity-assist trajectories for Electric Solar Wind Sails. Then, these trajectories have to be optimized in order to reduce the flight time. There are multiple optimization alternatives available, and out of these options, genetic algorithms have been specifically chosen. Genetic algorithms, an evolutionary algorithm that has experienced significant growth in the field of study over the last decade due to computational advancements, provide excellent results; however, they imply a substantial computational cost. Several variations on control parameters and operations are conducted, resulting in comparable results with reduced computational time.

# Contents

*Resumen* III
*Abstract* V
*Notation* IX

**1 Introduction** **1**
1.1 Motivation 1
1.2 Aim of the project 2
1.3 Structure of the project 3

**2 State of the art of Electric Solar Sails** **5**
2.1 Background 5
2.2 State of the art 5

**3 Background concepts in Orbital Mechanics** **11**
3.1 Equation of Motion 11
3.2 Dynamic equations in polar coordinates 12
3.3 E-sail continuous thrust model 13
3.3.1 Considerations about the E-sail control parameters 15
3.4 Gravity assist maneuvers 15
3.4.1 Sphere of influence 16
3.4.2 Patched conic method 17
3.4.3 Accomplishment of the gravity assist maneuver 18

**4 Optimization algorithms** **21**
4.1 Non linear optimization of continuous systems 21
4.1.1 Problem hypotheses 21
4.1.2 Optimal Control Problem formulation 21
4.1.3 Conversion of our OCP to a NLP problem 24
4.2 Genetic Algorithm 28
4.2.1 Metaheuristics 28
4.2.2 Background concepts in genetic algorithms 28
4.2.3 *Exploration* and *Exploitation* 29
4.2.4 Parts of a genetic algorithm 30
Creation of the initial population 30
Crossover 31
Mutation 31

Elitism 32
Selection 32
4.2.5 Procedure and relationship between the parts 35
4.2.6 Objective function and optimization variables of the problem 36

**5 Analysis of results 39**
5.1 Optimal transfer orbits between two planets 39
5.1.1 From Earth to Mars 39
5.1.2 From Earth to Jupiter 42
5.1.3 From Earth to Venus 45
5.1.4 From Mars to Jupiter 47
5.1.5 From Mars to Saturn 49
5.1.6 From Jupiter to Saturn 50
5.1.7 From Venus to Saturn 52
5.2 Optimal gravity-assist trajectories 53
5.2.1 Earth-Mars-Jupiter mission 53
Genetic algorithm in Earth-Mars-Jupiter 55
5.2.2 Earth-Mars-Saturn mission 62
Genetic algorithm in Earth-Mars-Saturn 63
5.2.3 Earth-Jupiter-Saturn mission 69
Genetic algorithm in Earth-Jupiter-Saturn 70
5.2.4 Earth-Venus-Saturn mission 75
Genetic algorithm in Earth-Venus-Saturn 77
5.2.5 Analysis of variations in the procedure 82

**6 Conclusions and future work 89**
6.1 Conclusions 89
6.2 Future work 90

**Appendix A Modified Genetic Algorithm process 93**

**Appendix B Modified Mutation process 95**

*List of Figures* 97
*List of Tables* 101
*Bibliography* 103

# Notation

| | |
|---|---|
| $\mathbf{a}$ | E-sail acceleration vector |
| $a$ | E-sail acceleration modulus |
| $a_c$ | E-sail characteristic acceleration |
| $a_r$ | E-sail acceleration in radial direction |
| $a_\theta$ | E-sail acceleration in tangential direction |
| $\mathbf{c}$ | Vector of constraints in NLP formulation |
| $E$ | Number of individuals of the elite |
| $\mathbf{f}$ | Set of state equations in OCP formulation |
| $\mathbf{g}$ | Set of boundary conditions in OCP formulation |
| $G$ | Universal Gravitational Constant |
| $\mathbf{h}$ | Set of path constraints in OCP formulation |
| $N$ | Number of time segments in NLP formulation. Maximum allowed number of generations |
| $n_c$ | Number of random crossovers in a generation |
| $p_c$ | Probability of an individual of becoming a parent |
| $p_m$ | Probability of mutation of a gene in an individual that mutates |
| $p_{mut}$ | Probability of an individual to mutate |
| $r$ | Distance from the Sun |
| $r_i$ | Planet's orbit mean radius |
| $R_e$ | Sphere of influence radius |
| $r_P$ | Approach radius in a gravity assist maneuver |
| $T$ | E-sail thrust modulus |
| $t$ | Time. Number of participants of a tournament |
| $t_N$ | Flight time |
| $TOL$ | Tolerance of difference between the mean value of the population in the objective function and that of the best individual |
| $\mathbf{u}$ | Set of the system's control parameters |
| $v_r$ | Radial velocity |
| $v_\theta$ | Tangential velocity |
| $v_\infty$ | Excess velocity |
| $\mathbf{x}$ | Set of the system's state variables |
| $X$ | Number of individuals of the base population |
| $\mathbf{y}$ | Vector of variables in NLP formulation |

| | |
|---|---|
| $\alpha$ | Thrust cone angle |
| $\alpha_n$ | Sail pitch angle |
| $\alpha_{n_{max}}$ | Maximum sail pitch angle |
| $\delta$ | Angle formed by the hyperbola asymptotes |
| $\gamma$ | Thrust nondimensional parameter in thrust model |
| $\Delta t$ | Time step size in NLP formulation |
| $\eta_c$ | Control parameter of similarity between offspring and parents |
| $\theta$ | True anomaly |
| $\theta_{P_i}$ | True anomaly of the planet i |
| $\mu_i$ | Standard Gravitational Parameter of body i (when omitted, referred to the Sun) |
| $\sigma_c$ | Denominator in the variance of the Normal distribution in mutation |
| $\tau$ | Thrust lever parameter |
| ♀ | Venus |
| ⊕ | Earth |
| ♂ | Mars |
| ♃ | Jupiter |
| ♄ | Saturn |

# 1 Introduction

In this chapter, the motivation and the aim of the project are presented. Furthermore, the hypothesis that are considered and the structure of the project are defined.

## 1.1 Motivation

The star in closest proximity to our Sun is “Proxima Centauri”, situated at a distance of 4.22 light-years from Earth. This implies that light requires 4.22 years to travel the distance between Earth and “Proxima Centauri”, accomplishing this feat at a velocity of 1,080,000,000 km/h. To provide context, the highest velocity achieved by any human-made object is 587,000 km/h, which is 0.05% of the velocity of light. This remarkable achievement was accomplished by NASA’s “Parker Solar Probe”, the spacecraft that has come closest to the Sun. However, even if we were capable of attaining such a velocity and escaping our Solar System, it would still require an 8,500-year journey to reach “Proxima Centauri”. Consequently, interstellar travel remains an inconceivable prospect, prompting us to focus on interplanetary missions within our Solar System.

Numerous interplanetary missions have been successfully executed, with a focus on adopting alternative approaches to minimize travel time. One such notable method employed is the utilization of gravity assist maneuvers, which have proven essential in achieving this objective.

The gravity assist maneuver was first attempted in 1959 when the Soviet probe “Luna 3” photographed the far side of the Moon [1]. This particular maneuver employs the relative movement and gravitational influence of celestial bodies, such as planets, to effectively modify the velocity of a spacecraft. Consequently, this results in a reduction in both propellant mass and flight duration. Numerous gravity assist maneuvers have been executed with the primary objective of reaching the remote regions within the solar system.

The successful execution of this maneuver relies on the precise alignment of planets, and the time required for these configurations to repeat can significantly increase when more than two planets are involved. As a result, the development of Low-Thrust Continuous Propulsion Systems emerges as a viable alternative for reaching remote celestial objects without dependence on gravity assist maneuvers. However, the applicability of these systems is limited by the required amount of propellant mass, giving rise to the development of Low-Thrust Propellantless Continuous Propulsion systems. The absence of propellant in these systems offers the advantage of accommodating a higher payload capacity. The basis of these propulsion systems lies in harnessing the Sun as the primary source of energy, utilizing the solar wind that reaches the spacecraft.

In recent years, a wide range of Solar Sail technologies has been studied, including Photonic, Magnetic, and Electric Solar Wind Sails (commonly known as E-sails). However, this project

specifically focuses on Electric Solar Wind Sails. These Low Thrust continuous propulsion systems have emerged as a promising alternative for space exploration. By harnessing the solar wind to generate thrust, E-sails offer an efficient mechanism for navigating the Solar System. The main objective of this project is to investigate mission design, leveraging the capabilities of Electric Solar Wind Sails as a viable solution for future interplanetary missions.

Furthermore, the optimization of interplanetary missions holds great importance. By optimizing mission trajectories, fuel consumption, and various parameters, we can minimize resource utilization, making missions more economically viable and environmentally sustainable. Moreover, optimization helps increase the probability of mission success by uncovering optimal paths, transfer orbits, and arrival times. Additionally, it aids in minimizing mission duration by identifying efficient trajectories, gravity assist maneuvers, and other techniques.

There are multiple alternatives available for optimization, and among these options, evolutionary algorithms emerge as a distinguished choice.

Evolutionary algorithms have been utilized in the optimization of interplanetary missions to tackle complex and multi-objective optimization problems. These algorithms are inspired by the process of natural evolution and employ the principles of selection, reproduction, and mutation to search for optimal solutions in a given problem space.

A widely employed strategy involves the utilization of evolutionary algorithms, such as genetic algorithms, to generate a population of candidate solutions representing different mission parameters. These algorithms provide a powerful tool to explore the vast search space of possible mission configurations and identify efficient and feasible solutions, what makes them suitable for tackling the complex problems associated with interplanetary travel.

Considering the shortage of existing studies on missions incorporating both gravity assist maneuvers and E-sails optimized with genetic algorithms, we find the integration of these three concepts to be of significant interest.

## 1.2 Aim of the project

The aim of this project is not to study the physical mechanisms that make the E-sail produce thrust, nor to understand its attitude behaviour, but to use them appropriately to accomplish different missions. Once we present an appropriate thrust model and solve the optimal control problem between two different planets, we are able to introduce gravity-assist maneuvers in the trajectories.

We center our focus on the design of optimal gravity-assist trajectories, establishing a method that provides us the trajectory with minimum flight time as well as the launch date for which it is given, and analyzing the evolution of the flight time for different launch dates in different missions. In addition, we analyze the effect of applying the genetic algorithm for the optimization of the trajectories, and some different variations on the parameters and operations of the algorithm.

Some hypotheses are considered in the realms of this project:

- The orbits of the planets are contained in the ecliptic plane of the Solar System. Therefore, the 2D simplification is assumed.
- The orbits of the planets are supposed circular and concentric, with the Sun in the center of them.
- Only Sun attraction and E-sail thrust are taken into account as forces. Gravitational effects of other planets and pressure of solar radiation are neglected.

- The launch date of the mission is a degree of freedom, therefore the position of the planets depends on the date we choose.
- The attitude problem is tackled as a black box, supposing that we are able to achieve the desired attitude instantaneously at any time.
- There is not any constraint about the approach radius in a gravity assist maneuver, therefore we have the ability to choose the proximity.

## 1.3 Structure of the project

The structure of the document is defined as follows:

**Chapter 1: Introduction.** This chapter serves as an introduction for the reader, covering the motivation, aim of the project, hypotheses, and other relevant aspects.

**Chapter 2: State of the art of Electric Solar Sails.** Here, the background and the state of the art of Electric Solar Sails are presented. In this chapter, the current progress and technology are analyzed.

**Chapter 3: Background concepts in Orbital Mechanics.** In this chapter, the background concepts in orbital mechanics are introduced. It starts by demonstrating basic equations. Then, a thrust model for E-sails is included, as well as its limitations. Lastly, basic concepts about gravity assist maneuvers are presented.

**Chapter 4: Optimization algorithms.** This chapter starts by formulating the Optimal Control Problem. After that, the problem is transformed to a NLP problem, in order to be solved by an optimization algorithm. Next, the process of the genetic algorithm and a development of this algorithm on the case of this project are presented.

**Chapter 5: Analysis of results.** Different scenarios and the obtained results are presented in this chapter, starting with optimal transfer orbits between two planets, and continuing with the introduction of gravity assist maneuvers in the trajectories.

**Chapter 6: Conclusions and future work.** Several conclusions are extracted from all the results. Furthermore, some aspects are included and proposed as future work.

# 2 State of the art of Electric Solar Sails

The exploration of deep space has been an objective for many countries and companies since the beginning of the space race, but within the reach of few given its high costs and required technologies. However, in recent decades the number of missions that are launched towards the exploration of our Solar System, and even beyond, has been constantly incresing.

## 2.1 Background

There have been numerous spatial missions in the realms of our Solar System. We have visited all the planets and various of their moons, including other celestial bodies such as asteroids or dwarf planets. Planets such as Jupiter have been visited in several missions: "Pioneer 10" (1973), "Pioneer 11" (1974), "Voyager 2" (1979), "Voyager 1" (1979), "Galileo" (1995-2003), "New Horizons" (2007) and Juno (2016-today). Other planets have been reached just once, like Uranus and Neptune, that were only visited by "Voyager 2" (1986 and 1989, respectively).

Many of those missions were achieved thanks to gravity assist maneuvers. In a gravity assist maneuver, an intermediate planet appears as a field of gravity moving relative to the inertial heliocentric coordinate system. Thus, spacecraft heliocentric energy changes when the encounter happens. This may imply a reduction of required flight time and launch energy. However, there is a problem with these maneuvers. We have to wait for the planets to align in a certain way, and the time necessary for these configurations to repeat can become really large. *Voyager 1* and *Voyager 2* are examples of this (as shown in Figure 2.1). Fly-bys around Jupiter, Saturn and Uranus allowed it to obtain the necessary speed to reach Neptune and even to achieve the Solar System escape velocity, but this planet configuration, known as the "Grand Tour", only repeats approximately every 175 years [2].

## 2.2 State of the art

Space missions are traditionally based on propulsion technologies, where a certain amount of propellant is used to generate thrust. This propellant needs to be stored on board, and it can dramatically increase both the total spacecraft mass and the overall mission costs. Moreover, the need for propellant on board limits the mission lifetime since orbital maintenance usually requires station-keeping maneuvers that are impossible to do when spacecraft is out of propellant [3].

As a possible alternative, some propellantless propulsion systems have been proposed. The most relevant example is represented by Solar Sails (or Photonic Solar Sails).

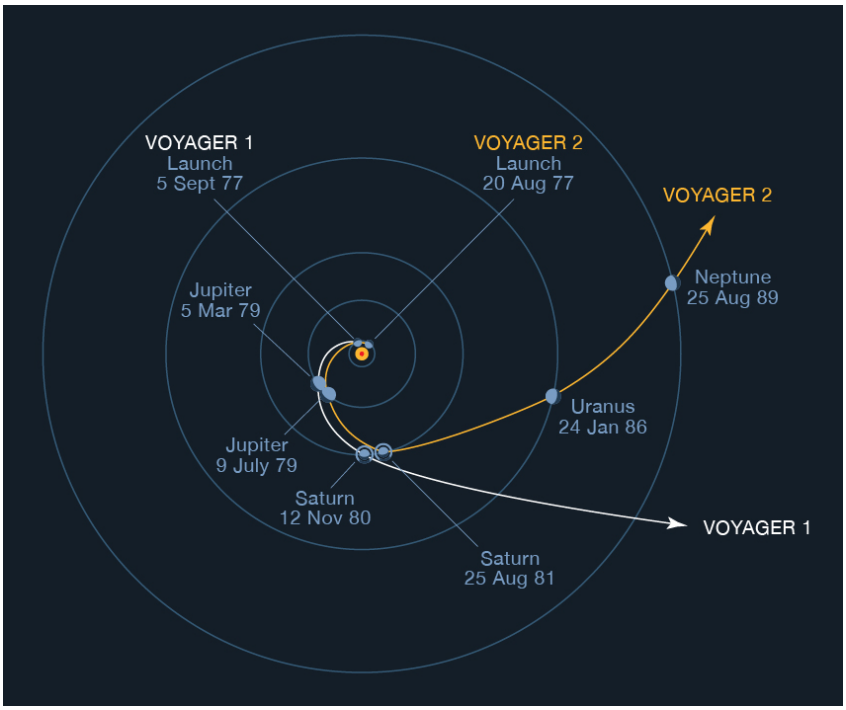


**Figure 2.1** *Voyager 1* and *Voyager 2* trajectories. (The "Grand Tour").

The concept of solar sailing is the use of photonic solar radiation as propellant of a spacecraft, potentially providing a continuous acceleration limited only by the lifetime of the sail materials, and a sustained and suitable distance to the Sun. The membrane where solar radiation impacts is packed during launch and deployed in space. It reflects the solar radiation such that it accelerates the spacecraft continuously and indefinitely without the need for an on-board propulsion system. However, the momentum carried by individual photons is extremely small. A solar sail with a perfectly reflective surface will experience approximately nine newtons of force per square kilometre of sail when located at one astronomical unit (AU) from the Sun, the average distance between Earth and Sun. Thus, to provide a suitably large momentum transfer, the sail must have a large surface area, with the lowest possible mass. It is found that the idealised thrust vector is directed normal to the surface of the sail with all incident photons reflected, therefore, we can modify the orbit energy controlling the orientation of the sail surface relative to the Sun, giving rise to a wide-range of potential missions [4].

One example of this technology is *LightSail 2* (see Figure 2.2), which is currently orbiting the Earth and changing its orbit exclusively with thrust from solar radiation pressure [5].

Another options are Magnetic and Electric Sails. The main difference is that Solar Sails gain momentum from solar radiation pressure (SRP), while Electric Sails [6] and Magnetic Sails [7] gain momentum from the interaction with the solar wind.

The concept of a magnetic sail is based on the fact that the magnetic field generated by a current-carrying coil can deflect incoming ions and therefore experiences a drag force. The application of this propulsion system is very attractive for interstellar missions where it can be used to decelerate the spacecraft allowing for an orbital insertion without additional propellant [8].

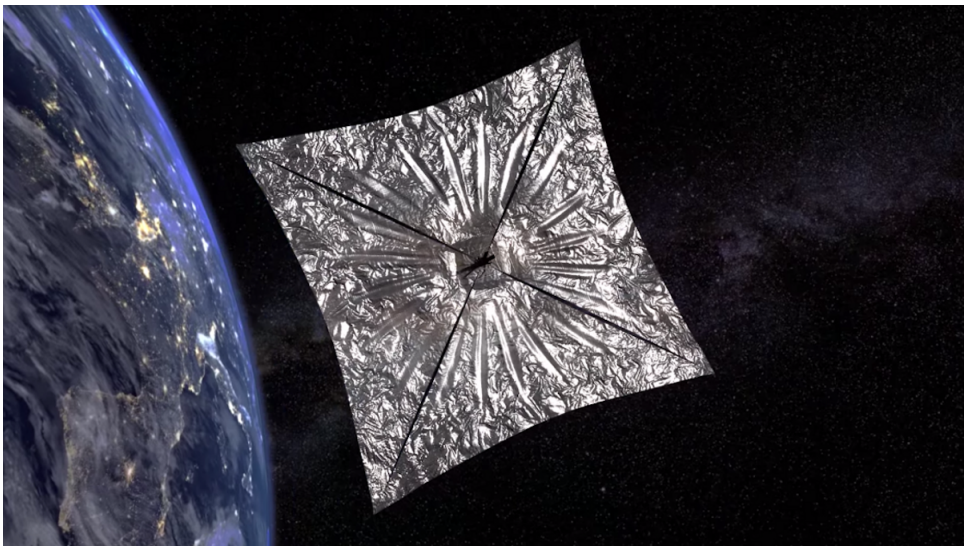

**Figure 2.2** *LightSail 2* deployed in space.

We will center our focus on Electric Sails, known as E-sails. For the first appearance of the concept of an Electric Solar Wind Sail, we have to date back to 2004, when Pekka Janhunen conceived this innovative propellantless propulsion system for use in interplanetary space [3].

Dr. Janhunen proposed the possibility of a system formed by a large grid of tether maintained at a high positive electrical voltage that repells protons instead of photons by using an electric field. Its concept scheme is shown in Figure 2.3.

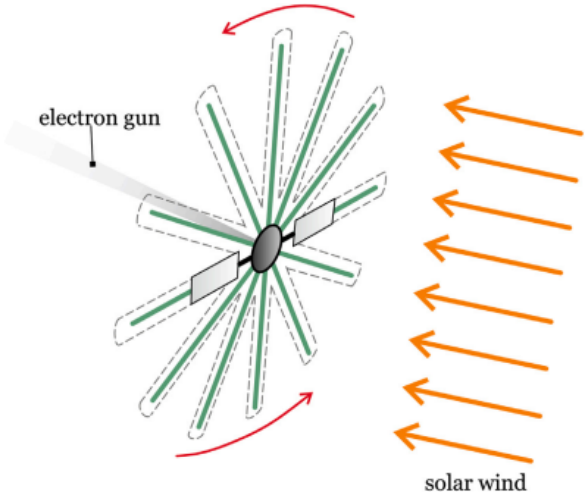


**Figure 2.3** E-sail concept scheme. Credit: [3].

The peculiar features of an E-sail are its lightness and the possibility of orienting the thrust vector, albeit within certain limits. There is also a distinguishing key. Thrust produced by an E-sail is proportional to $r^{-7/6}$ [3], where $r$ is the distance from the Sun, while the thrust produced by a Solar Sail decays with $r^2$ [9]. That makes E-sails feasible for missions to farther planets in a reasonable time.

Currently, the typical E-sail configuration consists of long conductive tethers (with a length of the order of km), arranged in a radial pattern, which are stretched out by the centrifugal force due to

the spacecraft spin. Each tether tip hosts a remote unit, which is generally equipped with a small thruster to adjust the E-sail spin rate. The remote units are connected to each other by auxiliary tethers in such a way as to form a circle centered at the spacecraft main body, where the payload rests (as shown in Figure 2.4) [10].

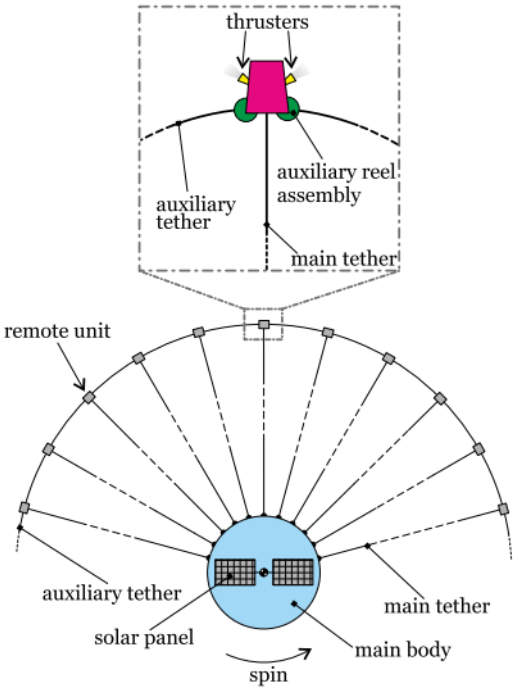


**Figure 2.4** E-sail typical configuration. Credit: [3].

Many other options have been proposed in the literature to maintain the desired tether spin rate, like the alternation of conductive and insulated tethers, or the use of photonic blades.

E-sails have been the focus of several studies and test missions. The first test was attempted with the Estonian student satellite *ESTCube-1*, and supported by ESA [11]. *ESTCube-1* was a CubeSat launched on 2013 onboard a Vega rocket, but unfortunately a failure of the tether unreel mechanism occurred during the launch phase, and the tether experiment did not take place. The lessons learned from the *ESTCube-1* failure have led to the design of *Aalto-1*, a Finnish CubeSat [12]. Currently, a possible scenario for a test mission of the E-sail-based propulsion in deep space is constituted by a fleet of nanosatellites equipped with a single positively charged tether [3].

NASA has also studied this concept with its *HERTS* project (Heliopause Electrostatic Rapid Transit System). Interested by such exploration opportunities, the Advanced Concepts Team at NASA's Marshall Space Flight Center (MSFC) began investigating the prospects of using an electric sail to travel to the edge of the solar system (the Heliopause). The *HERTS* study concluded an E-sail mission to the Heliopause could be completed in less than 15 years, which is much faster than with any other existing propulsion system [13]. A comparison between different propulsion system options can be seen in Figure 2.5.

The number of potential E-sail applications is large: missions to Venus, Mercury, Mars (and his moon, Phobos) or asteroids, maintaining non-Keplerian orbits (i.e. an orbit whose maintenance requires continuous propulsive thrust) , near-sun missions, boosting to outer solar system, among others [14]. An interesting example is "Off-Lagrange point solar wind monitoring". Nowadays, short-term forecasting of magnetospheric space weather (magnetic storms) is based on continuously

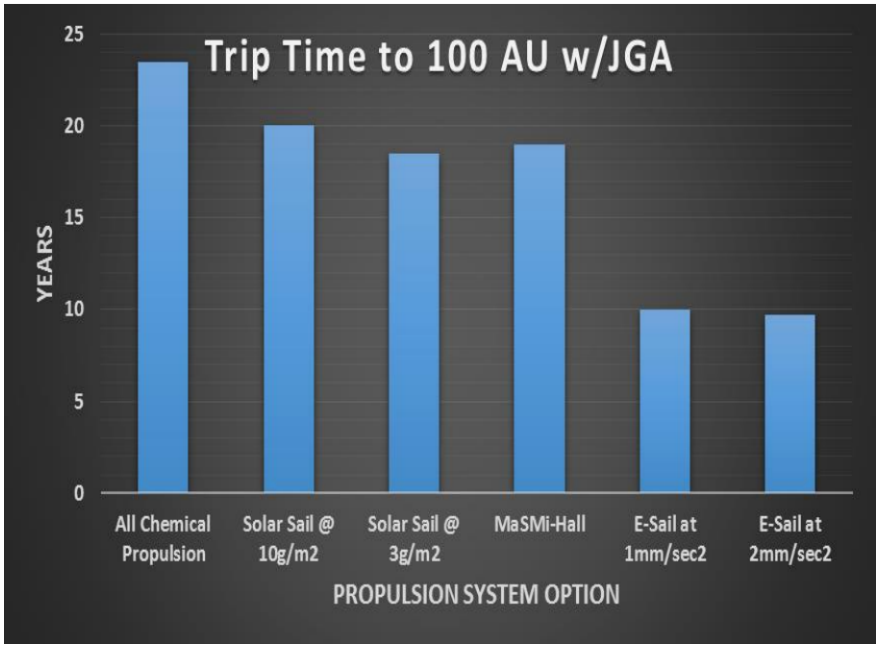


**Figure 2.5** Trip time to reach 100 AU using different propulsion systems. Credit: [13].

monitoring the solar wind plasma density, plasma velocity and interplanetary magnetic field (IMF) at the Earth-Sun Lagrange L1 point, by satellite such as *ACE* and *SOHO*. Because the solar wind takes about one hour to travel from the Lagrange L1 point to the magnetospheric nose, such monitoring can give about one hour of warning time for preparing to the radiation belt enhancement, geomagnetically induced current and other possible adverse effects of magnetic storms. The E-sail could be used to "hang" a spacecraft against the sun's gravity field closer to the sun than the Lagrange point (for example at twice the distance from the Earth than the Lagrange point so that the warning time would be twice ), without propellant [14].

Finally, much theoretical research related to planetary and interplanetary transfer trajectory design for solar sails have been conducted. Numerical optimization techniques are required to obtain an optimal solution. They are usually categorized as indirect or direct. The indirect method requires the use of the maximum principle to derive the first order necessary condition of the optimal solution. The minimum-time rendezvous problem can be formulated as an optimal-control problem, and the associated optimal-thrust profile can be derived by Pontryagin's maximum principle (PMP). The disadvantage of indirect method is that the solution is extremely sensitive to the initial guess. For direct methods, the trajectories are divided into discrete segments and the control laws are optimized to obtain a feasible solution satisfying boundary conditions. The scheme transcribes a continuous dynamic optimization problem to a nonlinear programming (NLP). The advantage of such methods is the capability to approximate the optimal trajectory through simple numerical methods, avoiding the difficulty of guessing the initial variables [4].

# 3 Background concepts in Orbital Mechanics

In this chapter, we introduce the basics of orbital mechanics. The equation of motion is presented and adapted to our case of continuous thrust, with a model to estimate the thrust produced by the E-sail. Finally, gravity assist maneuvers are presented.

## 3.1 Equation of Motion

The discovery of the equation of motion dates back to 1687, when Sir Isaac Newton published his *Philosophiæ Naturalis Principia Mathematica*. In that book, he included a law for gravitational force deducted empirically, known today as Newton's Law of Universal Gravitation. That law states that the gravitational force exerted by two massive bodies is directly proportional to the product of the masses and inversely proportional to the square of the distance between their centers of mass. The direction of the force is the line that connects both centers of mass, in the sense of attraction. The equations are:

$$\begin{aligned} \mathbf{F_{12}} &= G\frac{m_1 m_2}{r^2}\frac{\mathbf{R_2}-\mathbf{R_1}}{|\mathbf{R_2}-\mathbf{R_1}|} \\ \mathbf{F_{21}} &= G\frac{m_1 m_2}{r^2}\frac{\mathbf{R_1}-\mathbf{R_2}}{|\mathbf{R_1}-\mathbf{R_2}|} \end{aligned} \tag{3.1}$$

where G is the Universal Gravitational Constant, $G \approx 6.674 \cdot 10^{-11}\ m^3 kg^{-1} s^{-2}$, $F_{ij}$ is the force exerted by the body j to body i and $\mathbf{R_1}$, $\mathbf{R_2}$ are the position vectors of each body given an inertial frame of reference, as shown in Figure 3.1.

We can define vector $\mathbf{r}$, which is pointing from mass 1 to mass 2:

$$\mathbf{r} = \mathbf{R_2} - \mathbf{R_1}, \qquad r = |\mathbf{r}| \tag{3.2}$$

Introducing Newton's Second Law and dividing by $m_1$ in first equation and $m_2$ in second equation:

$$\begin{aligned} \ddot{\mathbf{R}}_\mathbf{1} &= \frac{\mathbf{F_{12}}}{m_1} = G\frac{m_2}{r^2}\frac{\mathbf{r}}{r} \\ \ddot{\mathbf{R}}_\mathbf{2} &= \frac{\mathbf{F_{21}}}{m_2} = -G\frac{m_1}{r^2}\frac{\mathbf{r}}{r} \end{aligned} \tag{3.3}$$

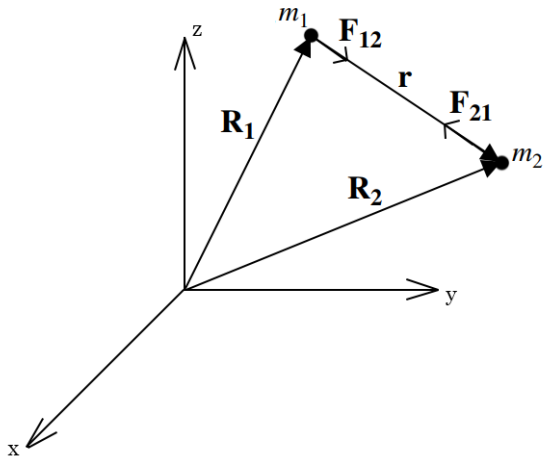


**Figure 3.1** The two-body problem.

Finally, recalling the definition of $\mathbf{r}$ in (3.2) and applying it to (3.3):

$$\ddot{\mathbf{R}}_\mathbf{2} - \ddot{\mathbf{R}}_\mathbf{1} = \ddot{\mathbf{r}} = -G\frac{m_1 + m_2}{r^2}\frac{\mathbf{r}}{r} \tag{3.4}$$

This equation is easier to solve than the case where more than 2 bodies with mass are involved (the number of degrees of freedom increases). The center of gravity of both bodies always moves with constant velocity, and we define our inertial frame of reference to be the one in which the center of mass of the system stays still. From that point of view, both of the bodies are "orbiting" this fixed point, also known as Keplerian motion.

If one of the bodies has a significantly higher mass than the other ($m_1 \gg m_2$), such as in our case, then the center of mass of the system is really close to the center of mass of that massive body, and so it can be assumed that they coincide. Given this simplification, $\mathbf{R_1}$ is constant, $m_1 + m_2 \approx m_1$ and the equation of motion for the second mass is now:

$$\ddot{\mathbf{r}} = -\frac{\mu}{r^2}\frac{\mathbf{r}}{r} \tag{3.5}$$

where $\mu = G \cdot m_1$, which is usually called the Standard Gravitational Parameter, widely used in orbital mechanics.

## 3.2 Dynamic equations in polar coordinates

It is reasonable to use polar coordinates to write the dynamic equations of the system given that our problem is assumed to be two-dimensional, and planets motion to be circular.

We first derive these equations keeping only the effects of the Sun's gravitational force, and later, we introduce the thrust produced by the E-sail. Since (3.5) involves a second order derivative of the position, and position is defined by two independent variables (in this two-dimensional problem, $r$ and $\theta$), we look for four first order differential equations, two for position and two for velocity.

To obtain these equations, we start differentiating the position vector $\mathbf{r} = r\mathbf{u_r}$ with respect to time in polar coordinates, to obtain the radial and tangential accelerations as follows:

$$\begin{aligned} \dot{\mathbf{r}} &= \frac{d\mathbf{r}}{dt} = \dot{r}\mathbf{u_r} + r\dot{\theta}\mathbf{u}_\theta \\ \ddot{\mathbf{r}} &= \frac{d\dot{\mathbf{r}}}{dt} = (\ddot{r} - r\dot{\theta}^2)\mathbf{u_r} + (2\dot{r}\dot{\theta} + r\ddot{\theta})\mathbf{u}_\theta \end{aligned} \tag{3.6}$$

Identifying terms with (3.5), we notice gravitational force is radial. Therefore the tangential component of acceleration is equal to 0.

$$\begin{aligned} \ddot{r} - r\dot{\theta}^2 &= -\frac{\mu}{r^2} \\ 2\dot{r}\dot{\theta} + r\ddot{\theta} &= 0 \end{aligned} \tag{3.7}$$

We now introduce tangential and radial velocities

$$\begin{aligned} v_r &= \dot{r} \\ v_\theta &= r\dot{\theta} \end{aligned} \tag{3.8}$$

and introduce them in (3.7), obtaining:

$$\begin{aligned} \dot{r} &= v_r \\ \dot{\theta} &= \frac{v_\theta}{r} \\ \dot{v}_r &= \frac{v_\theta^2}{r} - \frac{\mu}{r^2} \\ \dot{v}_\theta &= -\frac{v_r v_\theta}{r} \end{aligned} \tag{3.9}$$

In view of these equations, it is clear that the state variables of our problem are $\{r, \theta, v_r, v_\theta\}$. Given the values at an instant $t_0$, we can compute the orbit that the spacecraft follows.

## 3.3 E-sail continuous thrust model

In order to model the thrust force produced by an E-sail, the change of the angular momentum of the spacecraft, adding a possible perpendicular component of the thrust, has to be taken into account. This is achievable by inclining the E-sail nominal plane, that is, the plane containing the wires, which are stretched out by the E-sail spin [3]. The equations of radial and tangential thrust are then given by

$$\begin{aligned} T_r &= T\cos\alpha \\ T_\theta &= T\sin\alpha \end{aligned} \tag{3.10}$$

where T is the thrust modulus and $\alpha$ is the angle formed between the E-sail thrust vector and the position vector $\mathbf{r}$, known as thrust cone angle, which does not coincide with the sail pitch angle $\alpha_n$, as is shown in Figure 3.2, due to the surface created by the charged tethers is no longer supposed planar, among other reasons [15].

It is also common practice to use the acceleration produced by the E-sail thrust (the vector we call $\mathbf{a}$, as represented in Figure 3.2), rather than the thrust itself, because the motion is expressed in equations that involve accelerations, not forces.

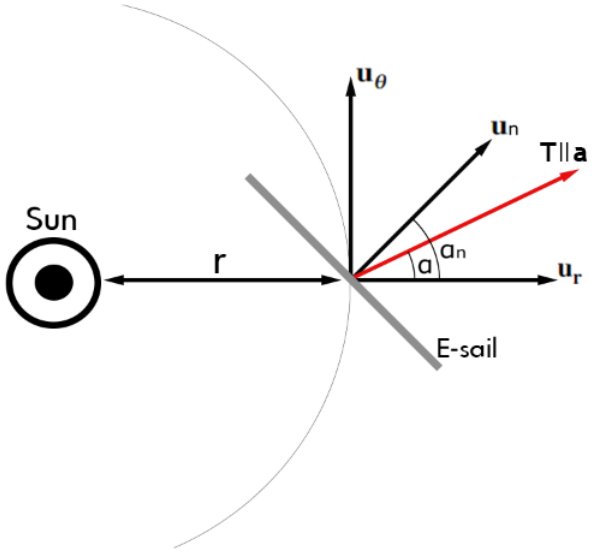


**Figure 3.2** Conceptual E-sail thrust model.

Regarding the thrust modulus, its dependence with respect to the distance of the Sun was estimated according to the evolution of the electrons temperature and density with that distance, where electron density decays with $r^{-2}$ and electron temperature decays with $r^{-1/3}$. With those results, it turns out that the thrust modulus decays with $r^{-7/6}$ [16].

Working with accelerations, it is typical to express the E-sail acceleration in terms of the maximum acceleration at 1AU distance from the Sun, usually denoted $a_c$, accompanied with a power parameter named $\tau$, which is a dimensionless parameter that is introduced to model the on/off modes of the electron gun. In particular, $\tau = 1$ means that the E-sail generates maximum acceleration and $\tau = 0$ means that the E-sail does not generate any acceleration.

In this model, we are assuming that we have actuators that can act instantaneously, what is not actually true. Nevertheless, comparing the acting time (in the order of minutes [17]) with the duration of typical orbit transfers (in the order of years [18]), it can be considered instantaneous.

With this, we obtain the E-sail thrust model determined by $\tau$ and $\alpha$, our control parameters.

$$\begin{aligned} a_r &= a_c \tau \cos\alpha \left(\frac{r_\oplus}{r}\right)^{7/6} \\ a_\theta &= a_c \tau \sin\alpha \left(\frac{r_\oplus}{r}\right)^{7/6} \end{aligned} \tag{3.11}$$

The relation between the thrust cone angle and the sail cone angle is given by

$$\cos\alpha = \frac{1+\cos^2\alpha_n}{\sqrt{1+3\cos^2\alpha_n}} \tag{3.12}$$

Our thrust model has two degrees of freedom: thrust modulus and its direction. Our control parameters can be either $\{\tau,\alpha_n\}$ or $\{\tau,\alpha\}$, since $\alpha_n$ and $\alpha$ are related by (3.12). We choose the first option as control parameters; $\tau$ and $\alpha_n$.

Rewriting (3.11) using (3.12), we have

$$\begin{aligned} a_r &= \tau \frac{a_c}{2} \left(\frac{r_\oplus}{r}\right) (1+\cos^2 \alpha_n) \\ a_\theta &= \tau \frac{a_c}{2} \left(\frac{r_\oplus}{r}\right) \sin \alpha_n \cos \alpha_n \end{aligned} \tag{3.13}$$

where the dependence of thrust modulus with respect to the distance from the Sun is estimated with a decay of $r^{-1}$, rather than $r^{-7/6}$, due to several made simulations [9].

Finally, introducing (3.13) in (3.9) accordingly, we obtain the motion of the E-sail when the only forces acting on it are the gravitational attraction of the Sun and its own thrust. These final equations of motion are

$$\begin{aligned} \dot{r} &= v_r \\ \dot{\theta} &= \frac{v_\theta}{r} \\ \dot{v}_r &= \frac{v_\theta^2}{r} - \frac{\mu}{r^2} + \tau \frac{a_c}{2} \left(\frac{r_\oplus}{r}\right) (1+\cos^2 \alpha_n) \\ \dot{v}_\theta &= -\frac{v_r v_\theta}{r} + \tau \frac{a_c}{2} \left(\frac{r_\oplus}{r}\right) \sin \alpha_n \cos \alpha_n \end{aligned} \tag{3.14}$$

We reach the dynamic equations according to the state variables of our problem, $\{r,\theta,v_r,v_\theta\}$, and the control parameters we have defined, $\{\tau,\alpha_n\}$. Nevertheless, there exists a variety of practical and physical limitations in the control parameters that we have to take into account, so not all the values are possible.

### 3.3.1 Considerations about the E-sail control parameters

We have assumed that thrust is independent of the spacecraft velocity, something that is not exactly correct. Considering that thrust produced by the E-sail comes from decelerating protons from the solar wind, the relative velocity between the E-sail and the solar wind should be considered. But, since the Earth average velocity is about 30 km/s (less in the case of planets that are farther from the Sun) and the solar wind average velocity is about 400 km/s, it can be assumed that the difference of velocities is sufficiently high to disregard this phenomenon [6].

There is also a limitation in the maximum sail pitch angle that the E-sail can reach. The current results in simulations and studies approximate this value in $\alpha_{n_{max}} = 60 - 70°$.

Apart from that, there are also limitations on how much acceleration the E-sail can produce at a given distance from the Sun. There exists a voltage of saturation $V$. That means that, given a distance from the Sun, and assuming that the grid voltage is high enough, one can calculate the maximum acceleration that can be generated.

There is a study that proposes a mass budget model, in order to estimate the characteristic accelerations [19]. It uses the results of thrust produced by a tether per unit of length to model a real spacecraft. By estimating the total mass of the E-sail and establishing the number of tether and their length, the maximum acceleration (at 1AU), $a_c$, that the E-sail can produce can be computed. It can typically range from 0.1 $mm/s^2$ to 6 $mm/s^2$.

## 3.4 Gravity assist maneuvers

As we pointed out in Section 2.1, a gravity assist maneuver, or swing-by, is the use of the relative movement and gravity of a planet or other celestial body to alter the path and speed of a spacecraft,

typically to save propellant and reduce expense. With a maneuver of this type, the modulus and direction of the spacecraft velocity can be changed, modifying the kinetic energy without additional thrust. In this section, we describe the gravity assist maneuvers in the planar case, where all the orbits are coplanar.

### 3.4.1 Sphere of influence

Let us consider a spacecraft under the influence of two massive bodies, body 1 and body 2, that are separated a distance $r_{12}$ (see Figure 3.3). When the spacecraft (body 3) is very close to body 1, the effect of 2 can be considered as a perturbation in the Keplerian motion of the spacecraft around 1.

$$\ddot{\mathbf{r}}_\mathbf{1} = -\mu_1 \frac{\mathbf{r_1}}{r_1^3} + \mu_2 \left| \frac{\mathbf{r_2}}{r_2^3} - \frac{\mathbf{r_{12}}}{r_{12}^3} \right| = \mathbf{g_1} + \mathbf{g_2'} \tag{3.15}$$

On the other hand, when the spacecraft is very close to body 2, the effect of 1 can be considered as a perturbation.

$$\ddot{\mathbf{r}}_\mathbf{2} = -\mu_2 \frac{\mathbf{r_2}}{r_2^3} + \mu_1 \left| \frac{\mathbf{r_1}}{r_1^3} - \frac{\mathbf{r_{12}}}{r_{12}^3} \right| = \mathbf{g_2} + \mathbf{g_1'} \tag{3.16}$$

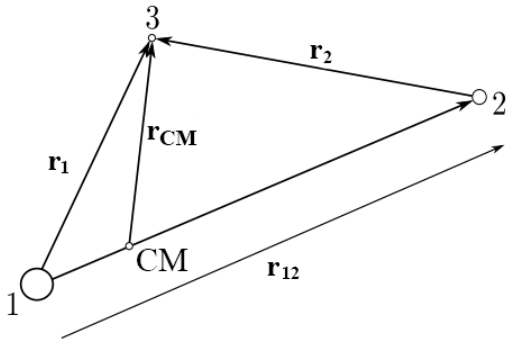


**Figure 3.3** Three-body problem. Center of mass is represented by CM.

With this, the locus of points where $\frac{g_2'}{g_1} = \frac{g_1'}{g_2}$ separates the influence zones of 1 and 2. When $m_1 \gg m_2$, this locus is approximated to a sphere, called sphere of influence, whose center is the body 2.

When the spacecraft is within the sphere of influence, it can be supposed that only body 2 acts over the vehicle, as a two body problem. In a similar way, outside of the sphere it can be supposed that only body 1 acts.

The radius of the sphere is given by

$$R_e = r_{12} \left( \frac{\mu_2}{\mu_1} \right)^{2/5} = r_{12} \left( \frac{m_2}{m_1} \right)^{2/5} \tag{3.17}$$

In order to show the order of magnitude of this radius, a comparison between different planets of Solar System is represented in Table 3.1.

**Table 3.1** Data of Solar System planets.

| | Planet radius (km) | Sphere of influence radius (km x $10^6$) | Mean distance to Sun (km x $10^6$) |
|---|---|---|---|
| Mercury | 2439 | 0.11 | 58 |
| Venus | 6051 | 0.62 | 108 |
| Earth | 6378 | 0.93 | 150 |
| Mars | 3397 | 0.58 | 228 |
| Jupiter | 71398 | 48 | 778 |
| Saturn | 60330 | 55 | 1426 |
| Uranus | 25400 | 52 | 2868 |
| Neptune | 24300 | 87 | 4494 |

### 3.4.2 Patched conic method

The patched conic method reduces the $n$-body problem to $n-1$ two-body problems. The simplification is achieved by dividing space into various parts by assigning each of the n bodies its own sphere of influence [20].

This method assumes that the sphere of influence of a planet has an infinite radius when it is observed from the planet, and has zero radius when it is observed from the Sun (due to $R_{planet} \ll R_{SoI_{planet}} \ll Distance_{Sun-Planet}$). Trajectories within the sphere of influence are two-body problems with the planet as the primary attracting body, and trajectories outside the sphere of influence are two-body problems with the Sun as the primary attracting body.

An example of an interplanetary transfer from Earth to Mars is shown in Figure 3.4.

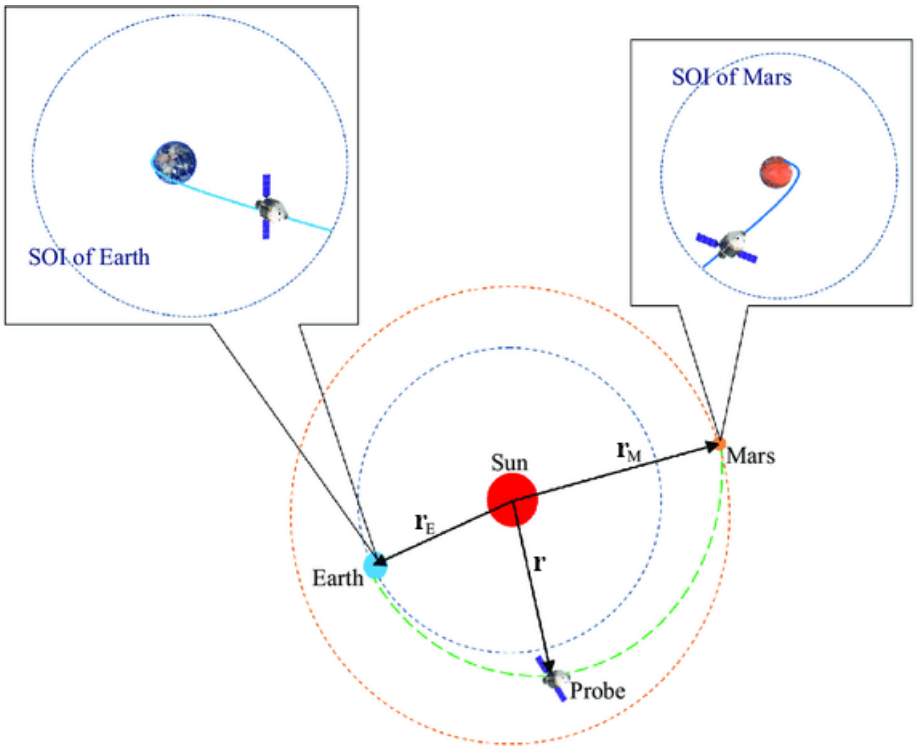


**Figure 3.4** Patched conic method for Earth-Mars direct interplanetary transfer. Credit: [21].

Therefore, in a planetocentric frame of reference, an hyperbolic orbit is needed to escape from the planet attraction. Then, once the spacecraft has reached the limit of the sphere of influence of the planet, we change to an heliocentric frame of reference, where elliptic or hyperbolic orbits are described.

The conditions going from planetocentric orbit to the heliocentric orbit or vice versa are called the "patch conditions". It consists in relating the velocity vector of the spacecraft with respect to the planet, $\mathbf{v^P}$, to the velocity vector of the spacecraft with respect to the Sun, $\mathbf{v^H}$, where the difference of the two is the velocity vector of the planet with respect to the Sun, $\mathbf{V_P}$. This relation can be represented as a triangle, called "triangle of velocities", and we discuss about it in Section 3.4.3.

### 3.4.3 Accomplishment of the gravity assist maneuver

The scenario in which a spacecraft enters the sphere of influence of planet "P", executes a gravity assist maneuver, and subsequently departs from said sphere of influence, is explicated. The notation we use is

- $\mathbf{v_1^H}$ : heliocentric velocity vector at the arrival to the planet.
- $\mathbf{v_2^H}$ : heliocentric velocity vector after the maneuver.
- $\mathbf{V_P}$ : heliocentric velocity vector of the planet "P".
- $\mathbf{v_1^P}$ : initial relative velocity vector.
- $\mathbf{v_2^P}$ : final relative velocity vector.

When the spacecraft goes into the sphere of influence of the planet "P", it describes an hyperbolic movement. The excess velocity (the velocity with which the spacecraft would reach infinity in a hyperbolic orbit) of the aforementioned hyperbola is $\mathbf{v}_\infty$, whose modulus verifies $|v_\infty| = |v_1^P| = |v_2^P|$.

On the one hand, the initial relative velocity $\mathbf{v_1^P}$ is defined as

$$\mathbf{v_1^P} = \mathbf{v_1^H} - \mathbf{V_P} \tag{3.18}$$

On the other hand, the final relative velocity $\mathbf{v_2^P}$ is defined as

$$\mathbf{v_2^P} = \mathbf{v_2^H} - \mathbf{V_P} \tag{3.19}$$

In Figure 3.5, triangles of velocities associated to the maneuver are presented.

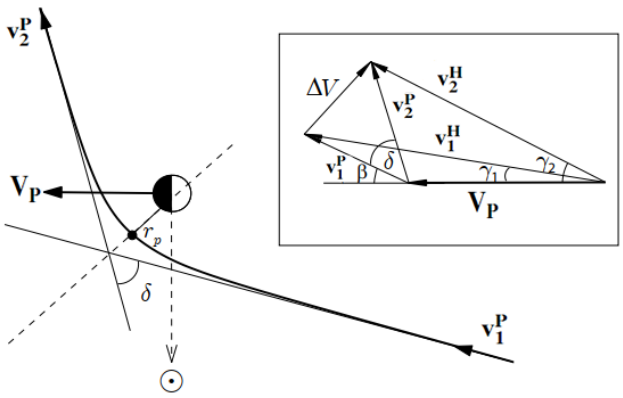


**Figure 3.5** Gravity assist maneuver. Triangles of velocities. Credit: [22].

The angle formed by $\mathbf{v_1^P}$ with the planet velocity $\mathbf{V_P}$ is called $\beta$. The angles formed by $\mathbf{v_1^H}$ and $\mathbf{v_2^H}$ with $\mathbf{V_P}$ are called $\gamma_1$ and $\gamma_2$ (trajectory angles), respectively. The trajectory angle is represented in an heliocentric frame of reference in Figure 3.6.

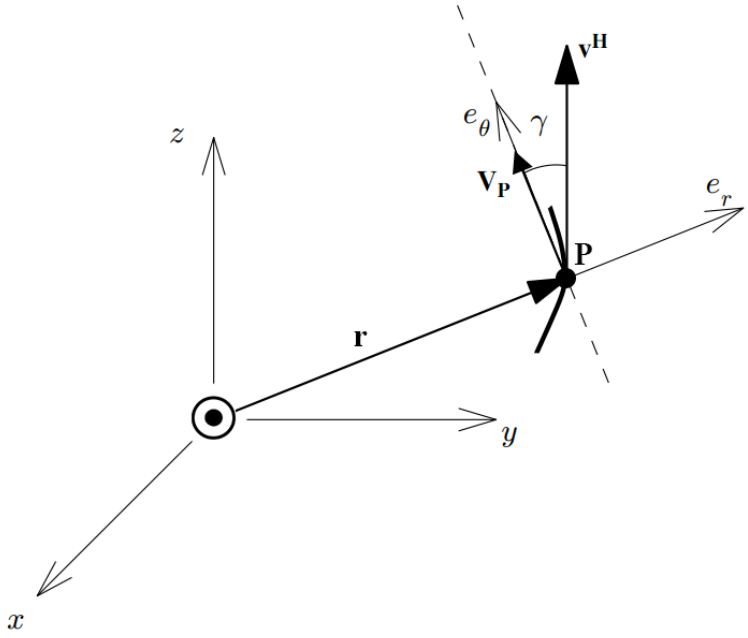


**Figure 3.6** Definition of the trajectory angle.

Lastly, the angle formed by the hyperbola asymptotes represents the deflection that the relative velocity vector experiments, and it is called $\delta$. Its value depends on the periapsis radius of the relative orbit to the planet, $r_P$, the excess velocity, $v_\infty$, and the Standard Gravitational Parameter of the planet, $\mu_P$.

$$\sin\left(\frac{\delta}{2}\right) = \frac{1}{1+\dfrac{r_P v_\infty^2}{\mu_P}} \tag{3.20}$$

The final relative velocity that we obtain of the triangle is based on $\delta$. We have two different options; $\delta$ can be added to $\beta$, or $\delta$ can be subtracted from $\beta$, as is shown in Figure 3.7. In both cases, the modulus of the final relative velocity is the same, but the modulus of heliocentric velocity after the maneuver is not the same.

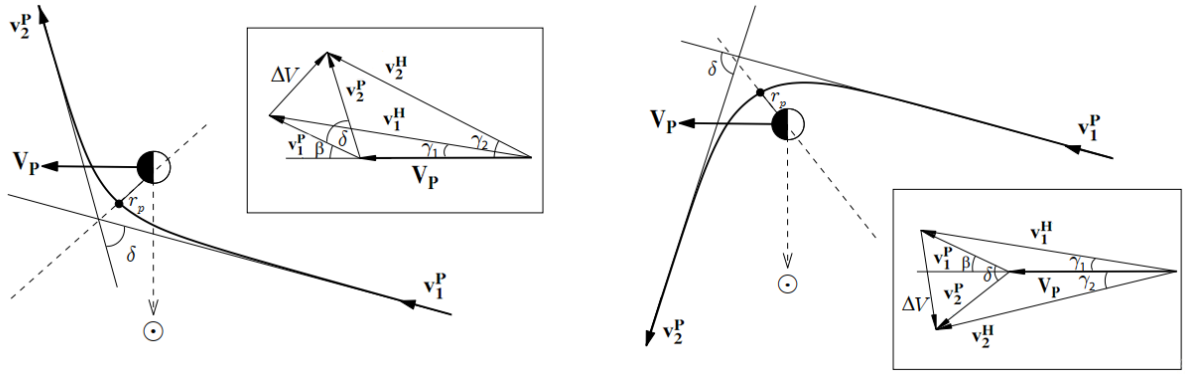


**Figure 3.7** Leading-side flyby and trailing-side flyby. Credit: [22].

When the spacecraft crosses the line between the planet and the Sun, the maneuver is known as a leading-side flyby and the spacecraft loses heliocentric velocity. The other case is known as a trailing-side flyby and the spacecraft gains heliocentric velocity [23]. However, not in all cases it is clearly distinguishable.

# 4 Optimization algorithms

There exists a variety of optimization algorithms applicable to the domain of this project. Our goal in this chapter is to define the algorithms that we use to find time-optimal transfer orbits, that is, find the necessary control parameters and variables of the problem as functions of time that lead to the fastest transfer orbit that takes the spacecraft from one planet to another, accomplishing the necessary gravity assist maneuvers in its path.

## 4.1 Non linear optimization of continuous systems

In this section, we center our focus on the optimal orbit control problem between two planets, in which the optimal orbit is defined as the one that requires the least time to be completed.

### 4.1.1 Problem hypotheses

To solve this, we recall some of the hypotheses and simplifications of Sections 1.2 and 3.2.

- **Coplanar orbits.** The orbits of the planets are contained in the ecliptic plane of the Solar System.
- **Circular orbits.** The orbits of the planets are supposed circular and concentric, with the Sun in the center of them.
- **Freedom in launch date choosing.** The launch date of the mission is a degree of freedom, therefore the position of the planets depends on the date we choose.
- **Only Sun attraction and E-sail thrust.** Only these forces are taken into account.

### 4.1.2 Optimal Control Problem formulation

In mathematics, optimal control theory is a branch of mathematical optimization where the main goal is to find a control for a dynamical system over a period of time such that an objective function is optimized [24]. These problems are usually denoted as Optimal Control Problems (OCP).

Our dynamic equations are defined in (3.14). We recall them here:

$$\begin{aligned}
\dot{r} &= v_r \\
\dot{\theta} &= \frac{v_\theta}{r} \\
\dot{v}_r &= \frac{v_\theta^2}{r} - \frac{\mu}{r^2} + \tau \frac{a_c}{2} \left(\frac{r_\oplus}{r}\right) (1 + \cos^2 \alpha_n) \\
\dot{v}_\theta &= -\frac{v_r v_\theta}{r} + \tau \frac{a_c}{2} \left(\frac{r_\oplus}{r}\right) \sin \alpha_n \cos \alpha_n
\end{aligned} \tag{4.1}$$

We have two path constraints, the boundary values of our control parameters. These constraints are defined in (4.2).

$$\begin{aligned} 0 \leq \tau(t) \leq 1 \\ -\alpha_n^{max} \leq \alpha_n(t) \leq \alpha_n^{max} \end{aligned} \tag{4.2}$$

Lastly, we have a series of conditions in the initial and final values of the state variables:

$$\begin{aligned} r(t_0) &= r_{P_i} & r(t_f) &= r_{P_f} \\ \theta(t_0) &= \theta_{P_{i,0}} & \theta(t_f) &= \theta_{P_{f,f}} \\ v_r(t_0) &= 0 & v_r(t_f) &= v_{r_f} \\ v_\theta(t_0) &= v_{P_i} & v_\theta(t_f) &= v_{\theta_f} \end{aligned} \tag{4.3}$$

where the subscript $P_i$ is referring to the initial planet, and the subscript $P_f$ is referring to the final planet. The initial velocity can be easily calculated as $v_{P_i} = \sqrt{\mu_{P_i}/r_{P_i}}$. Regarding the final velocity, its value is a degree of freedom and it depends on the final planet. Lastly, $\theta_{P_{i,0}}$ is referring to the position of the initial planet in $t_0$ and $\theta_{P_{f,f}}$ is referring to the position of the final planet in $t_f$.

Since $\theta_{P_{f,f}}$ depends on the final time $t_f$, and its value is unknown, this condition has to be replaced. Expressing $\theta_{P_{f,f}}$ in terms of $t_f$ and $t_0$ we have

$$\theta_{P_{f,f}} = \theta_{P_{f,0}} + (t_f - t_0)\sqrt{\frac{\mu}{r_{P_f}^3}} \tag{4.4}$$

where $\theta_{P_{f,0}}$ is referring to the position of the final planet in $t_0$, which is known.

Furthermore, the E-sail has to complete more revolutions than the final planet during the mission, therefore it is more correct to add the next constraint.

$$\theta(t_f) = \theta_{P_{f,0}} + (t_f - t_0)\sqrt{\frac{\mu}{r_{P_f}^3}} + 2\pi n \qquad\qquad n = 0,1,2,3... \tag{4.5}$$

Obviously, astronomical units are opted to be used, which are defined such that the mean distance from the Earth to the Sun equals 1 Astronomical Unit (AU), and the mean velocity of the Earth equals 1 Units of Velocity (UV). With this, the Standard Gravitational Parameter of the Sun equals to $\mu_\odot = 1$ AU UV$^2$, and we can also compute the rest of unit conversions:

$$\begin{aligned} 1 \text{ AU} &= 149.598 \cdot 10^6 \text{ km} \\ 1 \text{ UV} &= 29.7847 \text{ km/s} \\ 1 \text{ UT} &= 58.1324 \text{ days} \\ 1 \text{ UA} &= 5.9301 \text{ mm/s}^2 \end{aligned} \tag{4.6}$$

where UT means Units of Time and UA means Units of Acceleration.

There are more important observations that have to be made. In Section 3.3.1, a typically range of $a_c$ values is mentioned. For this project a conservative value of $a_c = 0.36$ mm/s$^2$ is used, which is less than the typical 1 mm/s$^2$ that is utilized in orbit determining investigations. In astronomical units, the value of the characteristic acceleration is $a_c = 0.0607$ UA.

We can also consider leaving some kind of margin in the sail pitch angle. Being the boundary value $\pm 70^o$, we may want to limit it to a lower value. However, recalling the relation between the thrust cone angle and the sail pitch angle, defined in (3.12), and adding the dependence of the modulus with the attitude of the spacecraft [25], which is given by a non-dimensional parameter ($\gamma$)

$$\begin{aligned} \cos\alpha &= \frac{1+\cos^2\alpha_n}{\sqrt{1+3\cos^2\alpha_n}} \\ \gamma &= \frac{\sqrt{1+3\cos^2\alpha_n}}{2} \end{aligned} \tag{4.7}$$

we can see in Figure 4.1 that there is no particular reason for the E-sail to opt for values of $\alpha_n$ much bigger than $55^o$, since that means reducing thrust modulus and cone angle. Given those reasons, the limit of the sail pitch angle keeps in $\pm 70^o$.

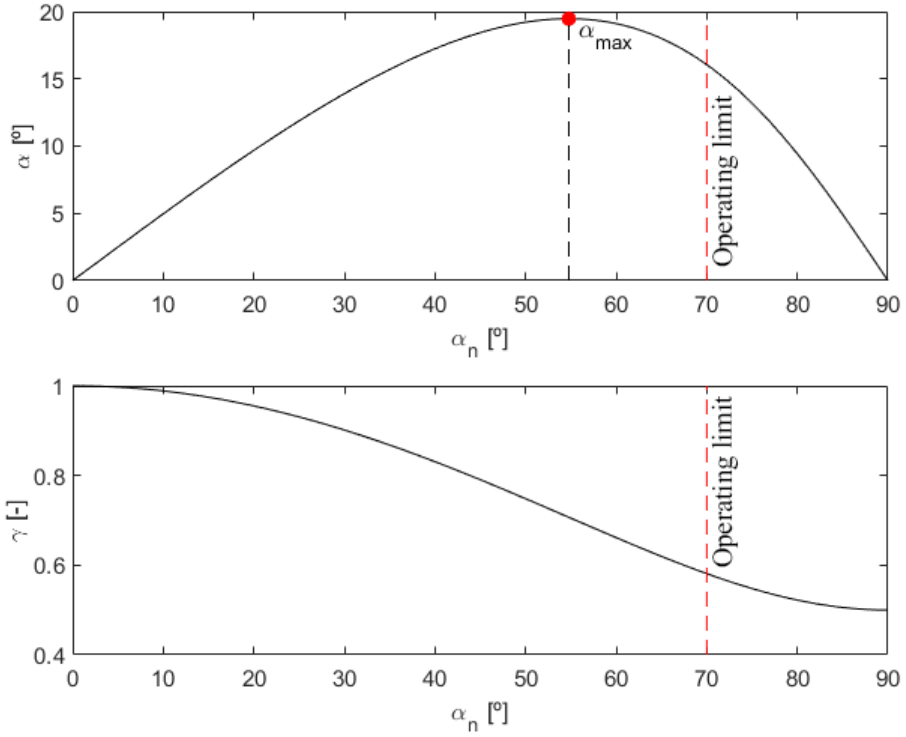


**Figure 4.1** Variation of $\alpha$ and $\gamma$ with respect to $\alpha_n$.

Lastly, to increase the robustness of the problem, we add an extra constraint that states that the final time must be positive ($t_f - t_0 \geq 0$).

Our final OCP formulation is presented in 4.8.

$$\min_{\tau,\alpha_n} \quad t_f - t_0$$

subject to

$$\begin{aligned}
\dot{r} &= v_r \\
\dot{\theta} &= \frac{v_\theta}{r} \\
\dot{v}_r &= \frac{v_\theta^2}{r} - \frac{\mu}{r^2} + \tau \frac{a_c}{2}\left(\frac{r_\oplus}{r}\right)(1+\cos^2\alpha_n) \\
\dot{v}_\theta &= -\frac{v_r v_\theta}{r} + \tau \frac{a_c}{2}\left(\frac{r_\oplus}{r}\right)\sin\alpha_n\cos\alpha_n
\end{aligned}$$

$$\begin{aligned}
0 \leq \tau(t) &\leq 1 \\
-\alpha_n^{max} \leq \alpha_n(t) &\leq \alpha_n^{max} \qquad\qquad t \in [t_0, t_f]
\end{aligned} \tag{4.8}$$

$$\begin{aligned}
r(t_0) &= r_{P_i} \\
\theta(t_0) &= \theta_{P_i} \\
v_r(t_0) &= 0 \\
v_\theta(t_0) &= v_{P_i} \\
r(t_f) &= r_{P_f} \\
v_r(t_f) &= v_{r_f} \\
v_\theta(t_f) &= v_{\theta_f} \\
\theta(t_f) &= \theta_{P_{f,0}} + (t_f - t_0)\sqrt{\frac{\mu}{r_{P_f}^3}} + 2\pi n \qquad\qquad n = 0,1,2,3...
\end{aligned}$$

$$t_f - t_0 \geq 0$$

where $a_c = 0.0607$ UA, $\alpha_n^{max} = 70^o$, $\mu = 1$ AU UV$^2$, $r_\oplus = 1$ AU, $v_{P_i} = \sqrt{\mu_{P_i}/r_{P_i}}$, $v_{r_f}$ and $v_{\theta_f}$ are free to choose, and $\theta_{P_{i,0}}$ and $\theta_{P_{f,0}}$ depend on the launch date chosen.

This time-optimal problem is difficult to solve. Our restrictions are non-convex and extremely non-linear, and that means that there possibly exist more than one local solution to our problem, what makes our solution extremely sensitive to the initial guess. Depending on it, and on the algorithm used, our problem can even end up being infeasible.

The numerical calculation of this problem is made using a direct transcription method that let us convert our problem into a Non Linear Programming (NLP) problem.

### 4.1.3 Conversion of our OCP to a NLP problem

In order to solve our OCP, we need to transform it to the form of a problem that can be solved using NLP optimization algorithms.

First, the standard formulation of NLP problems is presented.

A finite set of variables is needed, that we define as $\mathbf{y} = [y_1, y_2, ..., y_M]^T$. Then, the generic NLP problem is formulated as an optimization problem in which an objective function F is minimized as

$$\min_{\mathbf{y}} \quad F(\mathbf{y}) \tag{4.9}$$

These variables are subject to a set of inequality constraints and bounds represented as

$$\text{subject to} \quad \begin{cases} \mathbf{c}_L \leq \mathbf{c}(\mathbf{y}) \leq \mathbf{c}_U \\ \mathbf{y}_L \leq \mathbf{y} \leq \mathbf{y}_U \end{cases} \tag{4.10}$$

where initial and final conditions can be included by establishing the same value in lower and upper limit ($c_{L_i} = c_{U_i}$, $c_{L_f} = c_{U_f}$, $y_{L_i} = y_{U_i}$, $y_{L_f} = y_{U_f}$).

To adapt our OCP to this formulation, we need to discretize time in a number of intervals. Before that and without loss of generality, we assume the initial time of the problem to be $t_0 = 0$, what means our objective function is now $t_f$. Then, $t_f$ has become the flight time.

$$\mathbf{t} = [t_0 = 0, t_1, t_2, ..., t_N = t_f]^T, \quad \text{where} \quad t_{k+1} = t_k + h, \quad \forall k \in [0, N-1] \tag{4.11}$$

and $h$ is given by $h = t_f/N$.

Using a uniform time partition approach as (4.11) is common in trajectory optimization related problems [26].

Once we have a finite number of time instants, our set of unknowns has also become finite. At each instance of time $k$ of the N+1 total count, we have four state variables $\mathbf{x}_k$. On the other hand, for simplicity, the control parameters are chosen to be constant functions in each interval between time instants. Therefore, we have two control variables $\mathbf{u}_k$ at every interval of the N total count (a visual representation is presented in Figure 4.2). Lastly, since flight time is unknown, it is added to the vector of variables $\mathbf{y}$.

Therefore, in a time partition of N intervals with $n_x$ state variables, $n_u$ control parameters and one unknown flight time variable, the total amount of unknowns in the NLP problem can be expressed as

$$n_T = n_x \cdot (N+1) + n_u \cdot N + 1 \tag{4.12}$$

In our problem, where $n_x = 4$ and $n_u = 2$, if we opt for a time partition of 500 intervals we have a total of 3005 variables.

We now have to transform the state differential equations in (3.14), denoted as $\mathbf{f}$, into their algebraic finite differences equivalents, which are often called defect constraints. Using a classical Runge-Kutta method we can approximate the next value of a state variable depending on previous values of $\mathbf{x}$ and $\mathbf{u}$. This relation can be expressed as

$$\mathbf{x}_{k+1} = \mathbf{x}_k + h \sum_{i=1}^{s} b_i \mathbf{k}_i \tag{4.13}$$

where $s$ is the order of the Runge-Kutta method, $b_i$ are coefficients and $\mathbf{k}_i$ are midpoint state functions evaluations depending on the particular method scheme utilized.

It can be expressed as a defect constraint as

$$\zeta_k = \mathbf{x}_{k+1} - \mathbf{x}_k - h \sum_{i=1}^{s} b_i \mathbf{k}_i \tag{4.14}$$

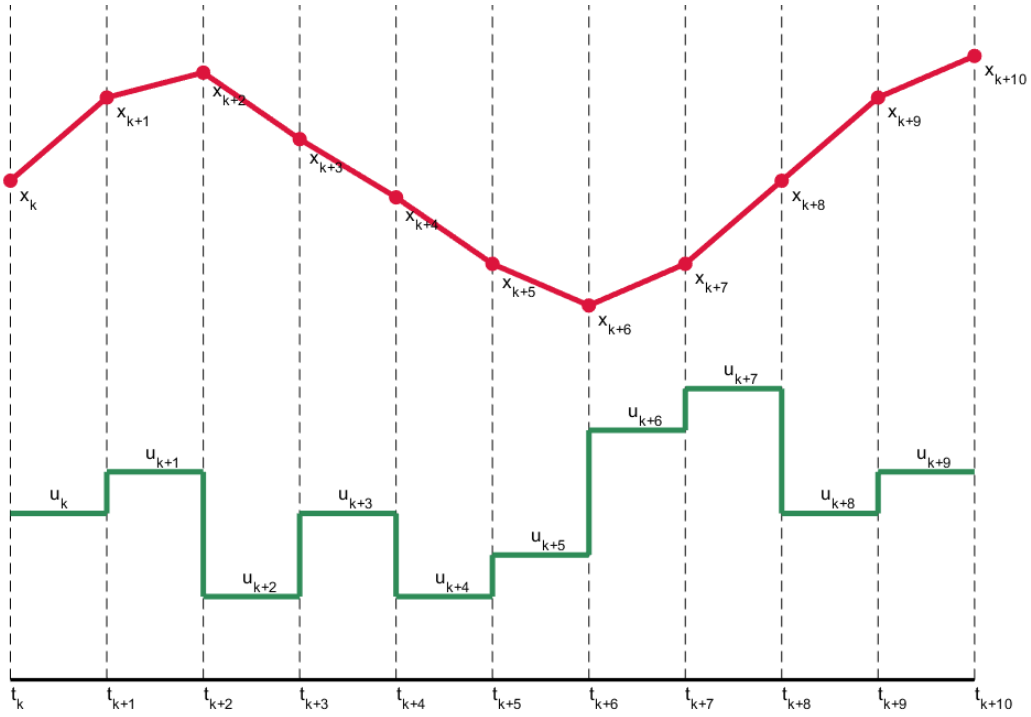


**Figure 4.2** Visual scheme of the transcription of an Optimal Control Problem.

The particular numerical integration method chosen for this project is the Classical Runge Kutta Fourth Order method, algebraically represented by the equations in (4.15).

$$\begin{aligned}
\mathbf{k}_{1_k} &= \mathbf{f}\left(\mathbf{x}_k, \mathbf{u}_k\right) \\
\mathbf{k}_{2_k} &= \mathbf{f}\left(\mathbf{x}_k + \frac{h}{2}\mathbf{k}_{1_k}, \mathbf{u}_k\right) \\
\mathbf{k}_{3_k} &= \mathbf{f}\left(\mathbf{x}_k + \frac{h}{2}\mathbf{k}_{2_k}, \mathbf{u}_k\right) \\
\mathbf{k}_{4_k} &= \mathbf{f}\left(\mathbf{x}_k + h\mathbf{k}_{3_k}, \mathbf{u}_k\right) \\
\mathbf{x}_{k+1} &= \mathbf{x}_k + \frac{h}{6}\mathbf{k}_{1_k} + \frac{h}{3}\mathbf{k}_{2_k} + \frac{h}{3}\mathbf{k}_{3_k} + \frac{h}{6}\mathbf{k}_{4_k}
\end{aligned} \tag{4.15}$$

This numerical integration method is good enough, since it represents a good compromise between simplicity and accuracy. Nevertheless, there exist better integration methods for more advanced applications, that compute extremely accurate approximations [27].

Apart form the equations already mentioned, we have the inequality path constraints about the maximum and minimum value of $\tau$ and $\alpha_n$, now defined for each interval, and the flight time positive constraint, as mentioned in Section 4.1.2. We can express it as

$$\begin{aligned}
0 \leq \tau_k \leq 1 \\
-\alpha_n^{max} \leq \alpha_{n_k} \leq \alpha_n^{max} \qquad & \forall k \in [0, N-1] \\
t_f \geq 0
\end{aligned} \tag{4.16}$$

In addition, the boundary conditions in their discrete version are presented in (4.17).

$$\begin{aligned} r_0 &= r_{P_i} \\ \theta_0 &= \theta_{P_i} \\ v_{r_0} &= 0 \\ v_{\theta_0} &= v_{P_i} \\ r_N &= r_{P_f} \\ v_{r_N} &= v_{r_f} \\ v_{\theta_N} &= v_{\theta_f} \end{aligned} \tag{4.17}$$

Lastly, the condition (4.5) can be expressed as

$$\theta_N = \theta_{P_{f,0}} + t_N \sqrt{\frac{\mu}{r_{P_f}^3}} + 2\pi n \qquad\qquad n = 0,1,2,3... \tag{4.18}$$

or, in a different way, as

$$\sin\left( \frac{\theta_N - \left( \theta_{P_{f,0}} + t_N \sqrt{\frac{\mu}{r_{P_f}^3}} \right)}{2} \right) = 0 \tag{4.19}$$

Summing all this up, the full problem in a NLP formulation is expressed in (4.20).

$$\min_{\mathbf{y}} \quad t_N$$

$$\text{subject to} \quad \begin{cases} \mathbf{c}_L \leq \mathbf{c}(\mathbf{y}) \leq \mathbf{c}_U \\ \mathbf{y}_L \leq \mathbf{y} \leq \mathbf{y}_U \end{cases}$$

where

$$\begin{aligned} \mathbf{y} &= [r_0,\theta_0,v_{r_0},v_{\theta_0},r_1,\theta_1,v_{r_1},v_{\theta_1},...,r_{N-1},\theta_{N-1},v_{r_{N-1}},v_{\theta_{N-1}},r_N,v_{r_N},v_{\theta_N},\tau_0,\alpha_{n_0},...,\tau_{N-1},\alpha_{n_{N-1}},t_N]^T \\ \mathbf{y}_L &= [r_{P_i},\theta_{P_i},0,v_{P_i},-,-,-,-,...,\ -\ ,\ -\ ,\ -\ ,\ -\ ,r_{P_f},v_{r_f},v_{\theta_f},0,-\alpha_n^{max},...,0,-\alpha_n^{max},0]^T \\ \mathbf{y}_U &= [r_{P_i},\theta_{P_i},0,v_{P_i},-,-,-,-,...,\ -\ ,\ -\ ,\ -\ ,\ -\ ,r_{P_f},v_{r_f},v_{\theta_f},1,\alpha_n^{max},...,1,\alpha_n^{max},-]^T \end{aligned}$$

and

$$\begin{aligned} \mathbf{c}(\mathbf{y}) &= [\zeta_0,\zeta_1,...,\zeta_{N-1},\zeta_N,\zeta_\theta]^T \\ \mathbf{c}_L &= [\ 0\ ,\ 0\ ,...,\ 0\ \ ,\ 0\ ,\ 0\ ]^T \\ \mathbf{c}_U &= [\ 0\ ,\ 0\ ,...,\ 0\ \ ,\ 0\ ,\ 0\ ]^T \end{aligned} \tag{4.20}$$

It should be pointed out that $\theta_N$ has been removed from $\mathbf{y}$ in (4.20), because it can be added as a non-linear constraint as it expressed in (4.19) (this constraint is called $\zeta_\theta$ in $\mathbf{c}(\mathbf{y})$).

Furthermore, the notation $-$ in a term of a vector means that there is not such restriction. For the example, in the case of $t_N$ there is a $-$ in the upper limit because $t_N$ is only limited to be positive (greater than 0).

Now that we have the problem in a NLP form, the next step is to use an optimization algorithm

to solve it, and we choose *CasADi* Toolbox for MATLAB [28]. *CasADi* Toolbox provides us the algorithm IPOPT (Interior Point OPTimizer), commonly used for large scale non linear optimization of continuous systems.

When the problem has convex constraints and a convex cost function in a convex domain, IPOPT is a deterministic algorithm that is able to find the global extremum rapidly. On the other hand, non-convex optimization, where there exist multiple local extrema, is more difficult and challenging. However, IPOPT is able to get a solution in many of these cases.

There is not a standardized procedure to ensure that the found solution is a global extremum, so it becomes to a new challenge. The procedure that we follow is to try with different initial orbit guesses, and see how the result changes. If the flight time remains the same for a variety of different initial guesses, the solution is surely globally optimal. Otherwise, if the result changes, our best option is to choose the orbit with less flight time than the rest (even if we can not ensure that this result is the global solution, it is probably close to it).

## 4.2 Genetic Algorithm

For the appearance of the genetic algorithms, by John Henry Holland, we have to date back to 70s. However, it has been in the last decade when its use in the space industry, as well as in many other fields, has increased notably thanks to advances in technology that allow its application. This algorithms imply a complex artificial intelligence methodology based on the *Darwin's Theory of Evolution*.

In this section, the algorithm is presented, and its different configurations are analyzed, in order to apply it to our optimization problem.

### 4.2.1 Metaheuristics

Before describing the genetic algorithms , we need to understand what metaheuristic algorithms consist. A metaheuristic is a higher-level procedure or heuristic designed to find, generate, tune, or select a heuristic (partial search algorithm) that may provide a sufficiently good solution to an optimization problem [29]. Metaheuristics sample a subset of solutions which is too large to be completely enumerated or otherwise explored.

Metaheuristic algorithms use artificial intelligence in order to seek the balance between randomness and local search, between *exploration* and *exploitation* (these terms are explained in detail in Section 4.2.3). With this, the metaheuristic algorithms are the perfect tool for the search for global optimums, although it is necessary to refine the final search with some conventional algorithm such as the use of deterministic methods.

### 4.2.2 Background concepts in genetic algorithms

The genetic algorithm distinguishes from the other metaheuristic algorithms in the way in which artificial intelligence is used. The number of solutions in which we work on at the same time or how this work is carried out are some of the features that characterize the method. To understand the methodology of a genetic algorithm, it is necessary to know *The theory of Natural Selection of Darwin* [30]:

- The individuals of species (population) have differences between them (different genes).
- In species, the individuals have more offspring than the (limited) resources and different dangers allow to survive.

- The individuals with the greatest survival capacity, the best, will be those with more likely to generate offspring, and with it, that their traits (genes) prosper.
- The offspring of two individuals in a population will randomly have genes of both parents (or mixtures).
- In any individual, a mutation can occur in one of their genes.
- The population will adapt to the environment while generations are advancing.

The algorithm uses the basis of the evolutionary theory to proceed, where the individuals are represented by the possible solutions of the optimization problem (called as candidates of the solution), and the genes are the values of the variables in each solution.

When the optimization problem is one in which a objective function is minimized, the individuals with the greatest survival capacity are those with the lowest value of the objective function once they are evaluated.

The first population is generated completely randomly (their genes can be delimited by a maximum and a minimum). Each individual is evaluated through the objective function, and then, the evolutionary process starts.

The way in which individuals are selected to generate offspring, how they interbreed the genes of the parents, or when and how they mutate are variables of the method, where we have a certain degree of freedom. This aspect is presented in Section 4.2.4, where genetic operators are defined.

Lastly, there exists different methods to close the optimization problem. Since neither the form of the optimal solution is known, nor is the value of the objective function in that optimal, the decision can not be made relative to reaching that point. We have two alternatives:

- A number of generations, N, is fixed, such that the best individual of the N population is chosen as the optimal.
- A value of tolerance is fixed, such that if a population is reached in which the best value of the objective function differs in less than this tolerance from the population mean, the best individual of this population is chosen as the optimal.

The second way is more reliable in order to find the global optimum, but, in complex problems, this way increases the computation time excessively. When the goal is simply to find a feasible solution, the first way is more appropriate. The common strategy (and the strategy we follow in this project) is to start fixing the number of generations, and once we analyze the behaviour of the problem we can set an appropriate value of tolerance to continue with the second alternative.

### 4.2.3 *Exploration* and *Exploitation*

It is important to distinguish between exploration and exploitation, two concepts that allow us to choose the degrees of freedom of the algorithm.

The exploration refers to the ability of the algorithm to explore the space of solutions. The more importance the randomness component has within the algorithm the greater this exploration will be. A good search ability allows the algorithm to get close to the surroundings of the global optimum.

On the other hand, the exploitation refers to the ability of the algorithm to improve a solution in order to converge to the closest optimum. The ability to reach an optimum is greater when the condition for an individual of the population to survive is more strict and the importance of the randomness component of the method is lower.

A good exploration at the beginning of the method and a great exploitation at the end is the ideal combination, without allowing the method to focus all its ability only in one of them in any point of the process [31]. This balance is reachable with the correct selection of the randomness parameters of the algorithm.

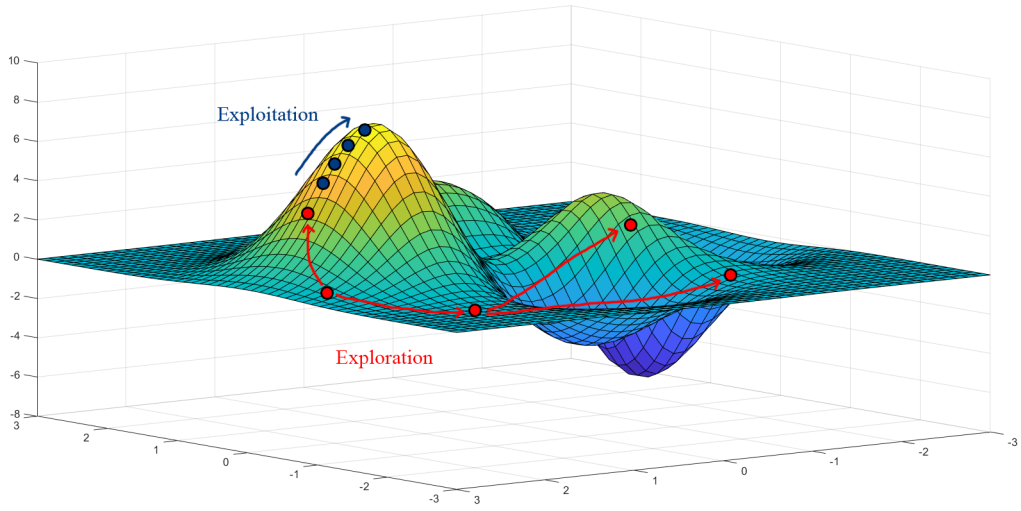


**Figure 4.3** Representation of exploration and exploitation.

### 4.2.4 Parts of a genetic algorithm

It is time to introduce the different parts of a genetic algorithm, also known as genetic operators, the degrees of freedom in each part and which of the different possibilities of operation is the best for the problem.

Among the different operators we have the creation of the initial population, the crossover, the mutation, the elitism and the selection.

#### Creation of the initial population

The creation of the initial population is purely random, without selecting a generation seed for the assignment of random numbers.

A seed is a number (or vector) used to initialize a pseudorandom number generator. Given the same seed number, a random number generator will generate the same series of random numbers each time a simulation is run.

In some problems it may be interesting to set all seeds of all processes involving randomness, being the solutions "seeded" in areas where optimal solutions are likely to be found.

Nevertheless, the algorithm that is used to obtain all the results exposed in this project does not have any of these seeds fixed. The extensive exploration offered by these methods is limited if you do not leave freedom in the initialization of the problem. To generate these individuals, the MATLAB "rand" order is used without fixing the seed, being each gene of each individual a random value between its maximum and minimum.

### Crossover

Crossover is the distinguishing feature of the genetic algorithm. It consists in mixing and matching genes of two parents to form children. The way of mixing and matching depends on the representation of the individuals [32]. Mainly, there are two ways to approach the process:

- Linear recombination: It consists in choosing the similarity with each parent. Then, the genes of the new individual are a linear combination of the predecessors.
- Recombination by substitution: It consists in choosing certain variables from one of the parents and completing the genes of the offspring with those of the other parent.

Looking for a method with selective pressure that guarantees exploration at the beginning and exploitation at the end, we opt to implement the linear recombination method known as Simulated Binary Recombination (SBR) [33]. In this method, the offspring is given by

$$\begin{aligned} x_{d_1} &= \frac{1}{2}[(1+\bar{\beta})x_{p_1} + (1-\bar{\beta})x_{p_2}] \\ x_{d_2} &= \frac{1}{2}[(1-\bar{\beta})x_{p_1} + (1+\bar{\beta})x_{p_2}] \end{aligned} \tag{4.21}$$

where $x_{p_i}$ are the parents and $\bar{\beta}$ is based on a random variable $u$, that is between 0 and 1, such that:

$$\begin{aligned} \bar{\beta} &= (2u)^{\frac{1}{\eta_c+1}}, \quad u \leq 0.5 \\ \bar{\beta} &= \left(\frac{1}{2(1-u)}\right)^{\frac{1}{\eta_c+1}}, \quad u > 0.5 \end{aligned} \tag{4.22}$$

The parameter $\eta_c$ is one of the control parameters of the algorithm. It consists in a positive real number that controls the probability that the offspring will be similar to the parents. Its value is determined by making some simulations with different parameters.

The selection of the parents is another aspect to be taken into account. In this project, the population of individuals is traversed, ordered from best (the best individual is the one with the least value of the objective function) to worst individual, deciding with a probability of $p_c$ each individual that becomes a parent. When we get two parents, crossover occurs (see in Figure 4.4). In addition, crossing is carried out randomly between any individuals, a low number of times (control parameter $n_c$). This helps that the exploration never stops.

### Mutation

Mutation of an individual causes some of its genes to change its value randomly. It is often used in conjunction with the crossover operator.

In order to control this operator when individuals are made up of non-binary genes, a good algorithm is the Gaussian Convolution [32]. The method consists in modifying random genes of a chosen individual, but such that the modifications (always between the maximum and minimum values of the gene) respond to a Normal distribution with zero mean and variance $\sigma$. By adjusting the value of $\sigma$ and the probability of mutation for a gene, $p_m$, (new control parameters) it is possible to focus more on exploitation (lower value of $\sigma$ and $p_m$) or on exploration (case contrary). $p_m$ can even be equal to 1, in which case the individual to be mutated undergoes changes in each of its genes. This case is especially useful to ensure that the genetic algorithm never stops exploring the space of solutions.

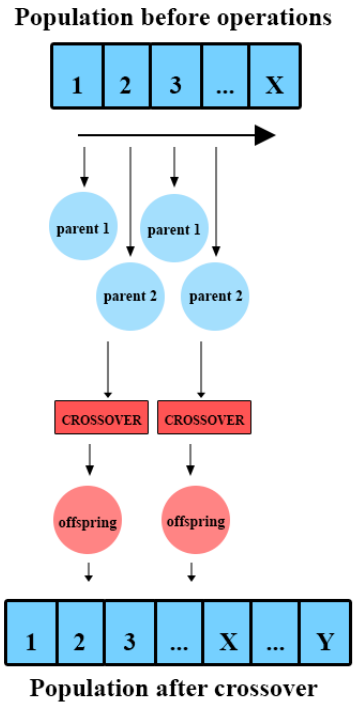


**Figure 4.4** Representation of Crossover.

In this project, a slight modification of the method is carried out. Instead of establishing a value of $\sigma$ for all the genes, we establish a value for each one of them. This value is given by

$$\sigma_i^2 = \frac{UB_i - LB_i}{\sigma_c} \tag{4.23}$$

where $UB_i$ and $LB_i$ are the upper and lower limits of the value of the gene, respectively, and $\sigma_c$ is a control parameter. The higher the value of $\sigma_c$, the lower the value of $\sigma$ and greater exploitation; the lower the value, the greater the exploration due to the increase in $\sigma$.

Therefore, the process we follow is the next: the population of individuals $Y$ (after the crossover is done) is traversed, deciding each individual that mutates (there is a probability, $p_{mut}$, that an individual will mutate). If mutation occurs, the Gaussian Convolution method is applied with a value of $p_m$ and $\sigma_c$. In addition, an individual is chosen arbitrarily from population $Y'$ (mutated population) and a mutation with $p_m = 1$ is applied to it. A representation of the process is presented in Figure 4.5.

### Elitism

The goal of Elitism is to preserve the $E$ best solutions (that are called the elites) of the population and avoid that these could be eliminated during the selection or subjected to mutation. This new control parameter $E$ must be at least one order of magnitude less than $X$ (size of the base population and total surviving population).

### Selection

Once the rest of the genetic operations is done and we have a number of individuals $Y > X$, the selection consists in choosing the $(Y - X)$ individuals to be removed.

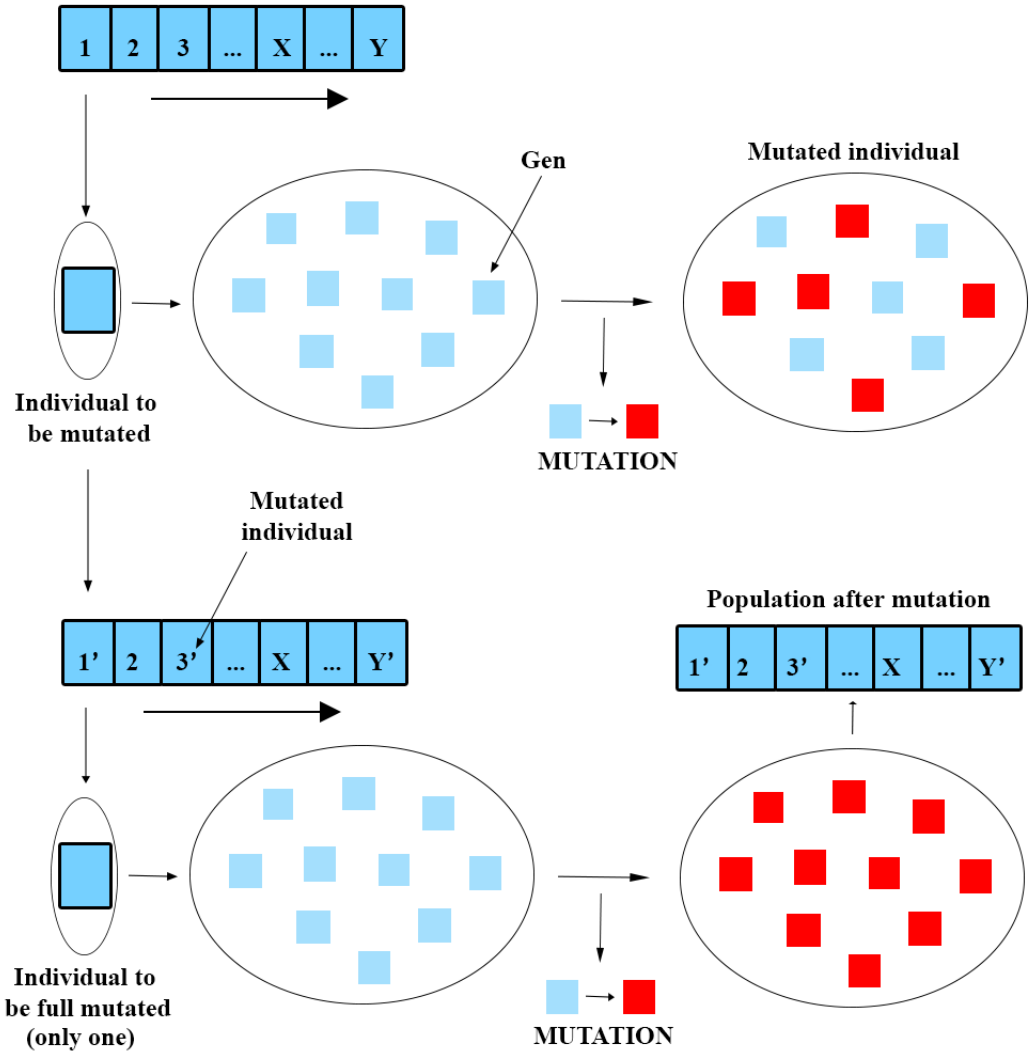


**Figure 4.5** Representation of Mutation.

The selection of individuals that survive probably is the part of the algorithm in which the decision of how to make it affects to the final result the most. It depends on the pressure on the population [34], a concept that is related to exploration and exploitation of the method.

With strict survival conditions, where the $X$ best individuals always survive (a procedure known as Truncation Selection), the pressure will be high and with it, the exploitation, but exploration capacity will be lost. In this case, the method will quickly converge to a local optimum. Otherwise, too low pressure (such as a random selection of surviving individuals) would lack exploitation capacity. Therefore, we look for a method with a low pressure at the beginning, favoring the exploration, and high in its last iterations to exploit the best area found.

To achieve this, there are different procedures [32], such as:

- **Fitness Proportionate Selection (FPS)**, sometimes known ad Roulette Selection. In this algorithm, individuals are selected in proportion to the value of the objective function. We "size" each individual according to (4.24),

$$p_i = 1 - \frac{F_i}{\sum^X F_i} \tag{4.24}$$

where $p_i$ is the probability of the i individual to be selected and $F_i$ is the value of the objective function for the i individual. The expression is the same in a maximization problem, replacing $p_i$ with $(1 - p_i)$. This procedure allows any solution the chance to survive, since there is never a strict probability of 0.

- **Stochastic Universal Sampling (SUS)** is a variant of Fitness Proportionate Selection, where we choose a number $n$ within $Y$, order the solutions according to their value in the objective function, and determine which survive using similar probabilities to those of the previous method, but ensuring the selection of at least one individual within each range (order of magnitude) of objective function values. With this, there is always the possibility of exploration.

However, the most appropriate procedure for a genetic algorithm is known as Tournament Selection [35].

Tournament Selection involves running several "tournaments" among a number $t$ of individuals chosen at random from the population $Y'$. The winner of each tournament is selected, becomes part of the next population and stops participating in the following tournaments. This tournament is repeated $X$ times, therefore the total number of individuals in the selected population is maintained (see in Figure 4.6). The parameter $t$ is another one of the mentioned control parameters on the genetic algorithm. By setting it, you can change how selective the technique is. At the extremes, if $t = 1$, this is just a random search. If $t$ is very large (much larger than the population size itself), then the process approaches Truncation Selection. The most popular setting is $t = 2$.

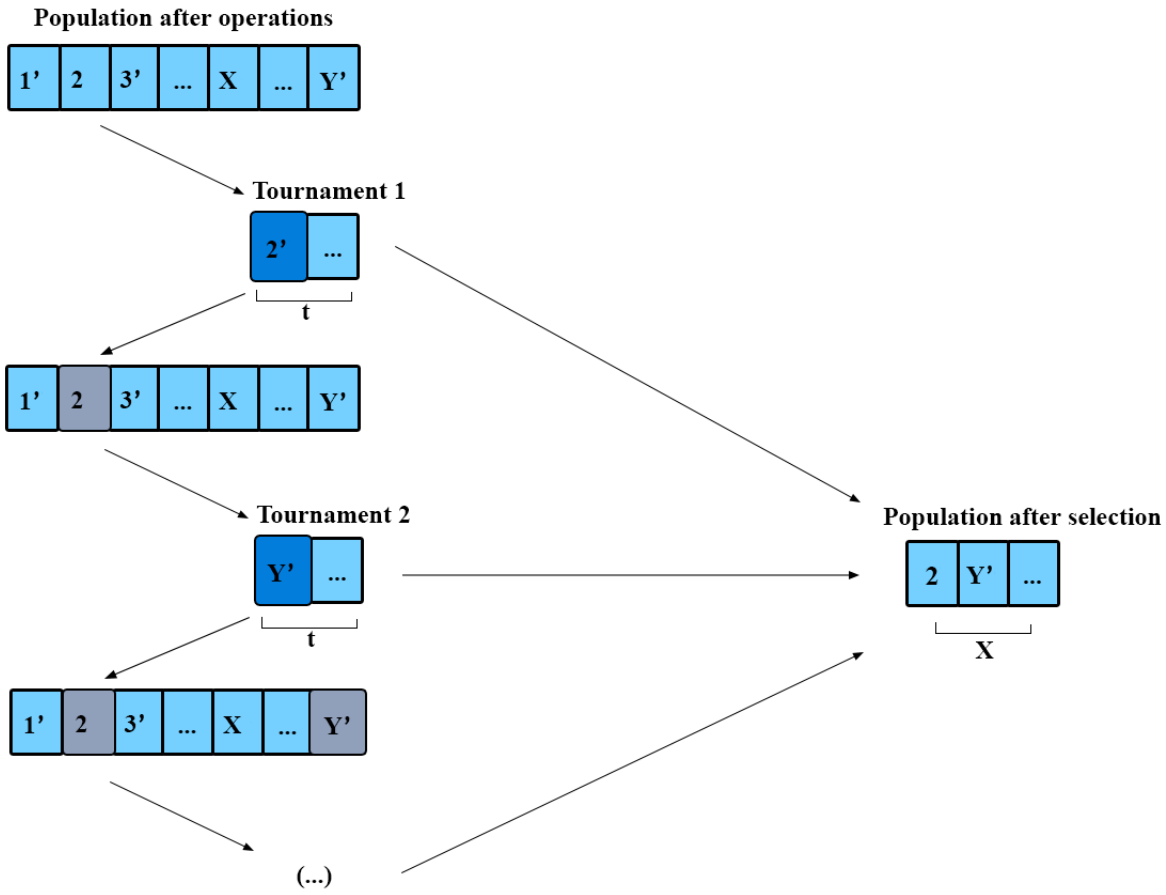


**Figure 4.6** Representation of Tournament Selection.

Slight modifications on Figures 4.5 and 4.6 would be necessary since the groups that are subjected to the operator in them are the complete population after the crossing process, being therefore necessary to extract from these groups those selected as elite. With this, we would carry out $X - E$ tournaments, instead of $X$. However, we decide to keep these figures in order to provide to the explanation a more generic value, since not all genetic algorithms have an elitism operator.

### 4.2.5 Procedure and relationship between the parts

A flowchart of the genetic algorithm is presented in Figure 4.7 in order to make the explanation of the process more understandable.

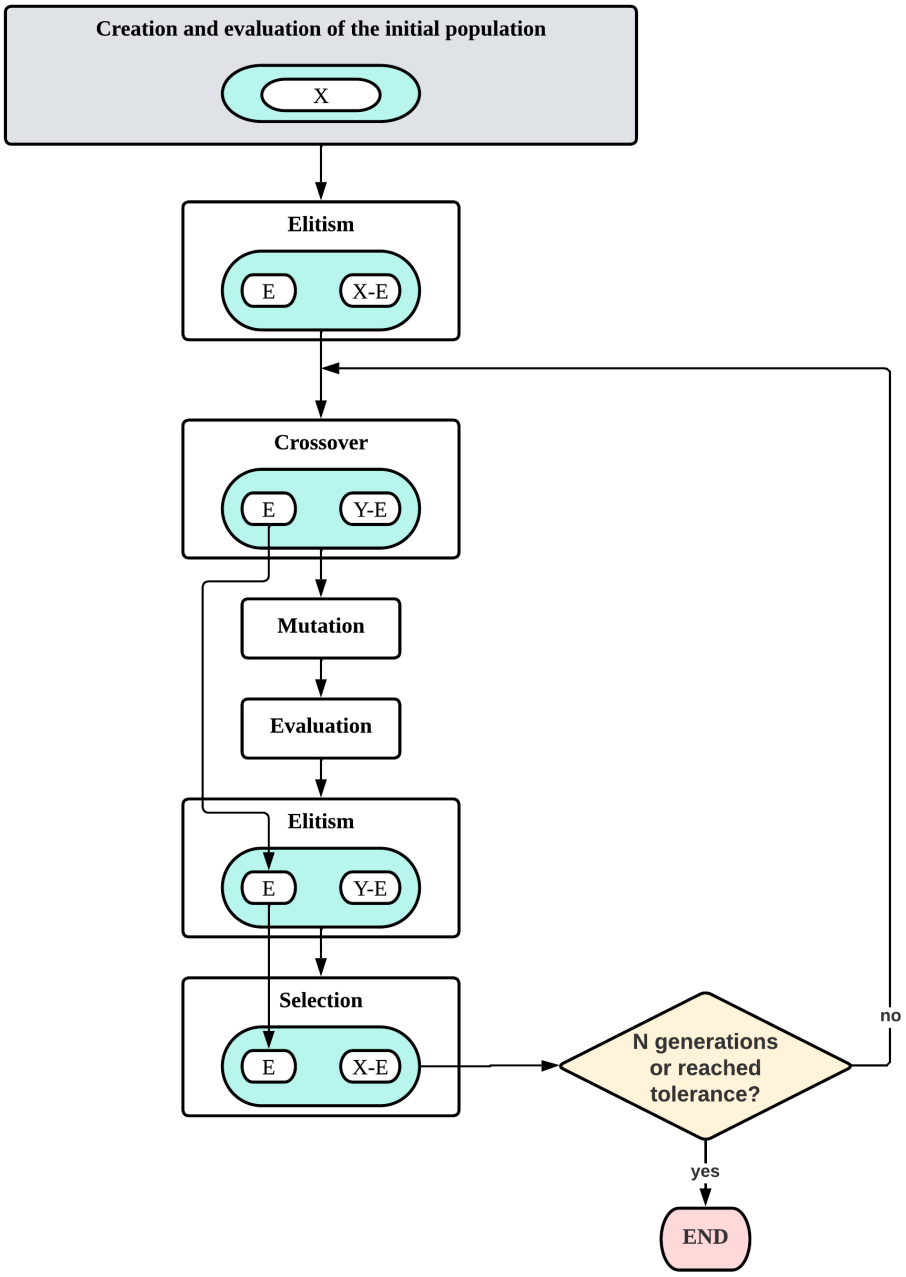


**Figure 4.7** Flowchart of the Genetic Algorithm process.

As a summary, the control parameters are finally:

- $X$: Number of individuals of the base population.
- $E$: Number of individuals of the elite.
- $N$: Maximum allowed number of generations.
- $t$: Number of participants of a tournament.
- $n_c$: Number of random crossovers in a generation.
- $\eta_c$: Control parameter of similarity between offspring and parents.
- $p_c$: Probability of an individual of becoming a parent.
- $\sigma_c$: Denominator in the variance of the Normal distribution in mutation.
- $p_{mut}$: Probability of an individual to mutate.
- $p_m$: Probability of mutation of a gene in an individual that mutates.
- $TOL$: Tolerance of difference between the mean value of the population in the objective function and that of the best individual.

Lastly, a genetic algorithm should not be launched only once. We opt to launch it several times comparing the different iterations in order to determine the closest solution to the global optimum.

### 4.2.6 Objective function and optimization variables of the problem

The problem where the genetic algorithm is applied consists in a trajectory with a gravity assist maneuver. Once the non linear optimization of a trajectory between two planets has been explained in Section 4.1, a flowchart with the objective function of the problem is presented in Figure 4.8

In a non linear optimization between two planets, there are two different cases: the arrival velocity (radial and tangential components) is fixed or not. In the first stretch, from Earth to the intermediate planet (where the gravity assist maneuver is accomplished), the two components of the arrival velocity are fixed and they are variables of the genetic algorithm. On the other hand, in the last stretch, there is not any constraint about the arrival velocity.

The third variable of the algorithm is $r_P$, the periapsis radius of the relative orbit to the intermediate planet in the gravity assist maneuver.

Another input of the non linear optimization is the position of the planets, that depends on the launch date chosen. Since the gravity assist maneuver is considered as instantaneous, the position of the planets in the second stretch only depends on the launch date and the flight time of the first stretch. This launch date can be set as another variable of the algorithm. However, in most of the simulations that are launched in this project, the launch date is fixed.

Therefore, the value of the objective function is the addition of the flight time in both stretches of the trajectory, and the variables are:

- **Radial component of the arrival velocity ($v_{r_f}$):** in UV. Its lower and upper limits depend on the intermediate planet.
- **Tangential component of the arrival velocity ($v_{\theta_f}$):** in UV. Its lower and upper limits depend on the intermediate planet.
- **Approach radius in the gravity assist maneuver ($r_P$):** it is expressed as a multiple of the radius of the intermediate planet.

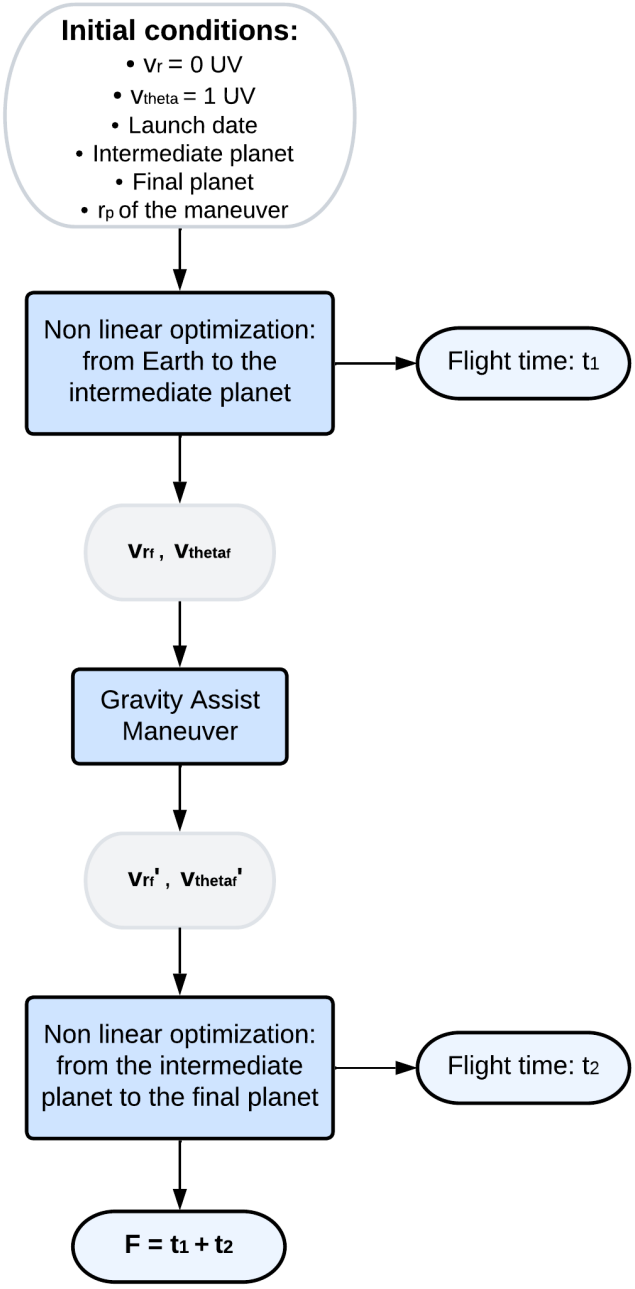


**Figure 4.8** Flowchart of the objective function.

# 5 Analysis of results

In this chapter, all the results that have been obtained are presented. First, different optimal transfer orbits between two planets are shown, in order to analyze the non linear optimization. Once the different paths are solved and the order of magnitude of the state variables and control parameters is known, we are able to introduce a gravity assist maneuver in the trajectories. Lastly, the flight time is optimized in the different studied cases through the genetic algorithm.

## 5.1 Optimal transfer orbits between two planets

All the orbits that are represented in this section have been obtained computing the time-optimal solution without the final velocity constraints. That is, we only care about reaching the final planet as fast as possible, ignoring the arrival velocity.

The studied cases are the optimal transfer orbits between Earth and Mars, Earth and Jupiter, Earth and Venus, Mars and Jupiter, Mars and Saturn, Jupiter and Saturn, and Venus and Saturn.

The code that has been employed in this project is based on a developed initial version by Fco. Javier Urrios Gómez [36]

### 5.1.1 From Earth to Mars

In Figure 5.1, the solution to the fastest orbit from Earth to Mars on 01/01/2024, with no arrival velocity constraints, is presented. Moreover, the evolution with time of state variables and control parameters is represented in Figure 5.2.

As we can see, a bang-bang structure is found for $\kappa$ ($= \tau a_c$), that is, it switches abruptly between two states. It is visible in the time evolution of the variables that the best strategy to reach Mars as fast as possible is to start with full throttle, coast when we are far from the Sun, so we can come again closer to it, and then go full throttle again.

An interesting remark is the evolution of the sail pitch angle $\alpha_n$ when we are in a coasting arc ($\kappa = 0$). This distribution does not really make a difference, since sines and cosines are then multiplied by 0 (thrust is off). The evolution that the algorithm calculates is then relatively arbitrary, and therefore it can be omitted and erased in Figure 5.2, not showing $\alpha_n$ when we are in a coasting arc. During those periods, it may be beneficial to position the E-sail perpendicular to the Sun.

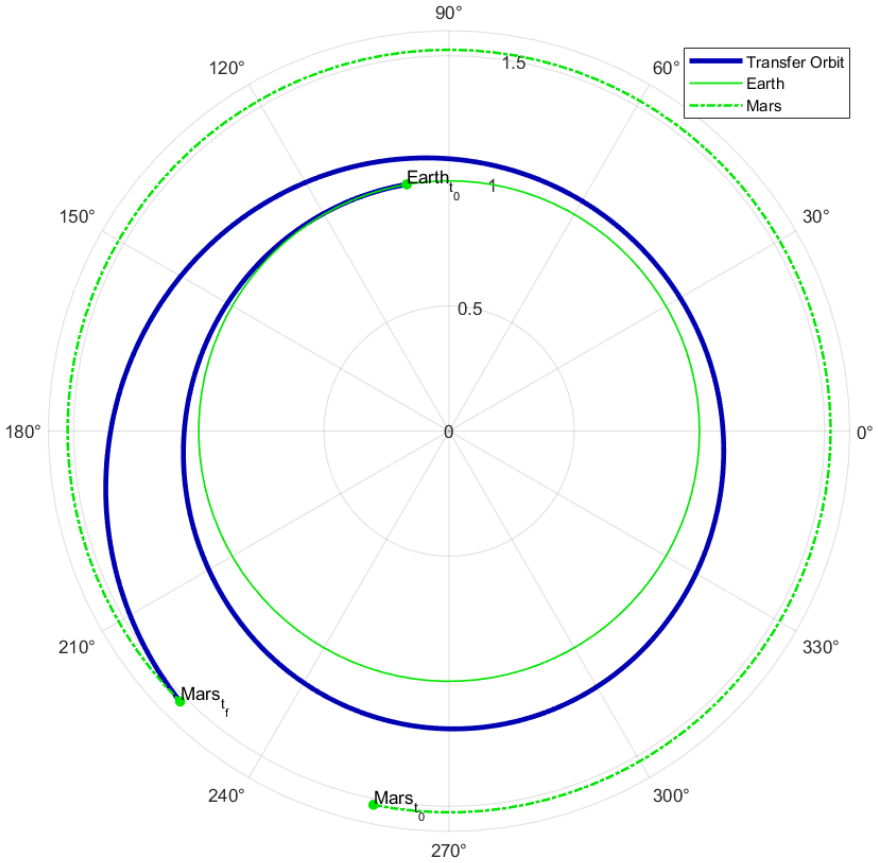


**Figure 5.1** Trajectory in a transfer orbit from Earth to Mars ignoring arrival velocity constraints.

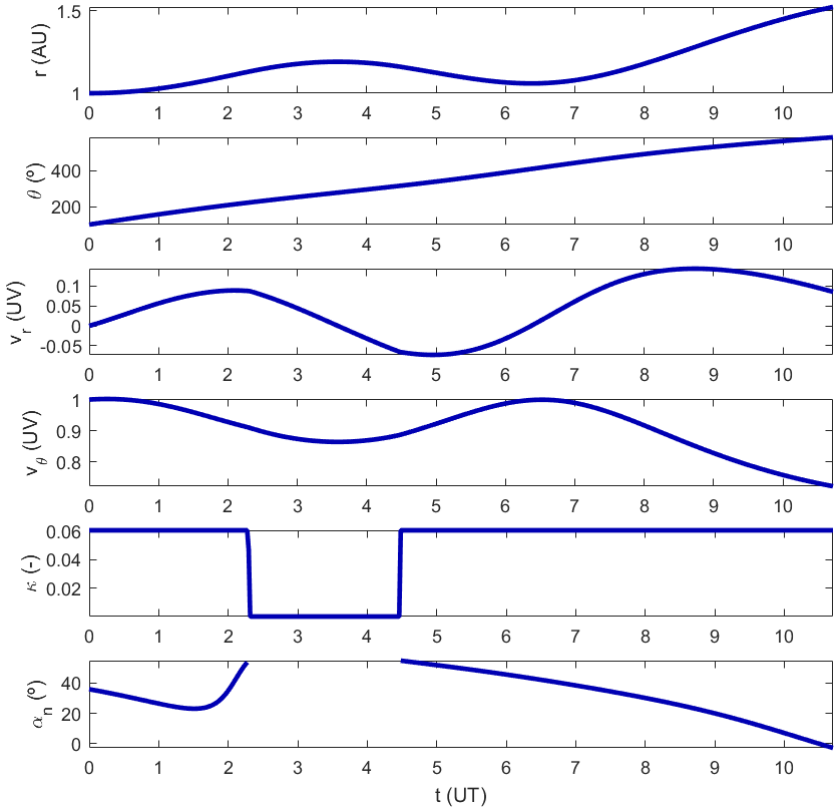


**Figure 5.2** Evolution of variables in a transfer orbit from Earth to Mars.

In this case, the initial conditions of the velocity are $v_{\theta_0} = v_{\oplus} = 1$ UV, $v_{r_0} = 0$ UV. The most significant values at the arrival, that are useful in next sections, are:

$$\begin{aligned} t_N &= 10.7210 \text{ UT} = 1.706 \text{ years} \\ v_{r_f} &= 0.0854 \text{ UV} \\ v_{\theta_f} &= 0.7225 \text{ UV} \end{aligned} \tag{5.1}$$

Once an example of a trajectory in a specific launch date has been represented, we proceed to calculate the flight time in an interval of dates, as is shown in Figure 5.3.

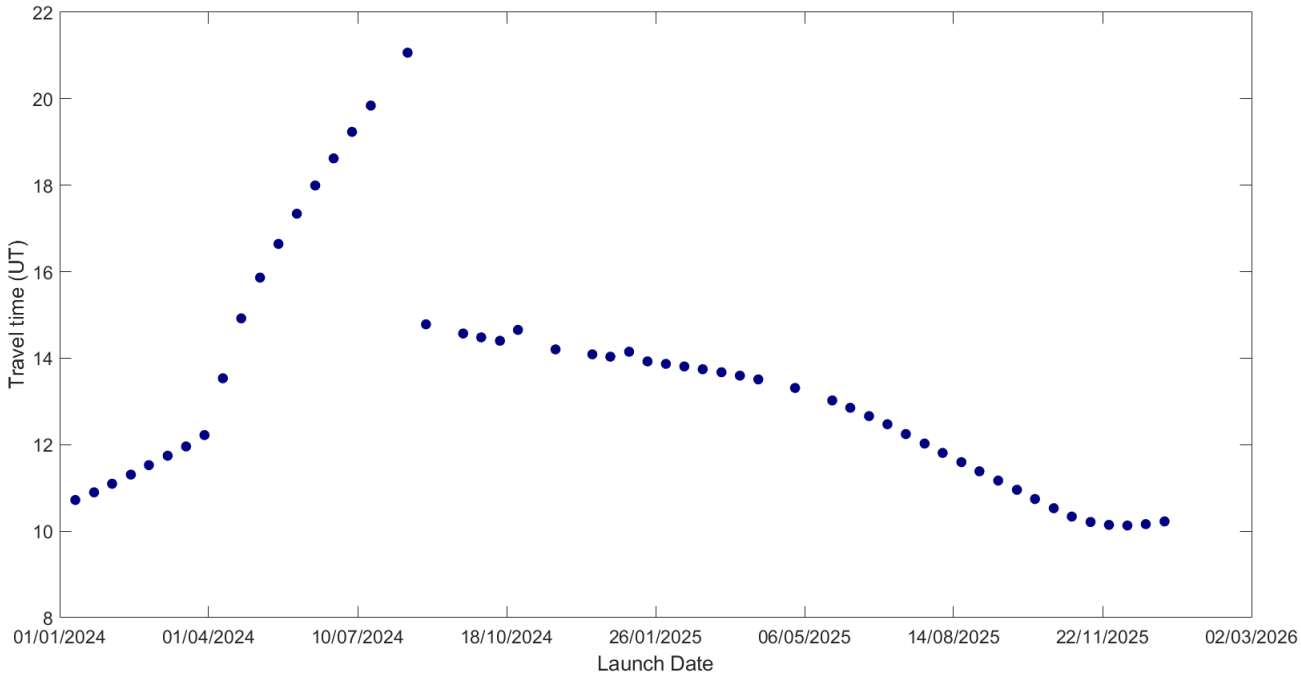


**Figure 5.3** Evolution of flight time in transfer orbits from Earth to Mars.

According to the results that have been obtained of the next two years, the synodic period between Earth and Mars can be verified. That is, the flight time repeats each 1.88 years since each phase configurations between Earth and Mars repeats each 1.88 years.

Furthermore, there is a discontinuity in the variation of the flight time. This discontinuity is associated with the way that *CasADi* sets the frame of reference and the origin of the angles. In Figure 5.4, the differences in the trajectory before and after the discontinuity are presented.

We can see in 5.4a that the final angle is close to $360^o$, but still lower. One day later, in 5.4b, the final angle should be close to $360^o$ too, but higher in this case, so it becomes to $0^o$ completing a revolution. Due to this passage through the origin of coordinates, the optimizer provides us another solution, in this case, that is better.

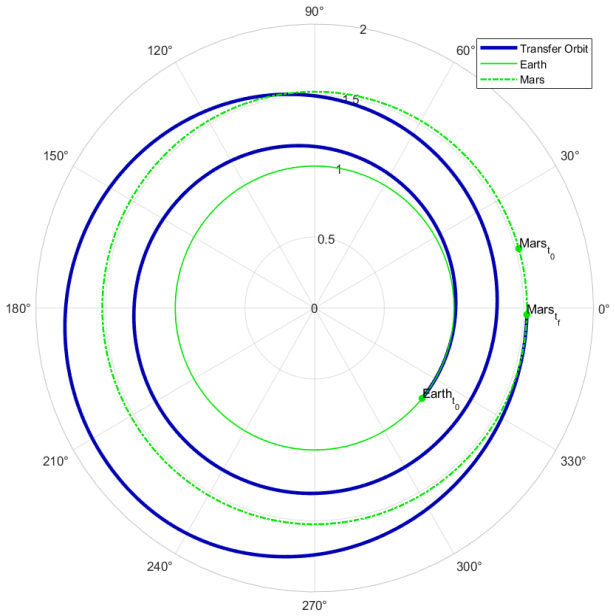


**(a)** Transfer orbit on 12/08/2024, with a flight time of 23.05 UT.

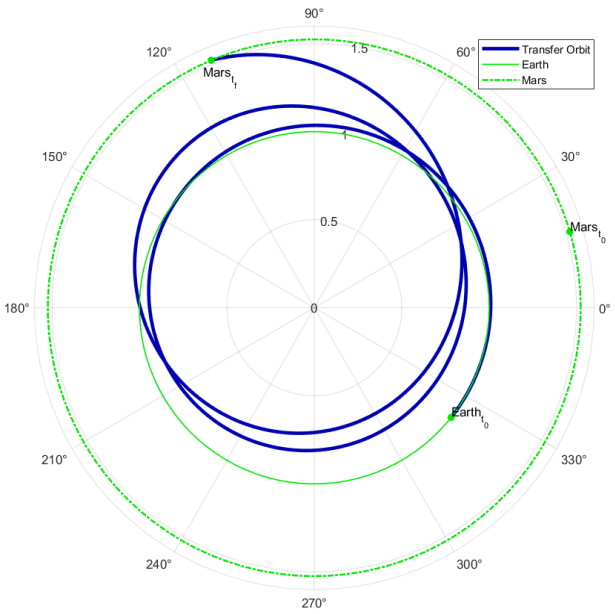


**(b)** Transfer orbit on 13/08/2024, with a flight time of 14.98 UT.

**Figure 5.4** Trajectories from Earth to Mars before and after the discontinuity.

### 5.1.2 From Earth to Jupiter

In Figure 5.5, the solution to the fastest orbit from Earth to Jupiter on 01/01/2024, with no arrival velocity constraints, is presented. Moreover, the evolution with time of state variables and control parameters is represented in Figure 5.6.

The bang-bang structure for $\kappa$ continues. In this case, the best strategy to reach Jupiter as fast as possible is to coast when we are far from the Sun, so we can come again closer to it, and then go full throttle, something very similar to the case of Mars.

Again, and for all other cases, the sail pitch angle $\alpha_n$ is erased in Figure 5.6 during the coasting arcs.

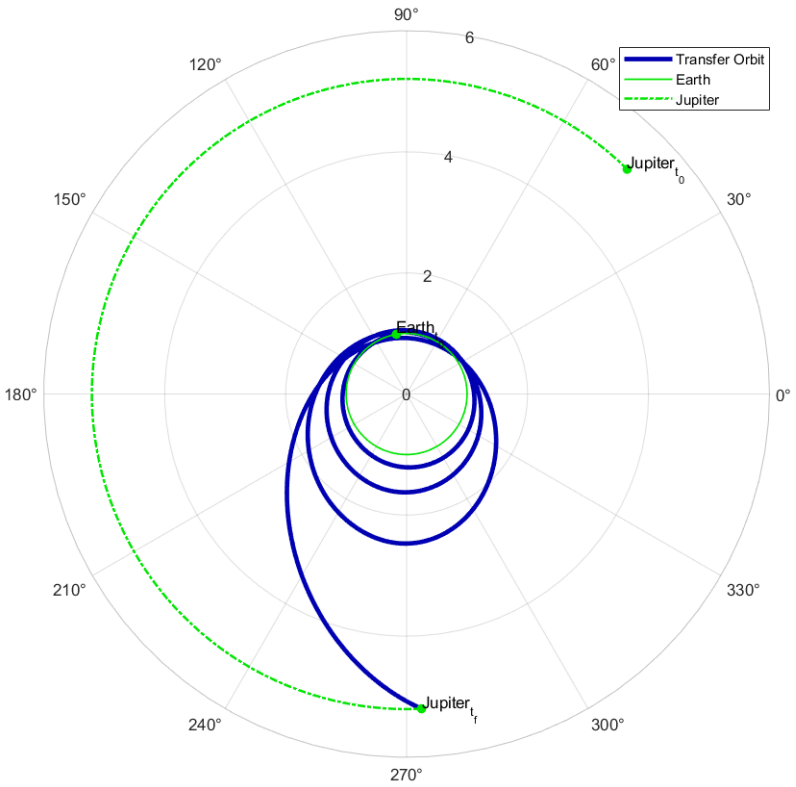


**Figure 5.5** Trajectory in a transfer orbit from Earth to Jupiter ignoring arrival velocity constraints.

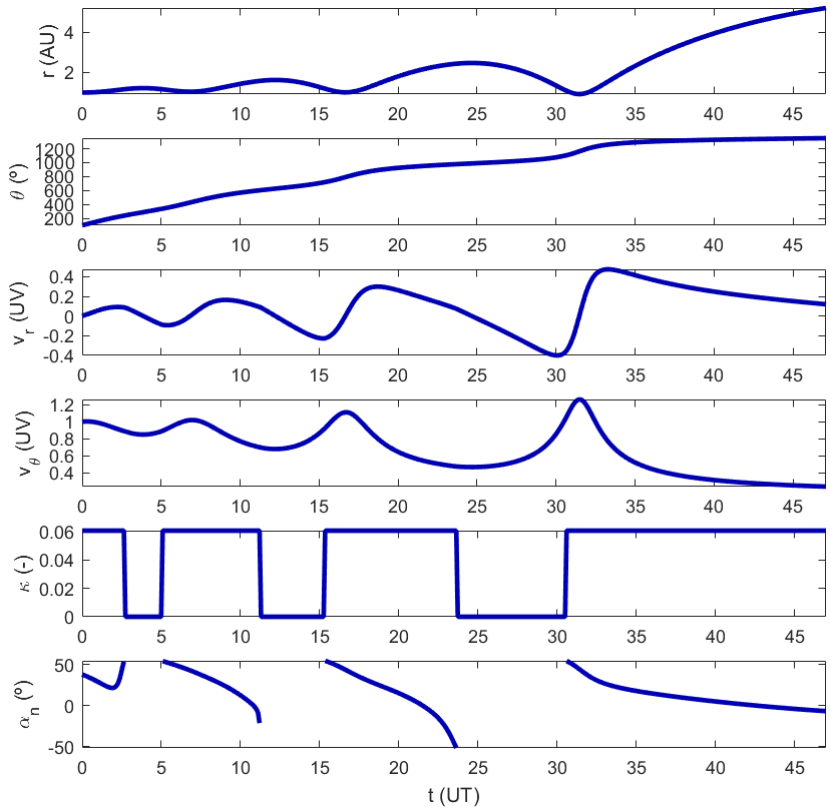


**Figure 5.6** Evolution of variables in a transfer orbit from Earth to Jupiter.

The initial conditions of the velocity are $v_{\theta_0} = v_{\oplus} = 1$ UV, $v_{r_0} = 0$ UV, and the most significant values at the arrival are:

$$\begin{aligned} t_N &= 47.0833 \text{ UT} = 7.49 \text{ years} \\ v_{r_f} &= 0.1193 \text{ UV} \\ v_{\theta_f} &= 0.2362 \text{ UV} \end{aligned} \tag{5.2}$$

Following the procedure that has been performed in Section 5.1.1, once an example of a trajectory in a specific launch date has been represented we calculate the flight time in an interval of dates, as is shown in Figure 5.7.

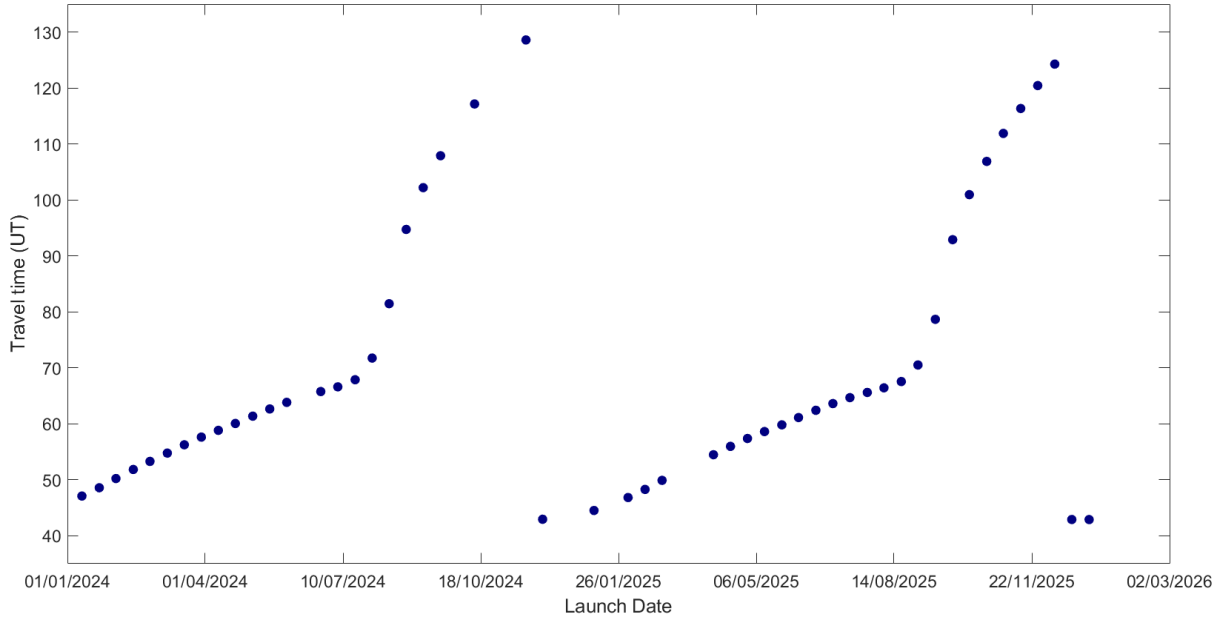


**Figure 5.7** Evolution of flight time in transfer orbits from Earth to Jupiter.

According to the results that have been obtained of the next two years, the synodic period between Earth and Jupiter can be verified. In this case, the flight time repeats each 400 days.

Furthermore, there is a discontinuity in the variation of the flight time again. In Figure 5.8, the differences in the trajectory before and after the discontinuity can be seen.

In this case, the discontinuity is not due to the final angle. We can see how, in 5.8a, the radial velocity is positive in the most of the trajectory, while in 5.8b, the solution follows the common structure that is found in most of the cases. This discontinuity could be reduced modifying the initial guess of the velocity, but we decide to keep the used one due to the optimizer finds a solution in most of the launch dates.

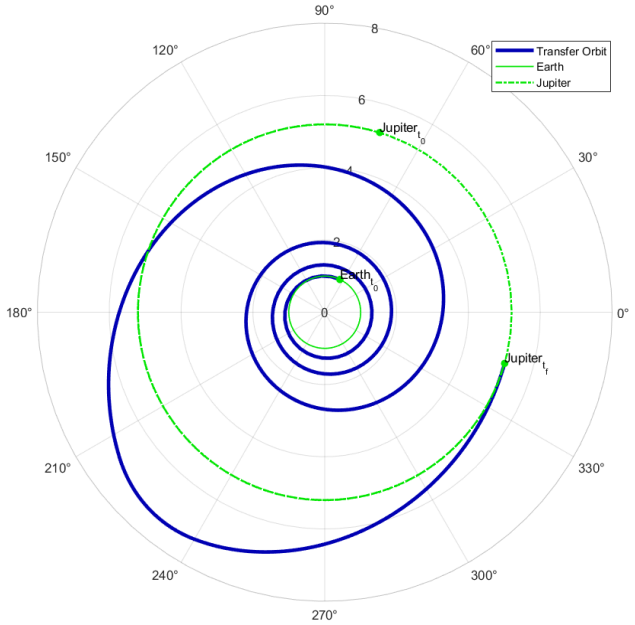


**(a)** Transfer orbit on 26/11/2024, with a flight time of 130.82 UT.

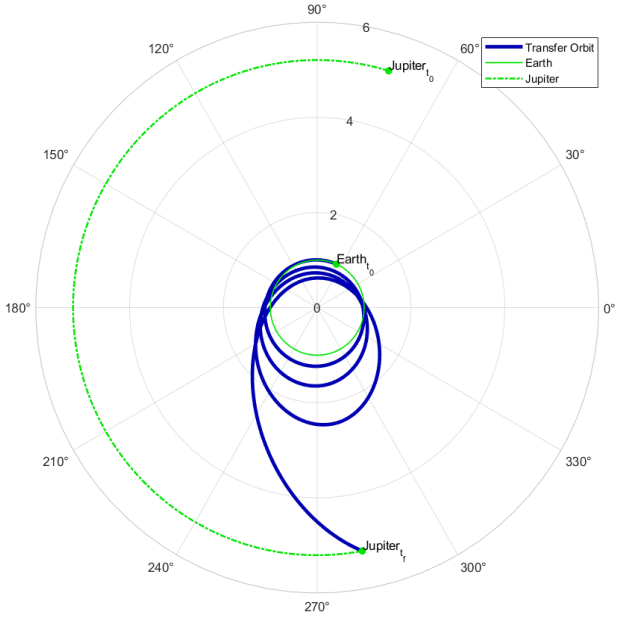


**(b)** Transfer orbit on 27/11/2024, with a flight time of 40.03 UT.

**Figure 5.8** Trajectories from Earth to Jupiter before and after the discontinuity.

### 5.1.3 From Earth to Venus

In Figure 5.9, the solution to the fastest orbit from Earth to Venus on 01/01/2024, with no arrival velocity constraints, is presented. Moreover, the evolution with time of state variables and control parameters is represented in Figure 5.10.

The initial conditions of the velocity are $v_{\theta_0} = v_{\oplus} = 1$ UV, $v_{r_0} = 0$ UV and the most significant values at the arrival are:

$$\begin{aligned} t_N &= 13.7891 \text{ UT} = 2.19 \text{ years} \\ v_{r_f} &= -0.2481 \text{ UV} \\ v_{\theta_f} &= 1.3191 \text{ UV} \end{aligned} \tag{5.3}$$

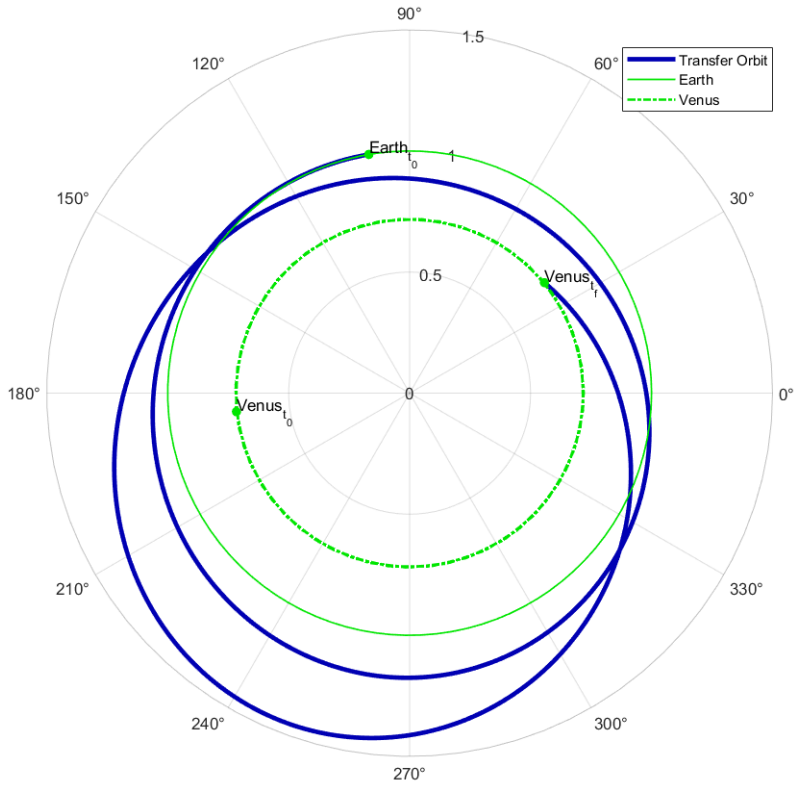


**Figure 5.9** Trajectory in a transfer orbit from Earth to Venus ignoring arrival velocity constraints.

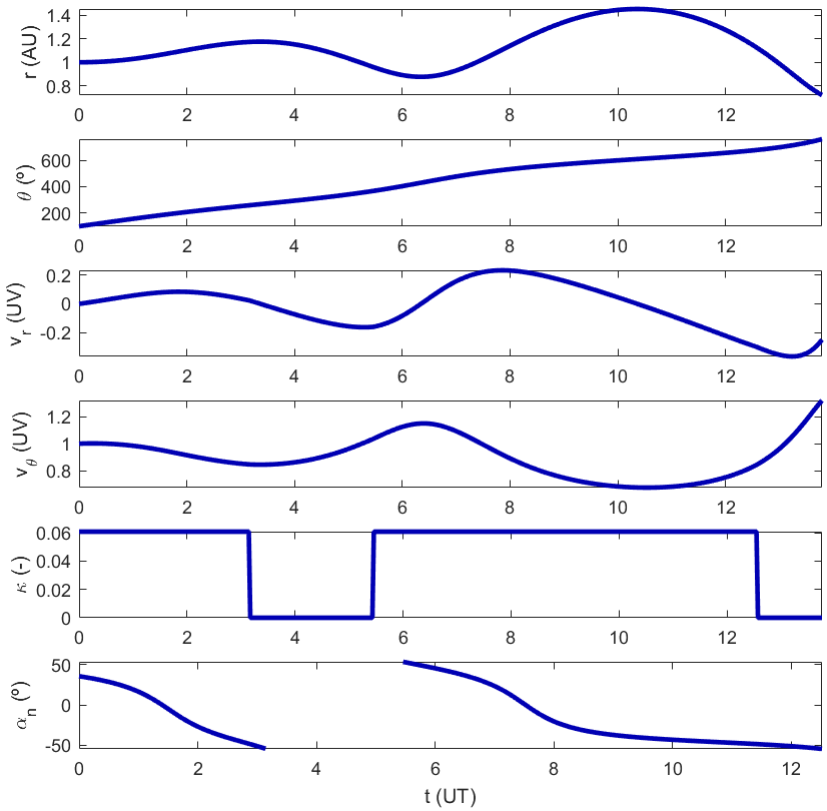


**Figure 5.10** Evolution of variables in a transfer orbit from Earth to Venus.

Even though Venus is closer to Earth than Mars, the E-sail covers a greater distance until reaching the destination due to the phase configuration of the planets. This means that the flight time is higher in this launch date, but not in all. A comparison of the flight times for a launch date in the first six months of 2024 can be seen in Figure 5.11.

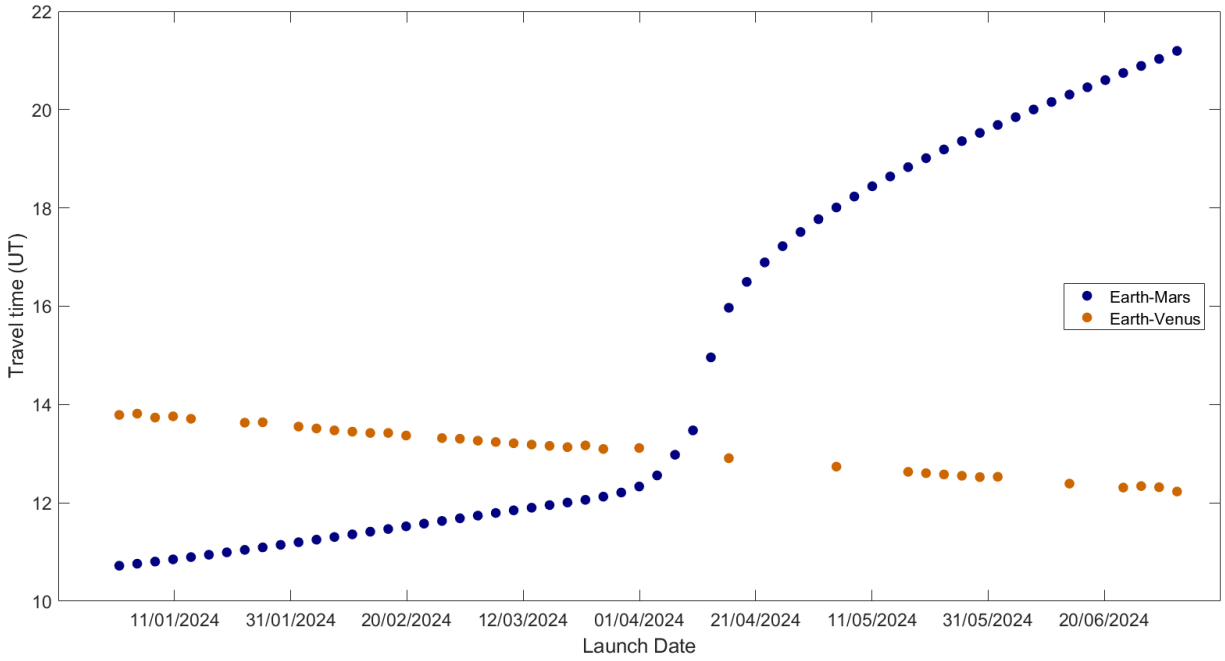


**Figure 5.11** Comparison of flight times in transfer orbits to Mars and Venus.

### 5.1.4 From Mars to Jupiter

In Figure 5.12, the solution to the fastest orbit from Mars to Jupiter on 01/09/2025, with no arrival velocity constraints, is presented. This launch date has been chosen based on the flight time that we get in the analysis of the trajectory from Earth to Mars. Moreover, the evolution with time of state variables and control parameters is represented in Figure 5.13.

A certain similarity can be verified with the case of the trajectory from Earth to Jupiter.

In this case, the initial conditions of the velocity are $v_{\theta_0} = v_{\male} = 0.81$ UV, $v_{r_0} = 0$ UV and the most significant values at the arrival are:

$$\begin{aligned} t_N &= 40.8586 \text{ UT} = 6.5 \text{ years} \\ v_{r_f} &= 0.1456 \text{ UV} \\ v_{\theta_f} &= 0.2632 \text{ UV} \end{aligned} \tag{5.4}$$

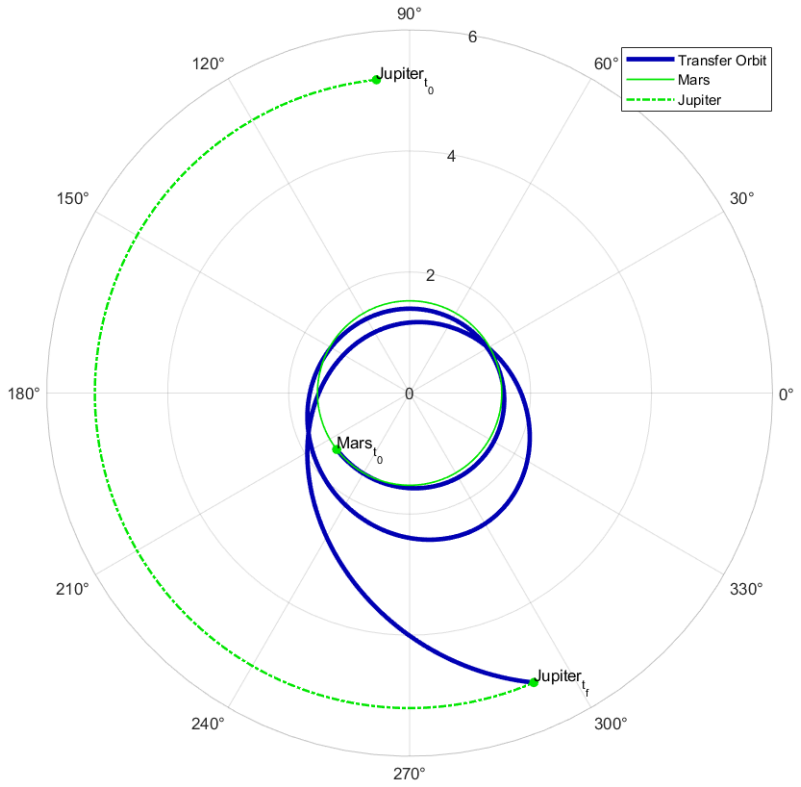


**Figure 5.12** Trajectory in a transfer orbit from Mars to Jupiter ignoring arrival velocity constraints.

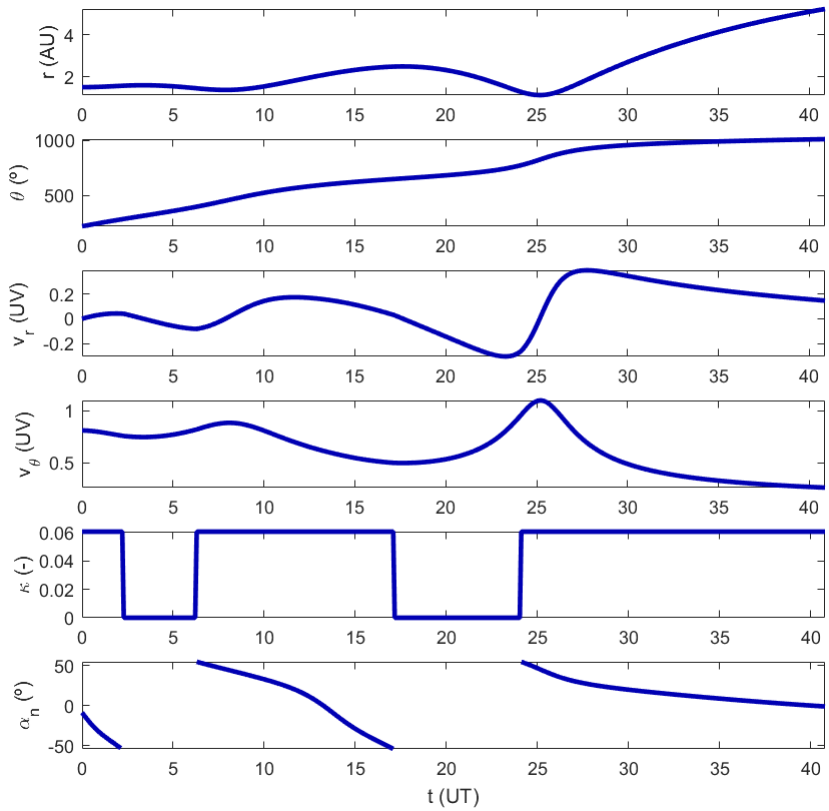


**Figure 5.13** Evolution of variables in a transfer orbit from Mars to Jupiter.

### 5.1.5 From Mars to Saturn

In Figure 5.14, the solution to the fastest orbit from Mars to Saturn on 01/09/2025, with no arrival velocity constraints, is presented. Moreover, the evolution with time of state variables and control parameters is represented in Figure 5.15.

In the same way that it happens in the trajectory from Earth to Jupiter, the best strategy is to coast when we are far from the Sun, coming again closer to it, and then go full throttle.

The initial conditions of the velocity are $v_{\theta_0} = v_{\male} = 0.81$ UV, $v_{r_0} = 0$ UV and the most significant values at the arrival are:

$$\begin{aligned} t_N &= 61.3813 \text{ UT} = 9.769 \text{ years} \\ v_{r_f} &= 0.3266 \text{ UV} \\ v_{\theta_f} &= 0.1233 \text{ UV} \end{aligned} \tag{5.5}$$

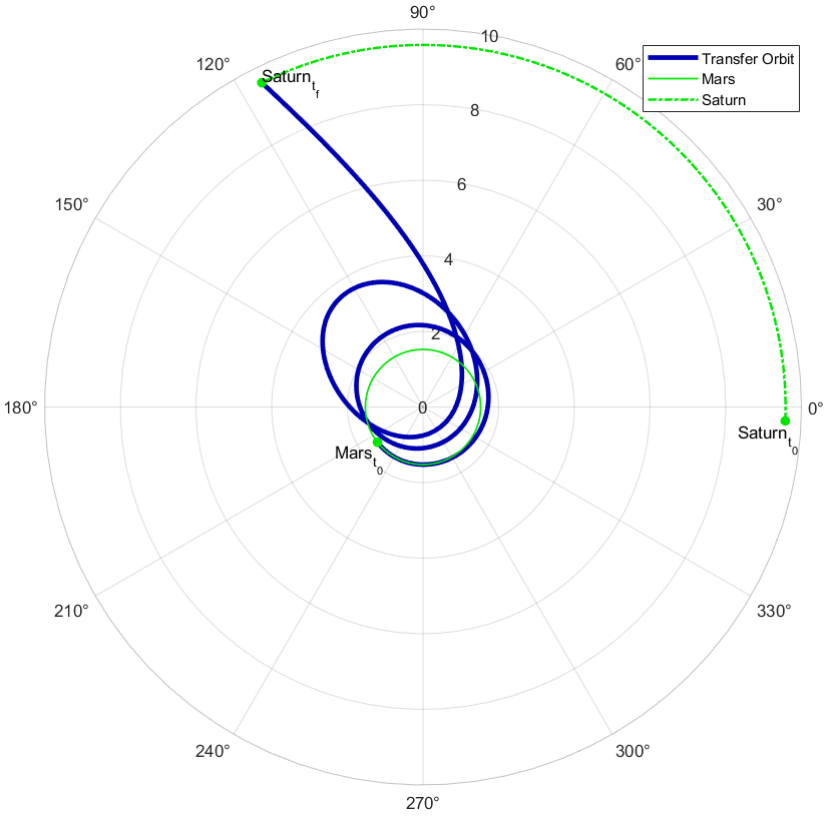


**Figure 5.14** Trajectory in a transfer orbit from Mars to Saturn ignoring arrival velocity constraints.

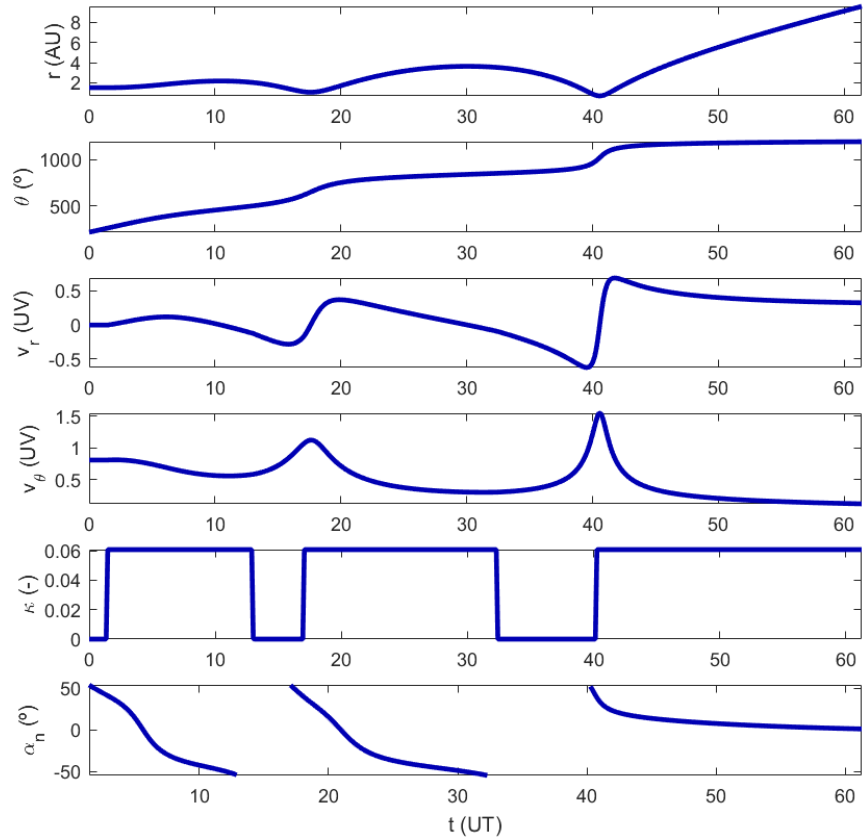


**Figure 5.15** Evolution of variables in a transfer orbit from Mars to Saturn.

### 5.1.6 From Jupiter to Saturn

In Figure 5.16, the solution to the fastest orbit from Jupiter to Saturn on 01/06/2031, with no arrival velocity constraints, is presented. Similarly, this launch date has been chosen based on the flight time that we get in the analysis of the trajectory from Earth to Jupiter. Moreover, the evolution with time of state variables and control parameters is represented in Figure 5.17.

In this case, the initial conditions of the velocity are $v_{\theta_0} = v_{\oplus} = 0.439$ UV, $v_{r_0} = 0$ UV and the most significant values at the arrival are:

$$\begin{aligned} t_N &= 67.5269 \text{ UT} = 10.75 \text{ years} \\ v_{r_f} &= 0.2565 \text{ UV} \\ v_{\theta_f} &= 0.2712 \text{ UV} \end{aligned} \tag{5.6}$$

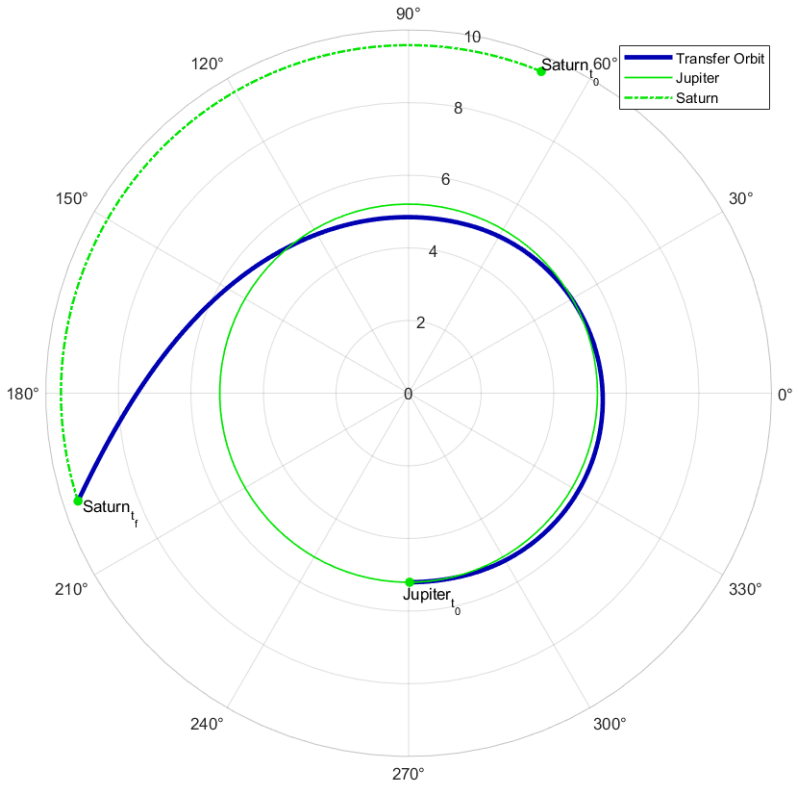


**Figure 5.16** Trajectory in a transfer orbit from Jupiter to Saturn ignoring arrival velocity constraints.

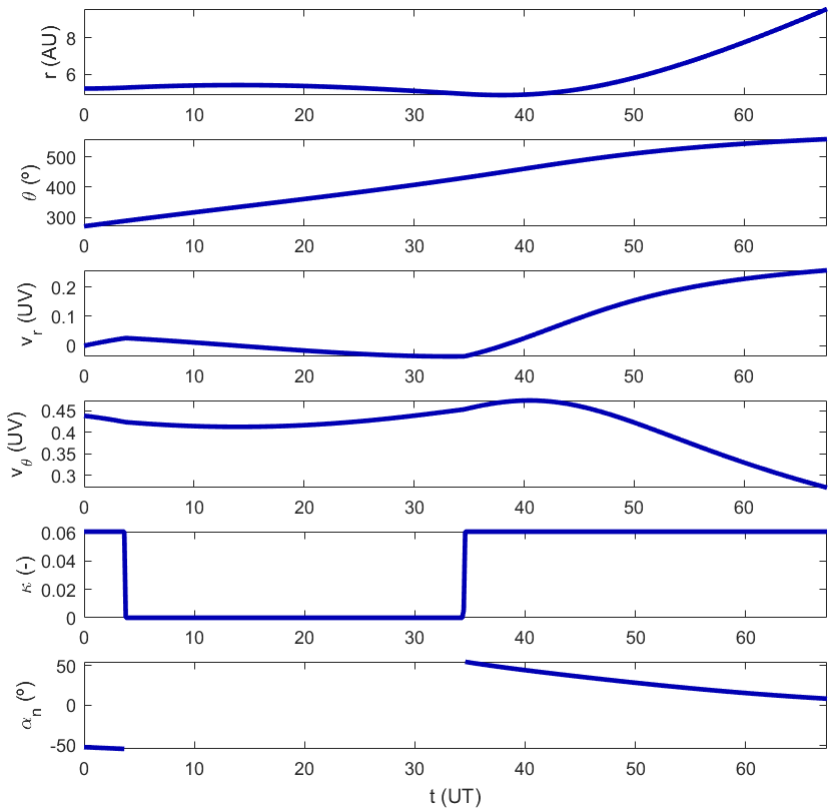


**Figure 5.17** Evolution of variables in a transfer orbit from Jupiter to Saturn.

### 5.1.7 From Venus to Saturn

In Figure 5.18, the solution to the fastest orbit from Venus to Saturn on 01/03/2026, with no arrival velocity constraints, is presented. Again, the launch date has been chosen based on the flight time that we get in the analysis of the trajectory from Earth to Venus. Moreover, the evolution with time of state variables and control parameters is represented in Figure 5.19.

In this case, the initial conditions of the velocity are $v_{\theta_0} = v_{\varphi} = 1.18$ UV, $v_{r_0} = 0$ UV and the most significant values at the arrival are:

$$\begin{aligned} t_N &= 77.2839 \text{ UT} = 12.3 \text{ years} \\ v_{r_f} &= 0.2603 \text{ UV} \\ v_{\theta_f} &= 0.1128 \text{ UV} \end{aligned} \tag{5.7}$$

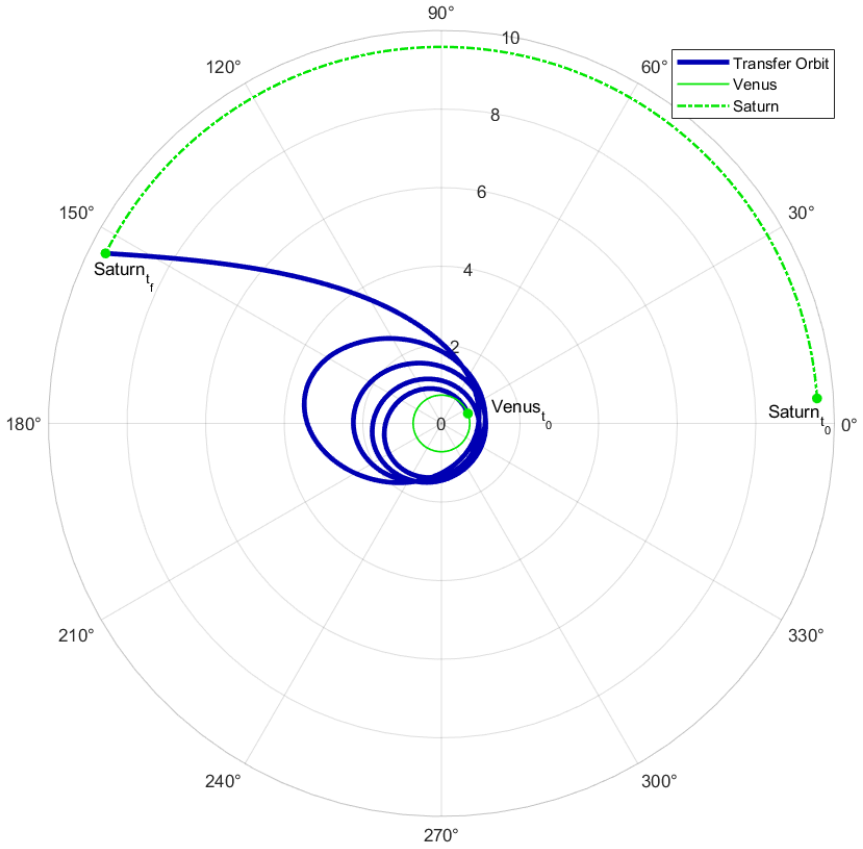


**Figure 5.18** Trajectory in a transfer orbit from Venus to Saturn ignoring arrival velocity constraints.

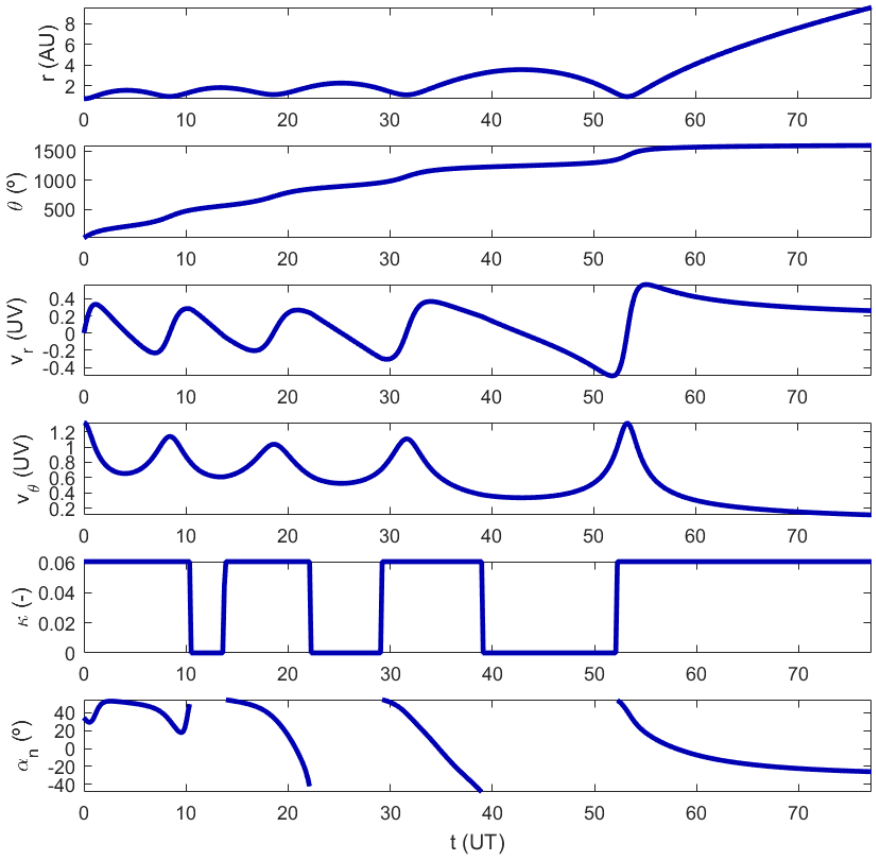


**Figure 5.19** Evolution of variables in a transfer orbit from Venus to Saturn.

## 5.2 Optimal gravity-assist trajectories

In this section, all the presented results have been obtained for missions with a launch date in the first six months of 2024. The studied missions are Earth-Mars-Jupiter, Earth-Mars-Saturn, Earth-Jupiter-Saturn and Earth-Venus-Saturn.

First, we join the different optimal transfer orbits analyzed in Section 5.1 through a gravity-assist maneuver, that is, with no arrival velocity constraints in any stretch. This is a procedure such that the first stretch does not depend on the second one. A flowchart of the procedure is identical to which is represented in Figure 4.8, being both non linear optimizations free of final velocity constraints.

With this, we obtain a possible optimal launch date. Next, the genetic algorithm is applied in different dates in order to check that possible optimal launch date that has been found in the independent optimization.

The code of the genetic algorithm that has been employed in this project is based on a developed version by Jesús F. Ramírez Sánchez, and the value of the control parameters has been selected attending to several analysis of sensitivity made in [37].

### 5.2.1 Earth-Mars-Jupiter mission

As a starting point, a mission with Mars as intermediate planet and Jupiter as final planet is analyzed. An example of trajectory of this mission is represented in Figure 5.20.

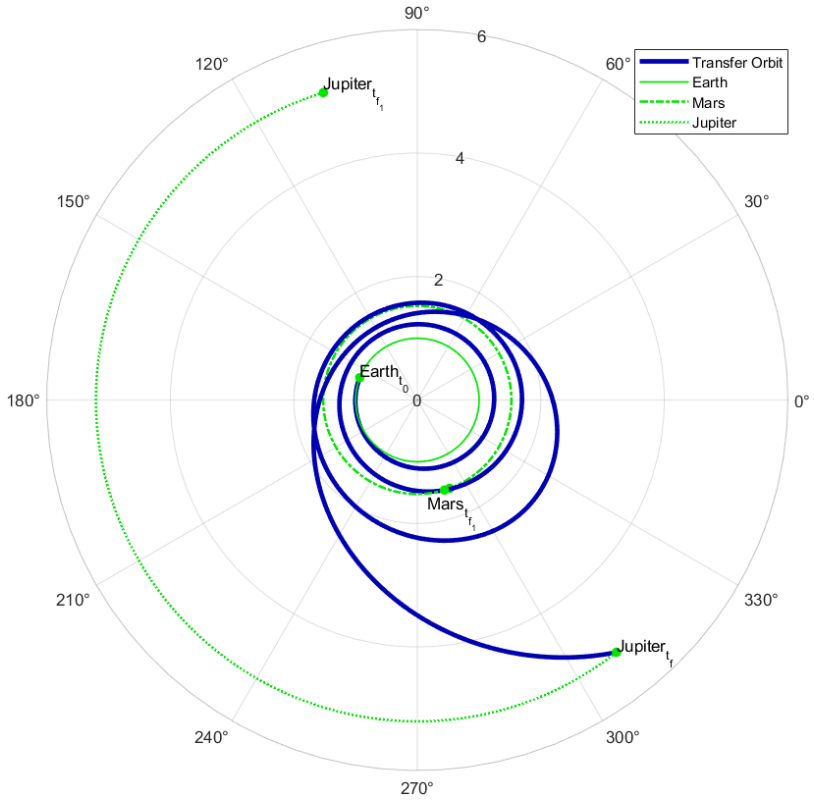


**Figure 5.20** Example of trajectory of the Earth-Mars-Jupiter mission.

This trajectory has been calculated for a launch on 01/03/2024, with an approach radius in the gravity assist maneuver of $r_P = 4R_{♂}$.

Next, in Figure 5.21, the results for the first six months of 2024 of the independent optimization, with $r_P = 4R_{♂}$ in the gravity assist maneuver, are presented.

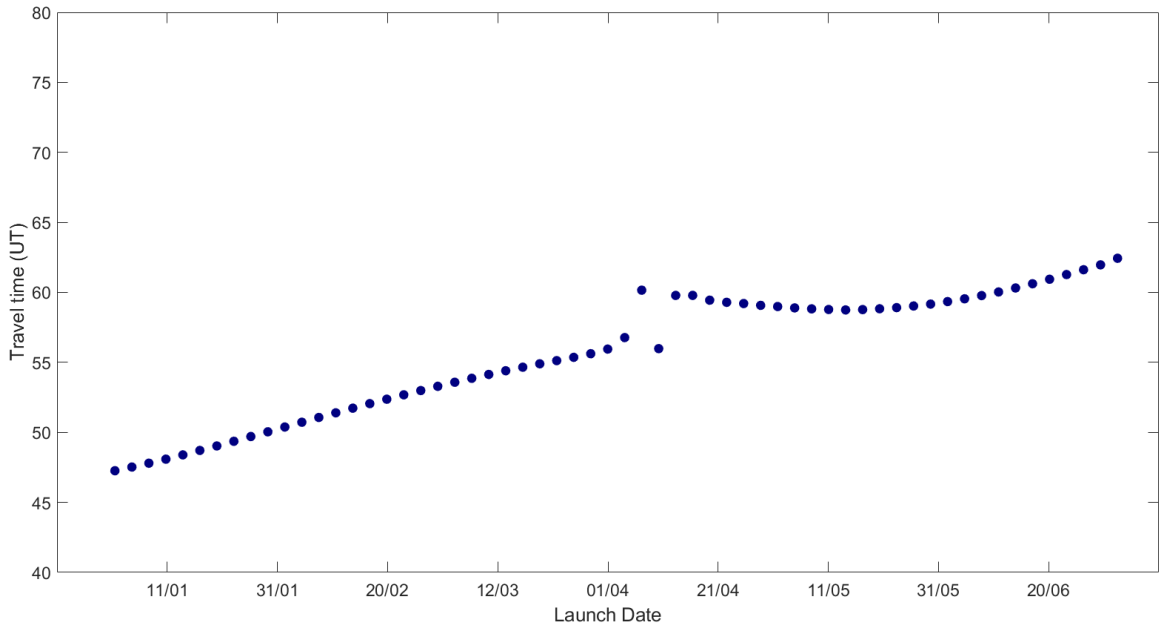


**Figure 5.21** Evolution of flight time in the independent optimization of Earth-Mars-Jupiter.

The flight time increases as the launch is delayed, so the best option should be a launch on 01/01/2024.

#### Genetic algorithm in Earth-Mars-Jupiter

Once we have analyzed the behaviour of the flight time according to the launch date, we discuss the appliance of the genetic algorithm in some points of the Figure 5.21. The value of the control parameters that we use in this section is:

$$[X,E,N,t,n_c,\eta_c,p_c,\sigma_c,p_{mut},p_m,TOL] = [15,6,50,6,2,3,0.4,30,0.15,0.3,0.1] \tag{5.8}$$

The number of individuals of the base population, $X$, and the maximum allowed number of generations, $N$, have been selected attending to the high computational time of the evaluation in the objective function. Given specific optimization variables, if the optimizer finds a solution, the computational time is about 100s. Otherwise, when the optimizer does not converge to a solution, the computational time can increase to 400s. On the other hand, the tolerance, $TOL$, has been selected attending to the obtained values in several tests.

Regarding the lower and upper limits of the value of the optimization variables, they have been selected based on the results at the arrival to Mars, that are presented in (5.1). Thus, the limits are included in Table 5.1.

**Table 5.1** Lower and upper limits of the value of optimization variables in Earth-Mars-Jupiter.

| | $v_{r_f}$ | $v_{\theta_f}$ | $r_P$ |
|---|---|---|---|
| LB | 0 | 0.7 | $3R_{♂}$ |
| UB | 0.15 | 0.9 | $7R_{♂}$ |

The first date on which we apply the genetic algorithm is when the flight time is minimum, that is, on 01/01/2024. In order to analyze the procedure of the genetic algorithm, it has been decided to create a typical representation consisting of representing for each generation the objective value of the best solution and the mean of the rest of the population. All the individuals that do not converge to a solution are excluded from this average. This evolution of generations is shown in Figure 5.22, where the red dots correspond to the best solution and the black dots correspond to the mean of the population.

The black curve must not be perfectly defined (in general), that is, it must present peaks, what indicates that the space of solutions is still being explored. The red curve must not be constant and as the algorithm progresses it must tend to a lower value than the initial one. We can see in Figure 5.22 that the curve represented by the mean tends to the curve represented by the best, therefore the method converges.

The algorithm stops when it reaches 27 generations because of the defined tolerance is reached. That is, the difference between the black dot and the red dot is lower than the tolerance that is defined in (5.8).

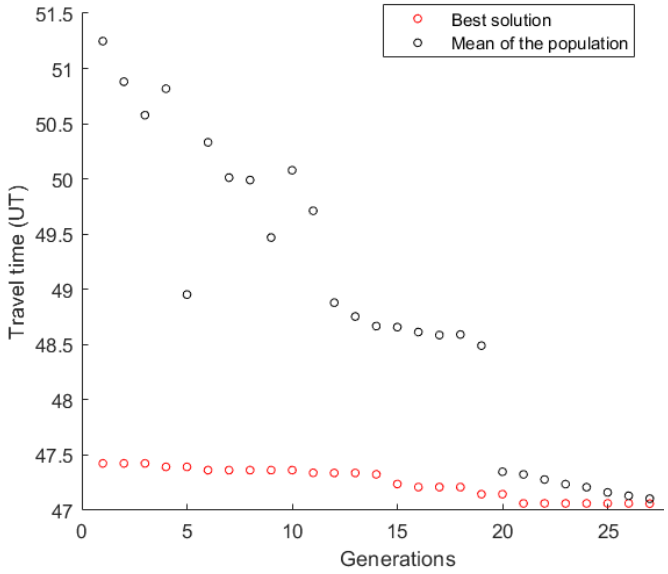


**Figure 5.22** Procedure of the genetic algorithm in Earth-Mars-Jupiter on 01/01/2024.

The solution that is obtained is:

$$v_{r_f} = 0.093 \text{ UV} \quad v_{\theta_f} = 0.7165 \text{ UV} \quad r_P = 3.8244 R_{\male} \tag{5.9}$$

We calculate the flight time for the first six months of 2024 with these arrival conditions to Mars, as shown in Figure 5.23 (green dots), where the date on which the genetic algorithm is applied is represented in red.

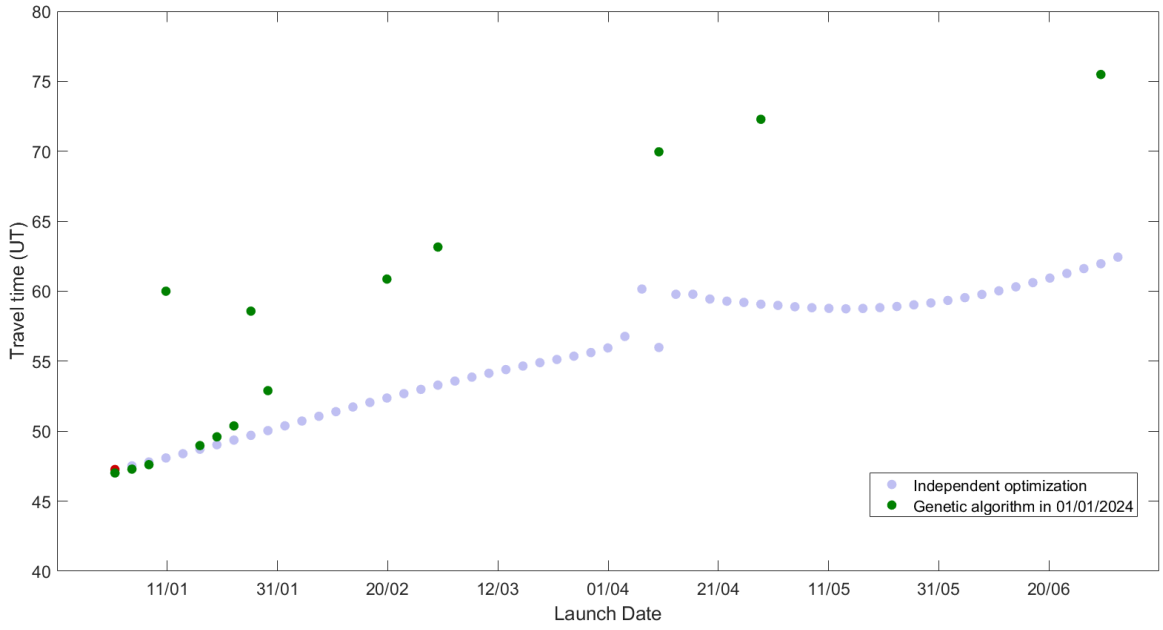


**Figure 5.23** Evolution of flight time of Earth-Mars-Jupiter after applying genetic algorithm on 01/01/2024.

The improvement on 01/01/2024 is not very high, from a flight time of 47.2615 UT to one of 47.0141 UT. The flight time has also improved in dates that are close to 01/01/2024. An interesting remark is that a solution with these arrival conditions is not found in all the dates, due to not all the phase configurations allow it.

The next date on which we apply the genetic algorithm is 01/02/2024. The evolution of generations is represented in Figure 5.24.

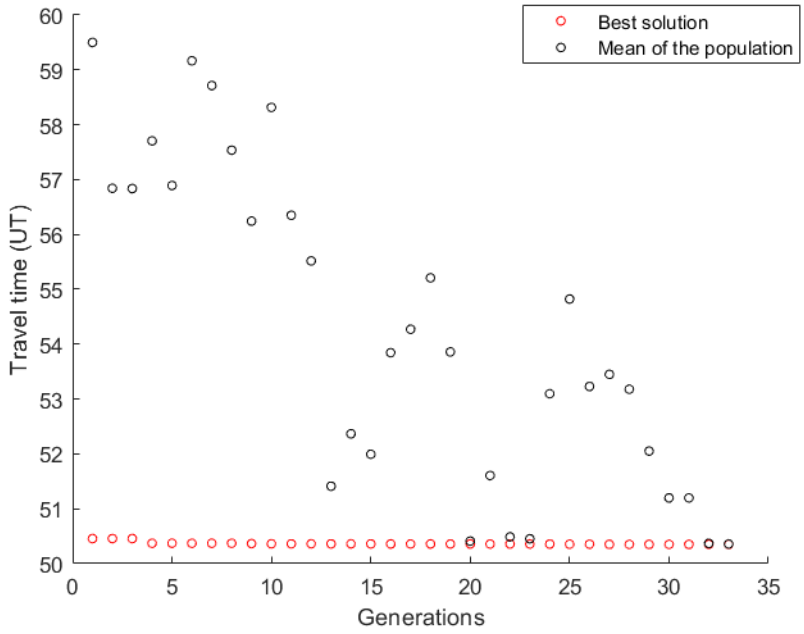


**Figure 5.24** Procedure of the genetic algorithm in Earth-Mars-Jupiter on 01/02/2024.

In this case, the tolerance has been modified to 0.01, in order to increase the exploitation, and the algorithm stops when it reaches 33 iterations. We can see that the best solution does not improve from the fourth iteration, so the algorithm could stop earlier.

The solution that is obtained is:

$$v_{r_f} = 0.0822 \text{ UV} \quad v_{\theta_f} = 0.7369 \text{ UV} \quad r_P = 5.1353 R_{\male} \tag{5.10}$$

Again, we calculate the flight time for the first six months of 2024 with these arrival conditions to Mars, as shown in Figure 5.25, where the date on which the genetic algorithm is applied is represented in red.

The improvement on 01/02/2024 is not evident, from a flight time of 50.384 UT to one of 50.3502 UT. The flight time has also improved in dates that are close to 01/02/2024. In this case, there are more found solutions with these arrival conditions, although the majority are worse than the solutions of the independent optimization.

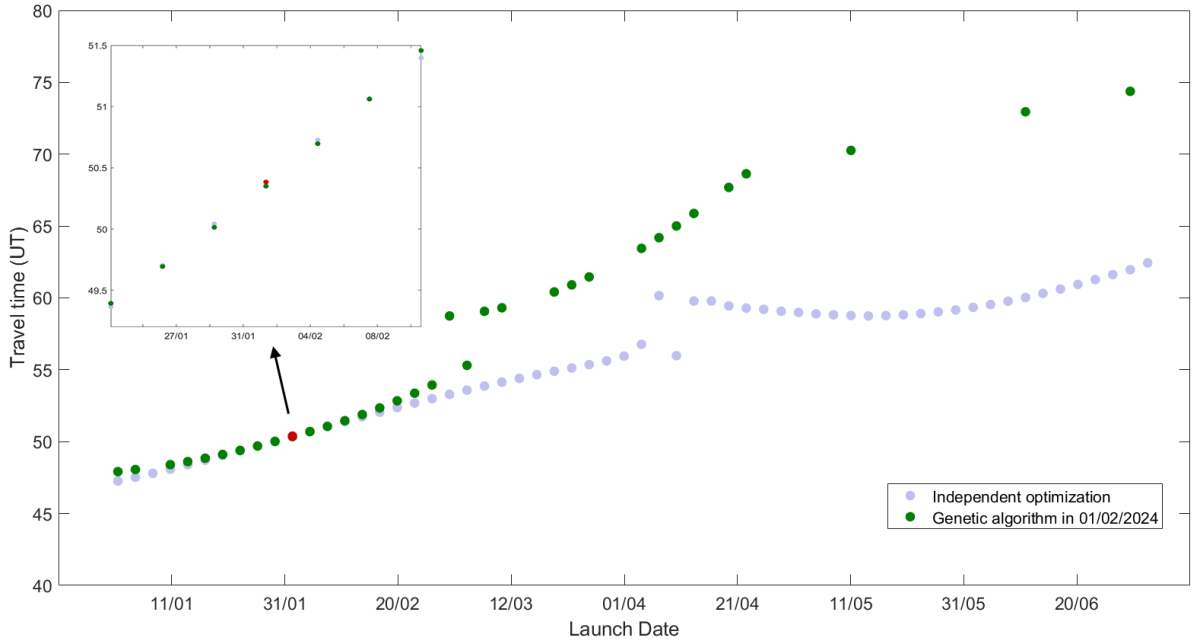


**Figure 5.25** Evolution of flight time of Earth-Mars-Jupiter after applying genetic algorithm on 01/02/2024.

Next, we apply the genetic algorithm on 07/04/2024. The evolution of generations is represented in Figure 5.26.

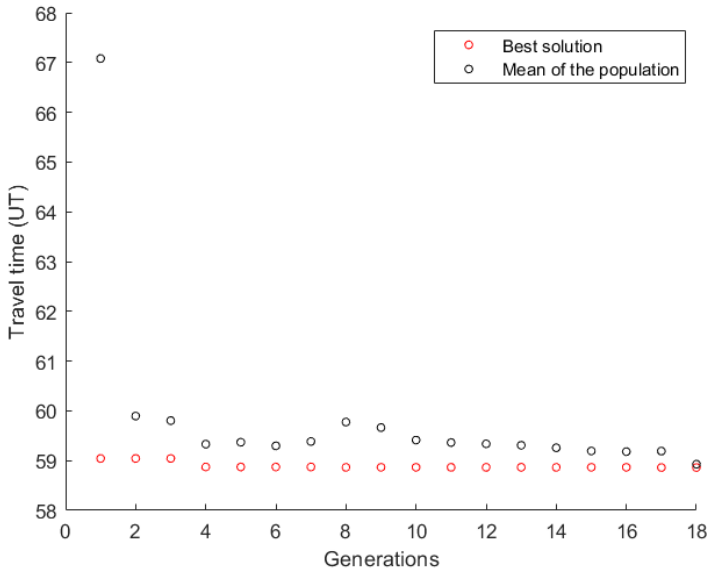


**Figure 5.26** Procedure of the genetic algorithm in Earth-Mars-Jupiter on 07/04/2024.

We can see that the best solution does not improve a lot from the initial population. The algorithm stops after 18 generations, when it reaches the defined tolerance.

The solution that is obtained is:

$$v_{r_f} = 0.0797 \text{ UV} \quad v_{\theta_f} = 0.7876 \text{ UV} \quad r_P = 6.1520 R_{\male} \tag{5.11}$$

Again, we calculate the flight time for the first six months of 2024 with these arrival conditions to Mars, as shown in Figure 5.27, where the date on which the genetic algorithm is applied is represented in red.

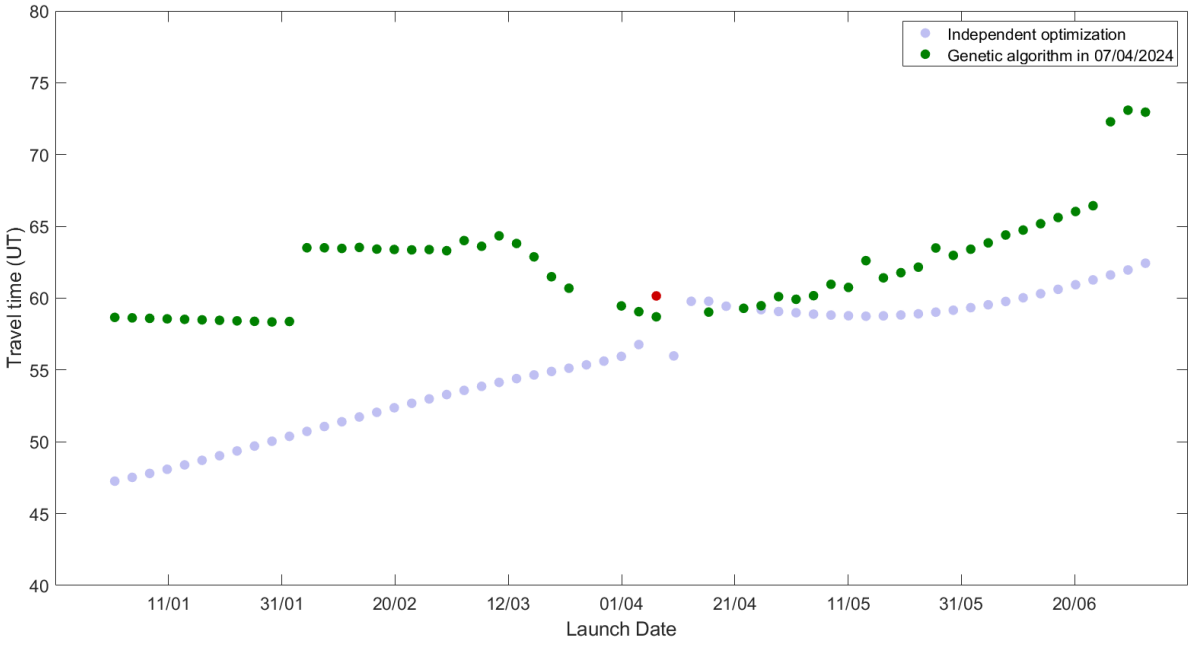


**Figure 5.27** Evolution of flight time of Earth-Mars-Jupiter after applying genetic algorithm on 07/04/2024.

The improvement on 07/04/2024 is from a flight time of 60.1572 UT to one of 58.7045 UT. In this case, the rest of the found solutions with these arrival conditions are worse than the solutions that are obtained in the independent optimization

The last date on which we apply the genetic algorithm is 02/07/2024. The evolution of generations is represented in Figure 5.28.

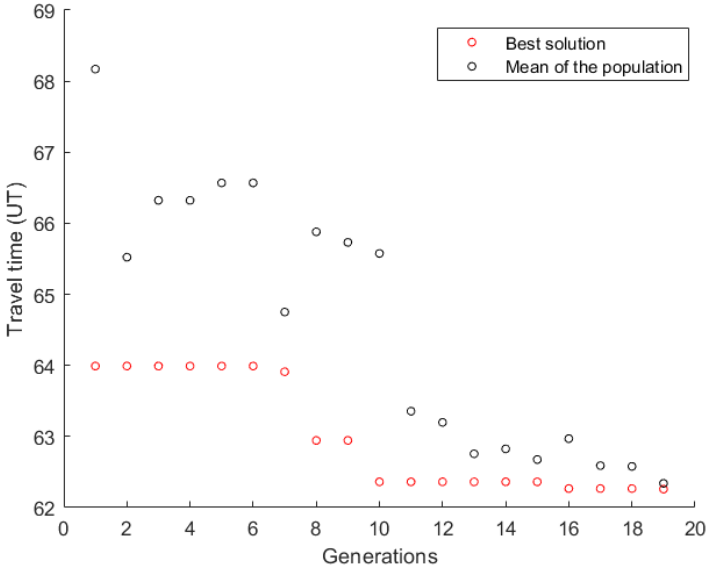


**Figure 5.28** Procedure of the genetic algorithm in Earth-Mars-Jupiter on 02/07/2024.

In this case, the algorithm stops when it reaches 19 generations because of the defined tolerance is reached.

The solution that is obtained is:

$$v_{r_f} = 0.0091 \text{ UV} \quad v_{\theta_f} = 0.7991 \text{ UV} \quad r_P = 6.8494 R_{\male} \tag{5.12}$$

We calculate the flight time for the first six months of 2024 with these arrival conditions to Mars, as shown in Figure 5.29.

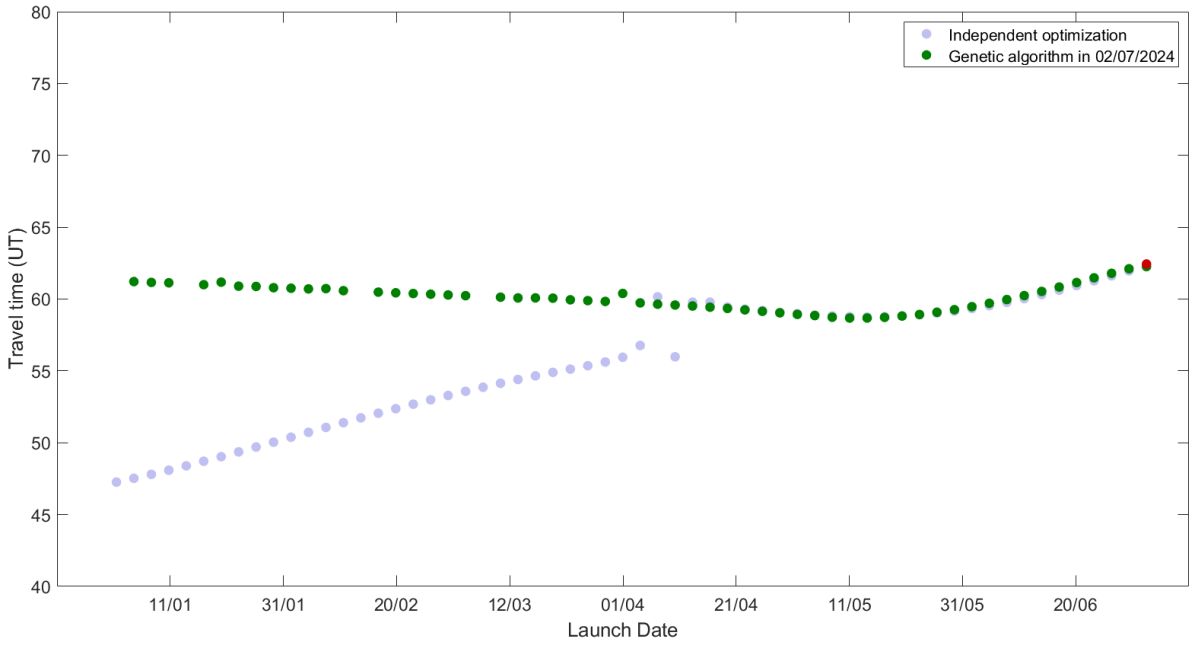


**Figure 5.29** Evolution of flight time of Earth-Mars-Jupiter after applying genetic algorithm on 02/07/2024.

Again, the improvement on 02/07/2024 is not evident, from a flight time of 62.4368 UT to one of 62.2595 UT. The solutions with these arrival conditions that are found are very similar to the solutions of the independent optimization around this date. The rest of found solutions are worse.

As a summary, the different flight times on the analyzed dates are presented in Table 5.2.

**Table 5.2** Improvement in flight times of Earth-Mars-Jupiter.

| Date | Independent optimization | Genetic algorithm |
|---|---|---|
| 01/01/2024 | 47.26 UT | 47.01 UT |
| 01/02/2024 | 50.38 UT | 50.35 UT |
| 07/04/2024 | 60.16 UT | 58.70 UT |
| 02/07/2024 | 62.44 UT | 62.26 UT |

Superimposing all the results, we can present the minimum flight time in each date, as is shown in Figure 5.30.

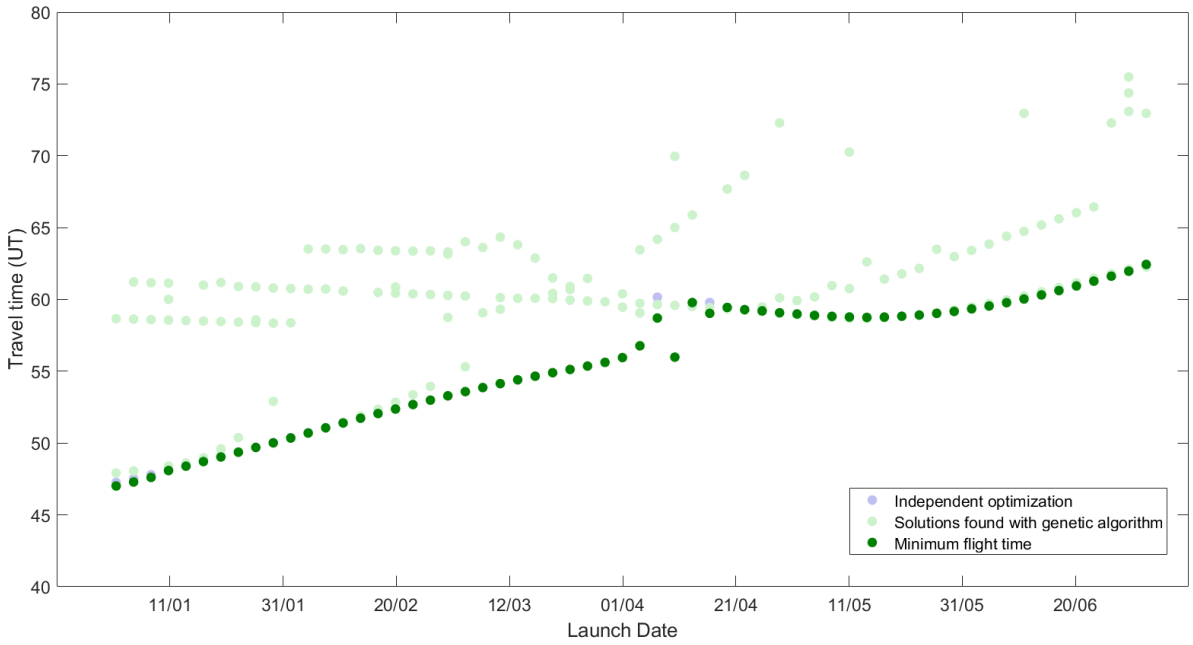


**Figure 5.30** Minimum flight time of Earth-Mars-Jupiter in each date.

In this case, the independent optimization presents very good results, that are close to the minimum flight times that we obtain after applying the genetic algorithm. An interesting remark is that the date with minimum flight time in the independent optimization coincides with the date with minimum flight time after applying the genetic algorithm.

Lastly, in order to improve the best solution and reduce the minimum flight time, we decide to apply a modification in the algorithm. We apply the genetic algorithm on 01/01/2024 again, but including the best found solution, (5.9), in the initial population. With this, we are forcing an exploitation around the found solution, without leaving the exploration. The evolution of generations is represented in Figure 5.31.

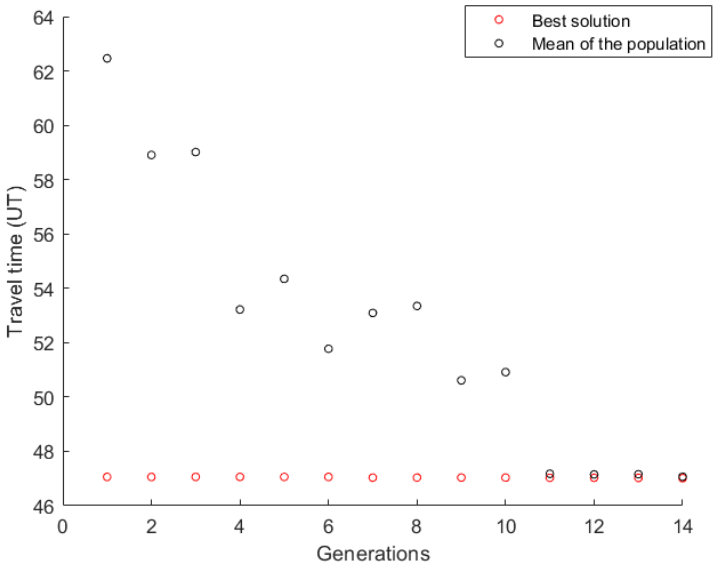


**Figure 5.31** Procedure of the genetic algorithm in Earth-Mars-Jupiter on 01/01/2024 including a known solution in the initial population.

We can see that the defined tolerance is reached and the best solution does not improve. Then, we are close to the global minimum.

### 5.2.2 Earth-Mars-Saturn mission

The next analyzed mission has also Mars as intermediate planet, but Saturn as final planet. An example of trajectory of this mission is represented in Figure 5.32.

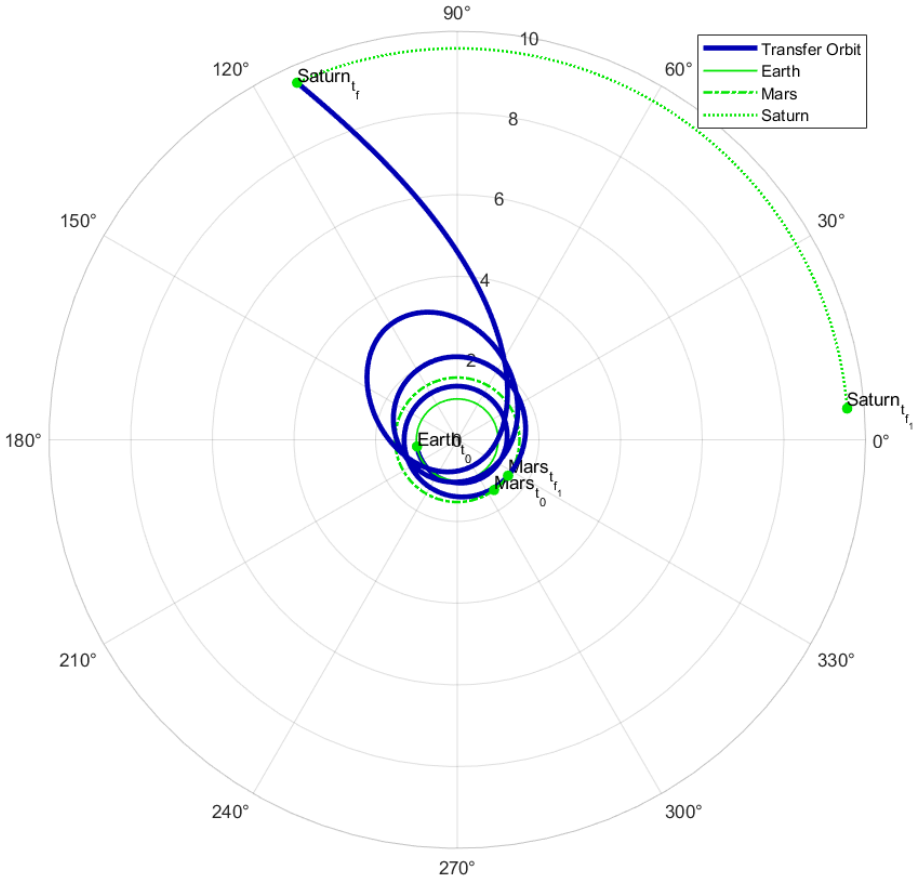


**Figure 5.32** Example of trajectory of the Earth-Mars-Saturn mission.

This trajectory has been calculated for a launch on 01/04/2024, with an approach radius in the gravity assist maneuver of $r_P = 4R_{\male}$.

Next, in Figure 5.33, the results for the first six months of 2024 of the independent optimization, with $r_P = 4R_{\male}$ in the gravity assist maneuver, are presented.

In this case, the flight time decreases as the launch is delayed until April, when we find the minimum. Then, it begins to increase until a discontinuity in May, when it becomes approximately constant.

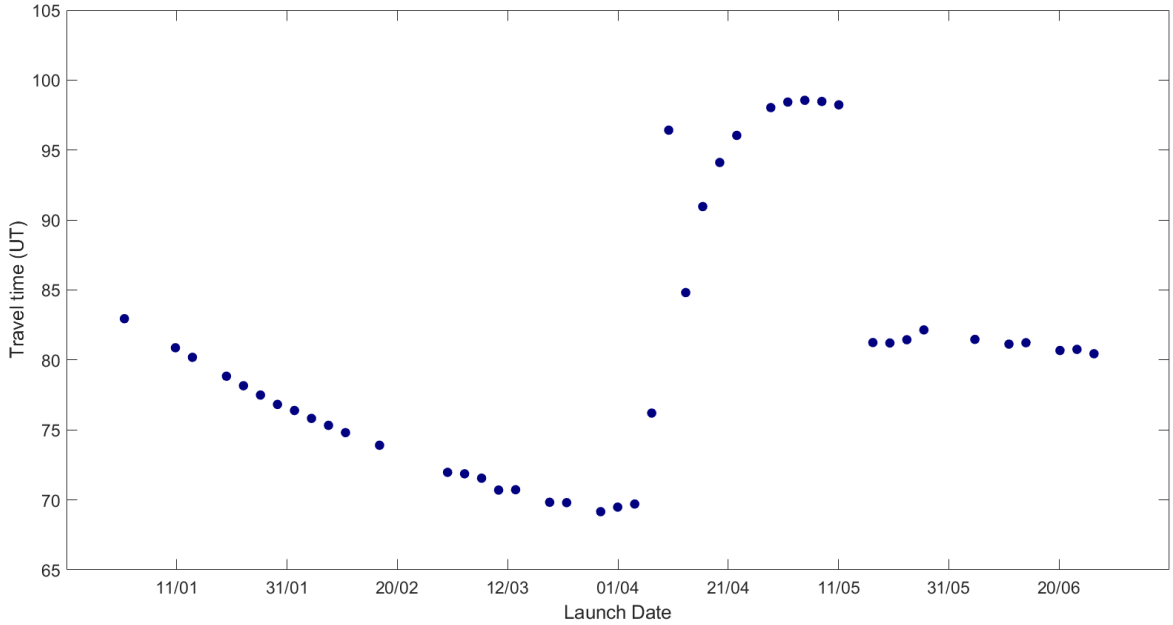


**Figure 5.33** Evolution of flight time in the independent optimization of Earth-Mars-Saturn.

### Genetic algorithm in Earth-Mars-Saturn

Once we have analyzed the behaviour of the flight time according to the launch date, we discuss the appliance of the genetic algorithm in some points of the Figure 5.33. The value of the control parameters that we use in this section is:

$$[X,E,N,t,n_c,\eta_c,p_c,\sigma_c,p_{mut},p_m,TOL] = [15,6,50,6,2,3,0.4,30,0.15,0.3,0.01] \tag{5.13}$$

Regarding the lower and upper limits of the value of the optimization variables, they have been selected based on the results at the arrival to Mars again, that are presented in (5.1). Thus, the limits are the same of the Earth-Mars-Saturn mission, and they are included in Table 5.3.

**Table 5.3** Lower and upper limits of the value of optimization variables in Earth-Mars-Saturn.

| | $v_{r_f}$ | $v_{\theta_f}$ | $r_P$ |
|---|---|---|---|
| LB | 0 | 0.7 | $3R_{\male}$ |
| UB | 0.15 | 0.9 | $7R_{\male}$ |

The first date on which we apply the genetic algorithm is 01/01/2024. The evolution of generations is shown in Figure 5.34.

In this case, the algorithm stops when it reaches 50 generations because of the defined tolerance is not reached, although the solution is reached in the generation 42. We can see some peaks again due to the exploration, and the black curve tending to the red one.

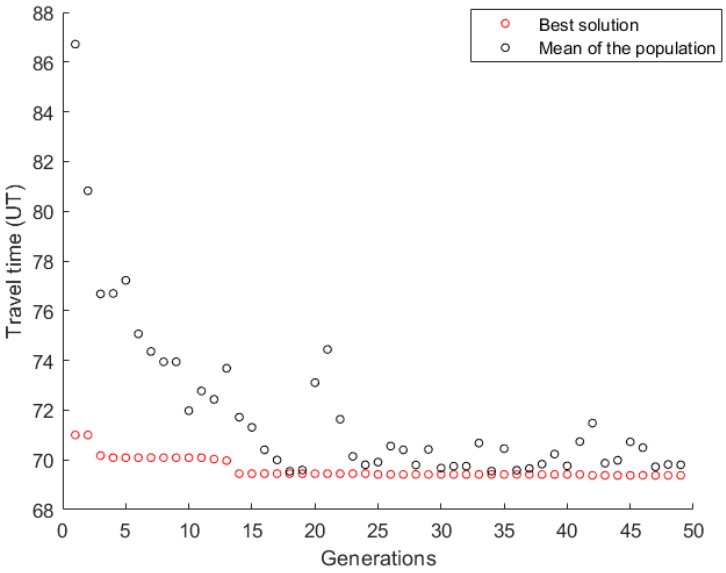


**Figure 5.34** Procedure of the genetic algorithm in Earth-Mars-Saturn on 01/01/2024.

The solution that is obtained is:

$$v_{r_f} = 0.1251 \text{ UV} \quad v_{\theta_f} = 0.7813 \text{ UV} \quad r_P = 3.8701 R_{\male} \tag{5.14}$$

We calculate the flight time for the first six months of 2024 with these arrival conditions to Mars, as shown in Figure 5.35, where the date on which the genetic algorithm is applied is represented in red.

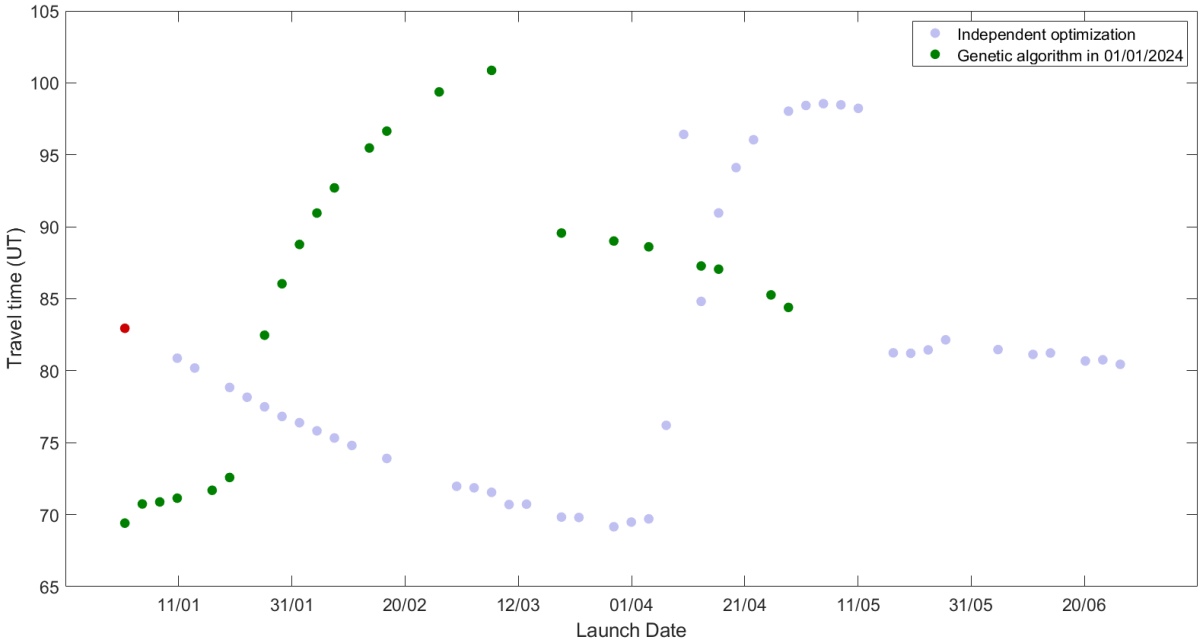


**Figure 5.35** Evolution of flight time of Earth-Mars-Saturn after applying genetic algorithm on 01/01/2024.

The improvement on 01/01/2024 is significant, from a flight time of 82.949 UT to one of 69.4118 UT. The flight time has improved in some dates, and, of course, it has gotten worse in another ones.

The next date on which we apply the genetic algorithm is 28/03/2024, when the flight time is minimum. The evolution of generations is represented in Figure 5.36.

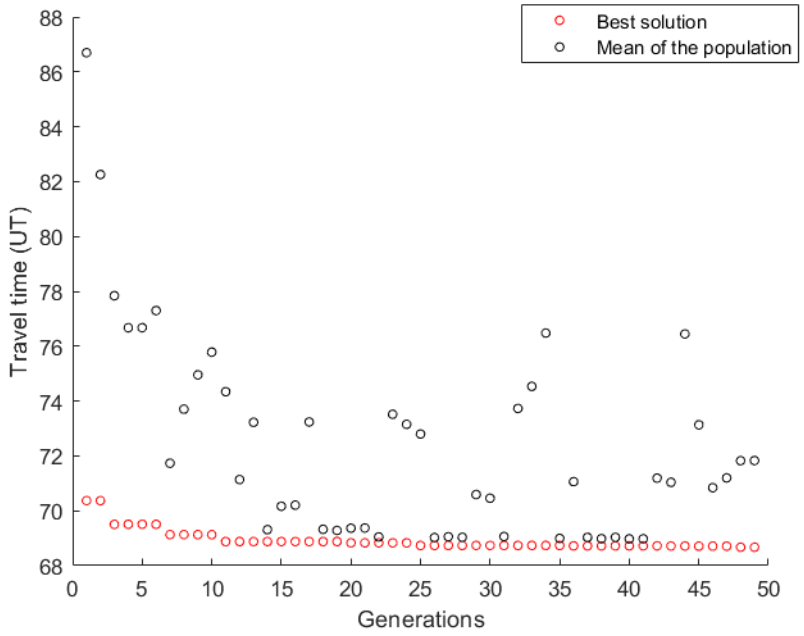


**Figure 5.36** Procedure of the genetic algorithm in Earth-Mars-Saturn on 28/03/2024.

In this case, the algorithm stops when it reaches 50 generations, not reaching the defined tolerance. However, the best individual does not improve much in the last 40 generations.

The solution that is obtained is:

$$v_{r_f} = 0.0733 \text{ UV} \quad v_{\theta_f} = 0.7628 \text{ UV} \quad r_P = 3.7605 R_{\male} \tag{5.15}$$

Again, we calculate the flight time for the first six months of 2024 with these arrival conditions to Mars, as shown in Figure 5.37, where the date on which the genetic algorithm is applied is represented in red.

The improvement on 28/03/2024 is not so high, from a flight time of 69.16 UT to one of 68.671 UT. The flight time improves on most dates, keeping the same date for the minimum flight time.

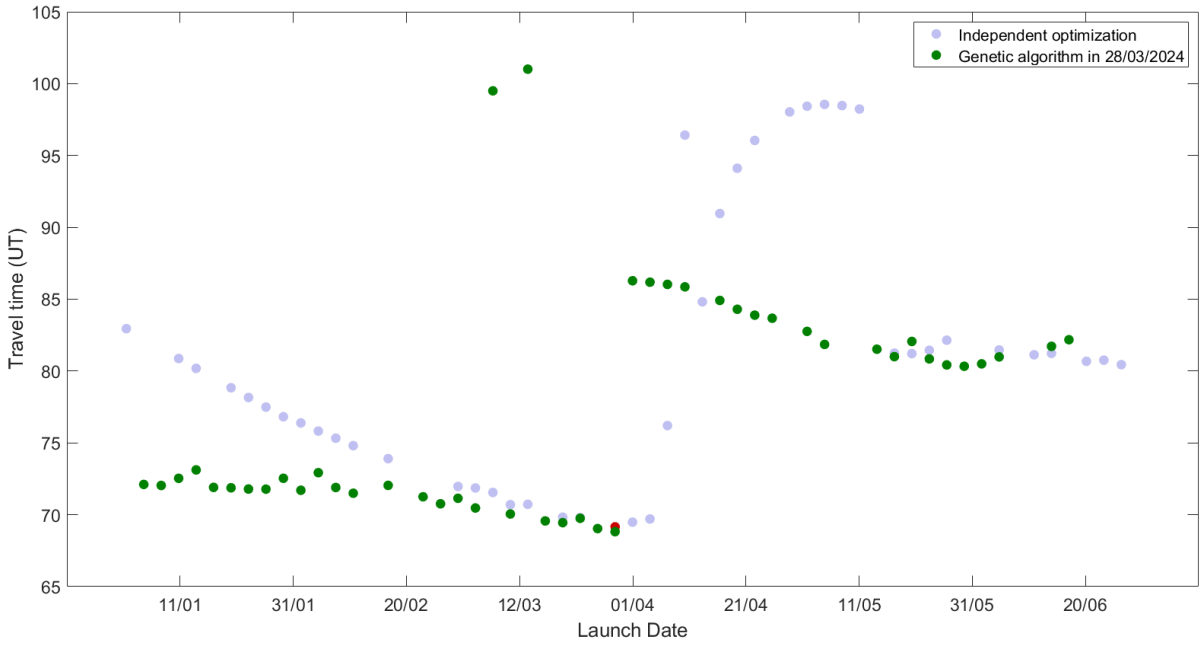


**Figure 5.37** Evolution of flight time of Earth-Mars-Saturn after applying genetic algorithm on 28/03/2024.

Next, we apply the genetic algorithm on 11/05/2024, just before the discontinuity. The evolution of generations is represented in Figure 5.38.

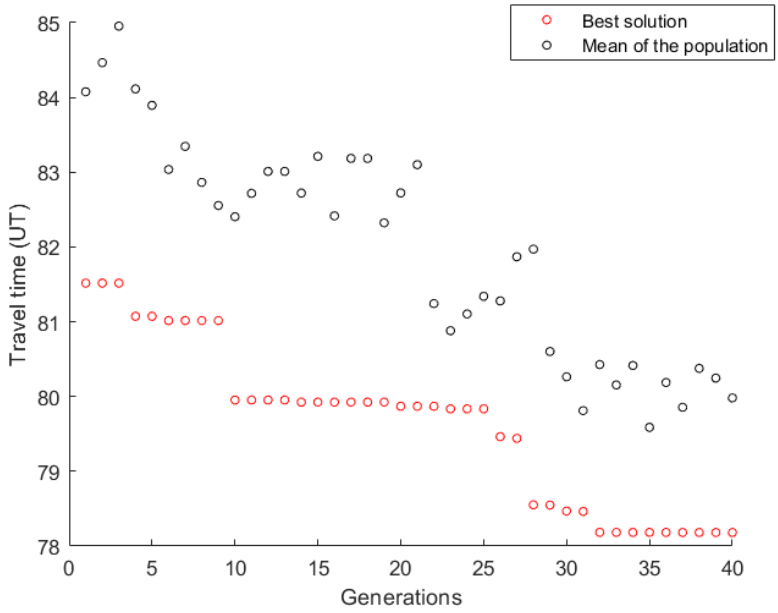


**Figure 5.38** Procedure of the genetic algorithm in Earth-Mars-Saturn on 11/05/2024.

In this case, we decide to change the maximum allowed number of generations to 40, due to the improvement of the best solution in the last generations is not too high, and the difference between the black curve and the red curve is high in all generations, so it does not look like it is going to converge soon.

The solution that is obtained is:

$$v_{r_f} = 0.014 \text{ UV} \quad v_{\theta_f} = 0.8435 \text{ UV} \quad r_P = 6.7236 R_{\male} \tag{5.16}$$

We calculate the flight time for the first six months of 2024 with these arrival conditions to Mars, as shown in Figure 5.39.

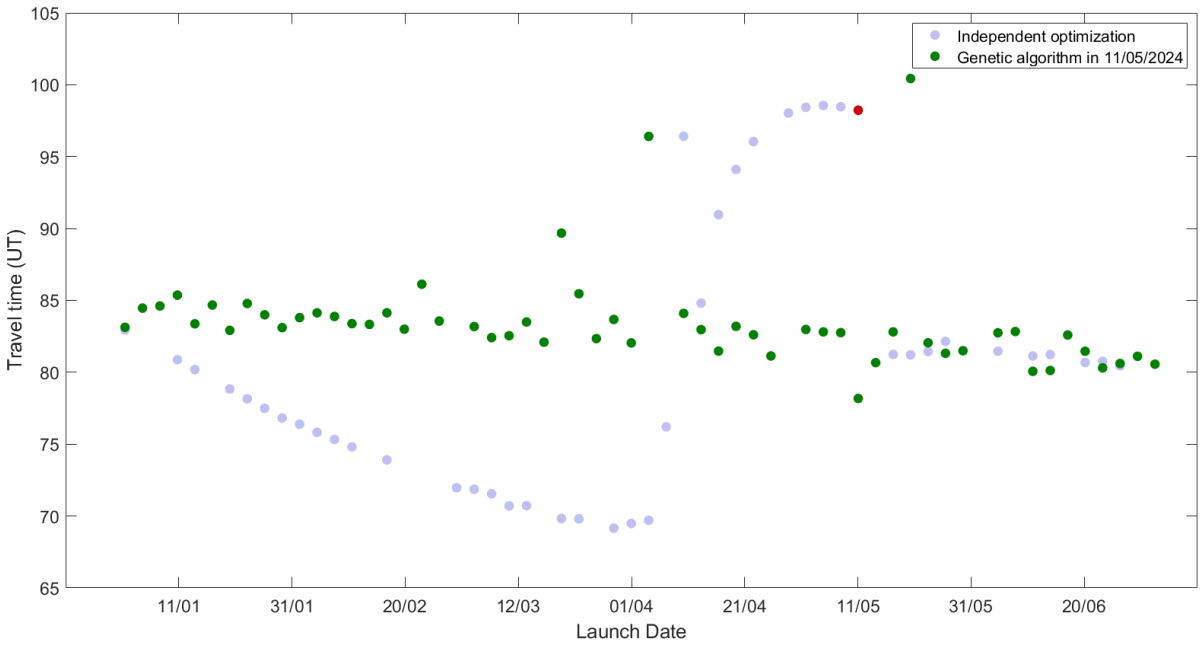


**Figure 5.39** Evolution of flight time of Earth-Mars-Saturn after applying genetic algorithm on 11/05/2024.

The improvement on 11/05/2024 is from a flight time of 98.2317 UT to one of 78.1816 UT. We can see that, with these arrival conditions, the evolution of flight time is approximately constant.

The last date on which we apply the genetic algorithm is 30/06/2024. The evolution of generations is represented in Figure 5.40.

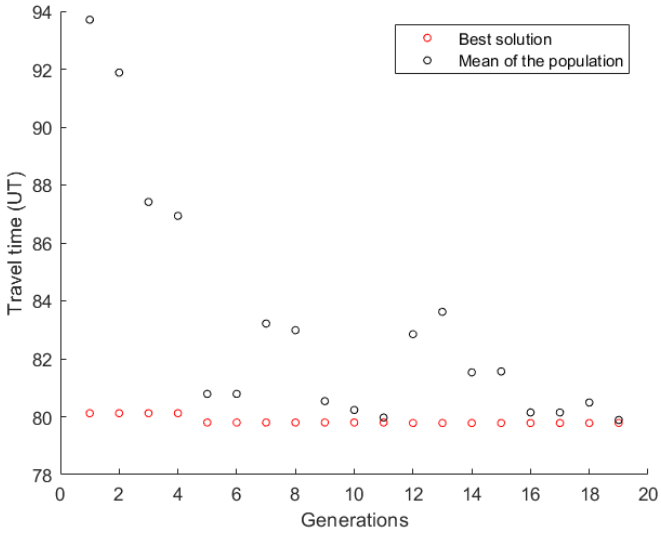


**Figure 5.40** Procedure of the genetic algorithm in Earth-Mars-Saturn on 30/06/2024.

In this case, the algorithm stops when it reaches 19 generations because of the defined tolerance is reached.

The solution that is obtained is:

$$v_{r_f} = 0.019 \text{ UV} \quad v_{\theta_f} = 0.8402 \text{ UV} \quad r_P = 5.4703 R_{\male} \tag{5.17}$$

We calculate the flight time for the first six months of 2024 with these arrival conditions to Mars, as shown in Figure 5.41.

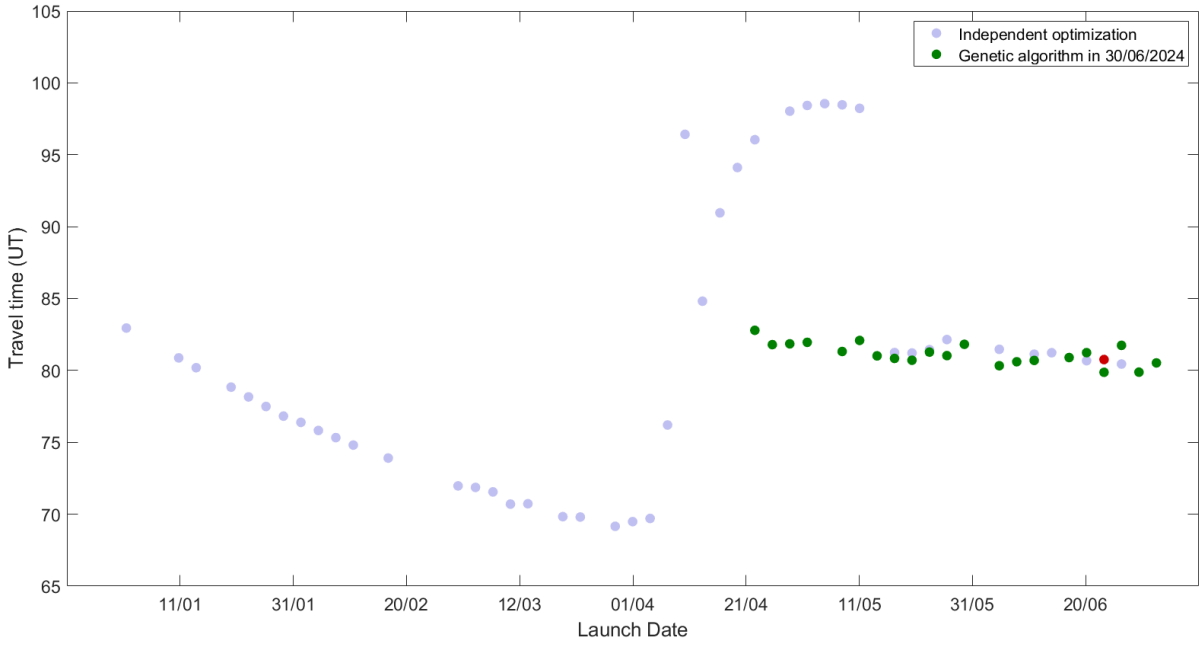


**Figure 5.41** Evolution of flight time of Earth-Mars-Saturn after applying genetic algorithm on 30/06/2024.

The improvement on 30/06/2024 is from a flight time of 80.7574 UT to one of 79.8706 UT. Solutions with these arrival conditions are found only on dates that are close to 30/06/2024.

As a summary, the different flight times on the analyzed dates are presented in Table 5.4.

**Table 5.4** Improvement in flight times of Earth-Mars-Saturn.

| Date | Independent optimization | Genetic algorithm |
|---|---|---|
| 01/01/2024 | 82.95 UT | 69.41 UT |
| 28/03/2024 | 69.16 UT | 68.67 UT |
| 11/05/2024 | 98.23 UT | 78.18 UT |
| 30/06/2024 | 80.76 UT | 79.87 UT |

Lastly, superimposing all the results, we can present the minimum flight time in each date, as is shown in Figure 5.42.

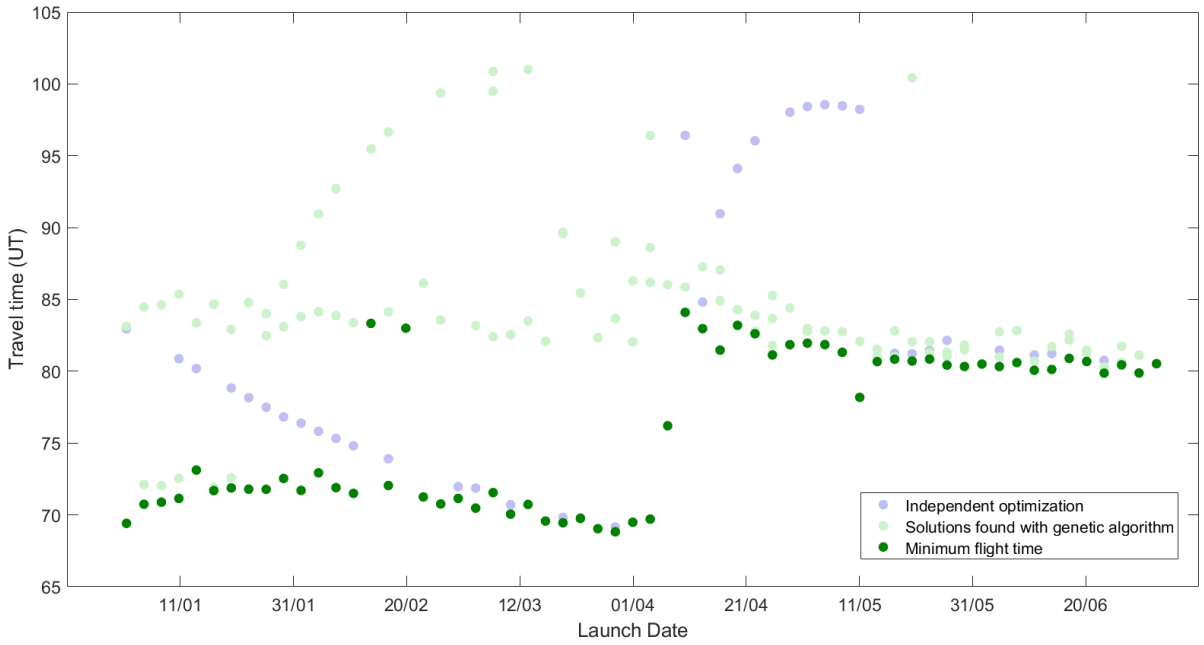


**Figure 5.42** Minimum flight time of Earth-Mars-Saturn in each date.

We can see that the date with minimum flight time in the independent optimization coincides with the date with minimum flight time after applying the genetic algorithm.

### 5.2.3 Earth-Jupiter-Saturn mission

The next analyzed mission has also Saturn as final planet, but Jupiter as intermediate planet. An example of trajectory of this mission is represented in Figure 5.43.

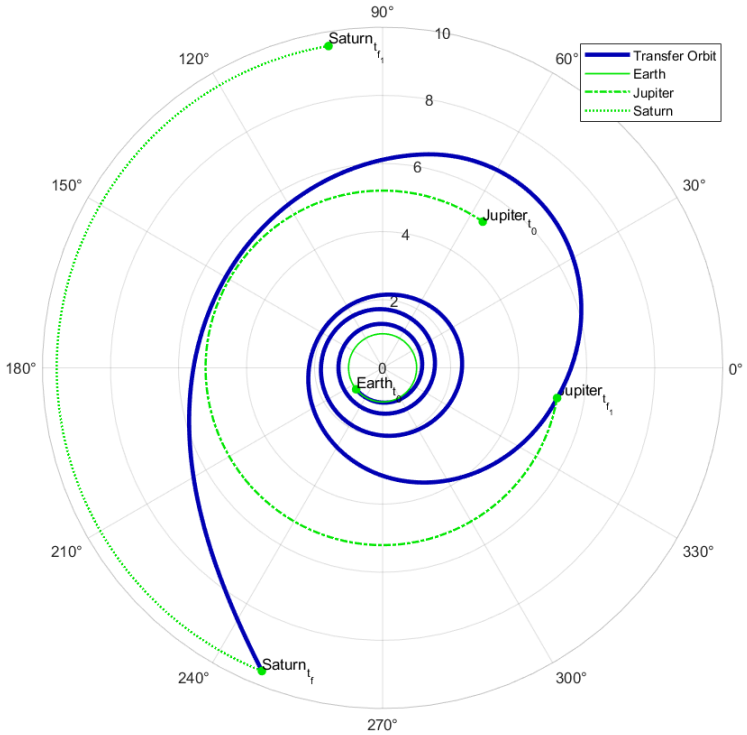


**Figure 5.43** Example of trajectory of the Earth-Jupiter-Saturn mission.

This trajectory has been calculated for a launch on 01/05/2024, with an approach radius in the gravity assist maneuver of $r_P = 4R_{\varphi_+}$.

Next, in Figure 5.44, the results for the first six months of 2024 of the independent optimization, with $r_P = 4R_{\varphi_+}$ in the gravity assist maneuver, are presented.

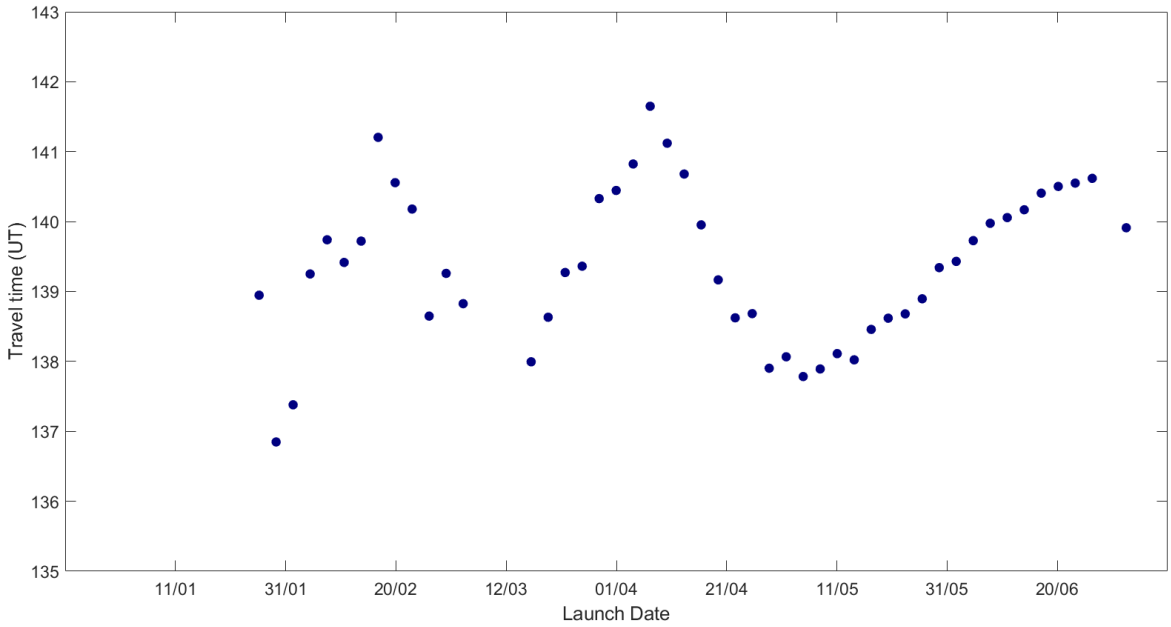


**Figure 5.44** Evolution of flight time in the independent optimization of Earth-Jupiter-Saturn.

In this case, no solutions are found for the independent optimization until 27/01/2024, close to the date on which the minimum flight time is found. We can see that the flight time varies around a value, which is greater than for the Earth-Mars-Saturn mission.

### Genetic algorithm in Earth-Jupiter-Saturn

Once we have analyzed the behaviour of the flight time according to the launch date, we discuss the appliance of the genetic algorithm in some points of the Figure 5.44. The value of the control parameters that we use in this section is:

$$[X,E,N,t,n_c,\eta_c,p_c,\sigma_c,p_{mut},p_m,TOL] = [15,6,50,6,2,3,0.4,30,0.15,0.3,0.01] \tag{5.18}$$

Regarding the lower and upper limits of the value of the optimization variables, they have been selected based on the results at the arrival to Jupiter, that are presented in (5.2). Thus, the limits are included in Table 5.5.

**Table 5.5** Lower and upper limits of the value of optimization variables in Earth-Jupiter-Saturn.

| | $v_{r_f}$ | $v_{\theta_f}$ | $r_P$ |
|---|---|---|---|
| LB | 0.07 | 0.2 | $3R_{\varphi_+}$ |
| UB | 0.15 | 0.4 | $7R_{\varphi_+}$ |

The first date on which we apply the genetic algorithm is 29/01/2024, when the flight time is minimum. The evolution of generations is shown in Figure 5.45.

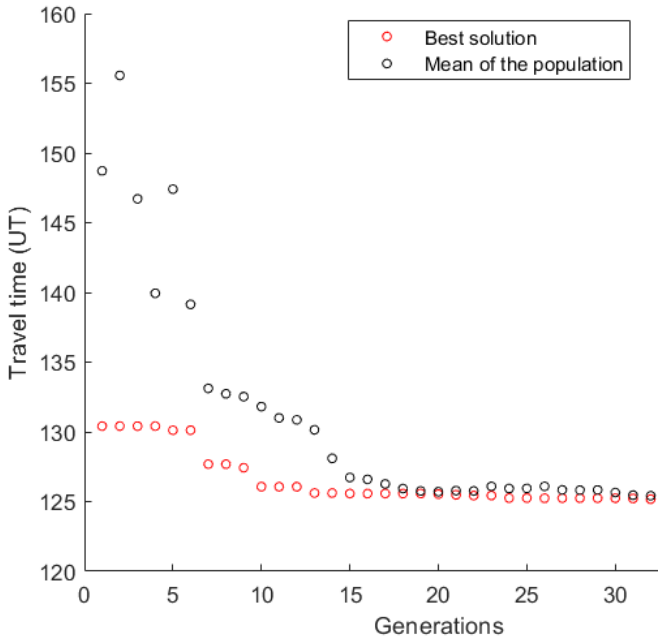


**Figure 5.45** Procedure of the genetic algorithm in Earth-Jupiter-Saturn on 29/01/2024.

The algorithm stops when it reaches 32 generations because of the defined tolerance is reached. In this case, the black curve tends to the red one quickly, but such a low value of the defined tolerance makes the procedure take longer.

The solution that is obtained is:

$$v_{r_f} = 0.0701 \text{ UV} \quad v_{\theta_f} = 0.3168 \text{ UV} \quad r_P = 6.4885 R_{\oplus} \tag{5.19}$$

We calculate the flight time for the first six months of 2024 with these arrival conditions to Jupiter, as shown in Figure 5.46, where the date on which the genetic algorithm is applied is represented in red.

The improvement on 29/01/2024 is significant, from a flight time of 136.85 UT to one of 124.8 UT. The flight time improves in all the dates when a solution is found.

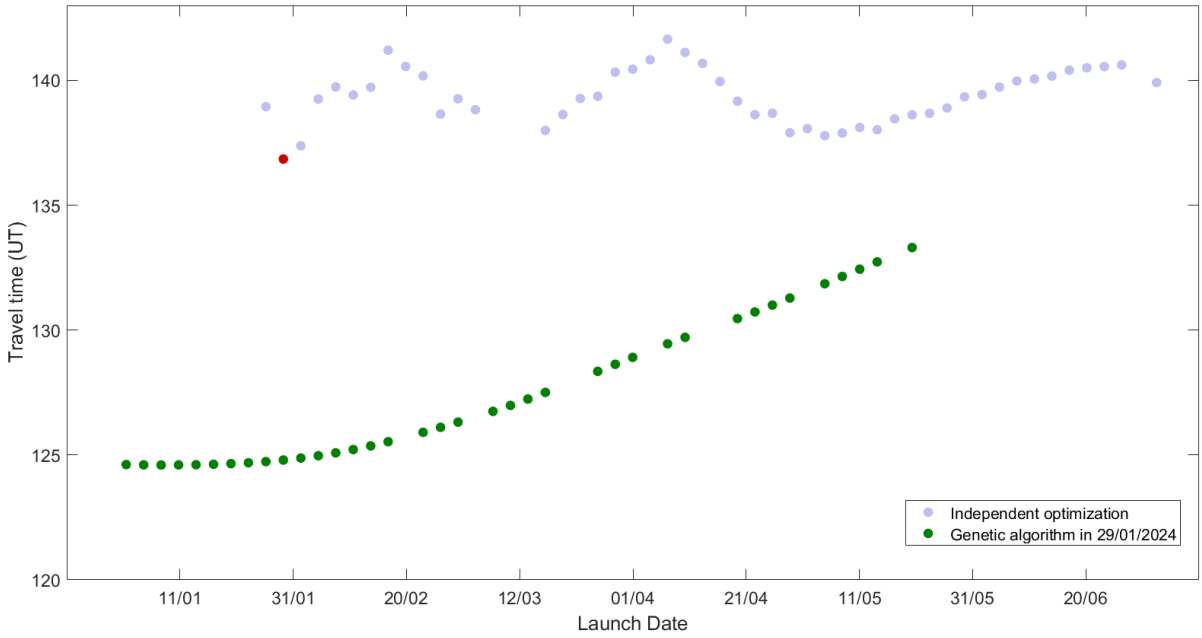


**Figure 5.46** Evolution of flight time of Earth-Jupiter-Saturn after applying genetic algorithm on 29/01/2024.

The next date on which we apply the genetic algorithm is 01/06/2024. The evolution of generations is represented in Figure 5.47.

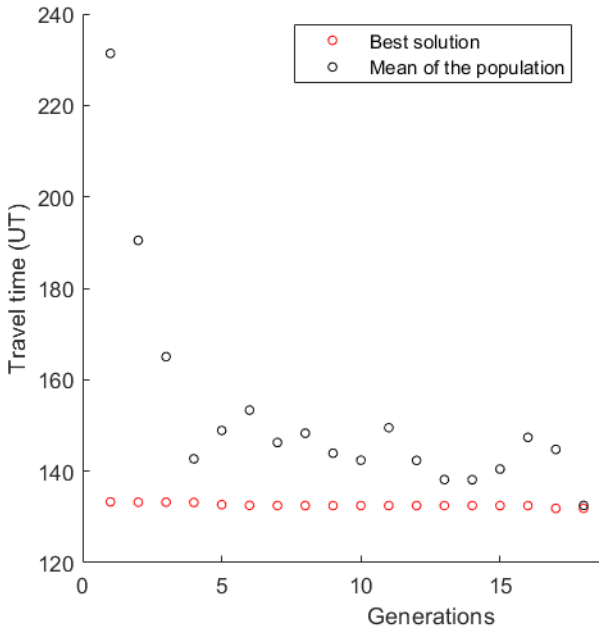


**Figure 5.47** Procedure of the genetic algorithm in Earth-Jupiter-Saturn on 01/06/2024.

In this case, the algorithm stops when it reaches 18 generations because of the defined tolerance is reached. We can see that the best individual (red dots) remains almost constant in all generations, so the best individual of the initial population is close to the optimal solution.

The solution that is obtained is:

$$v_{r_f} = 0.0778 \text{ UV} \quad v_{\theta_f} = 0.3412 \text{ UV} \quad r_P = 6.9588 R_{\oplus} \tag{5.20}$$

Again, we calculate the flight time for the first six months of 2024 with these arrival conditions to Jupiter, as shown in Figure 5.48, where the date on which the genetic algorithm is applied is represented in red.

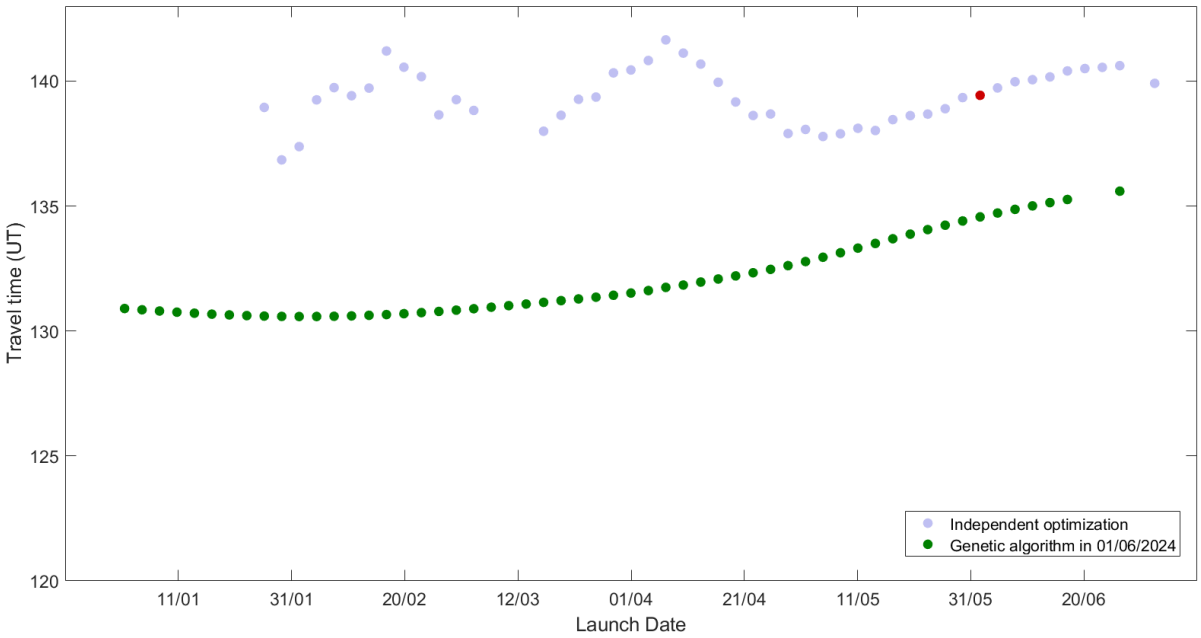


**Figure 5.48** Evolution of flight time of Earth-Jupiter-Saturn after applying genetic algorithm on 01/06/2024.

The improvement on 01/06/2024 is from a flight time of 139.43 UT to one of 134.57 UT. All the found solutions with these arrival conditions are better than the obtained solutions in the independent optimization again.

The last date on which we apply the genetic algorithm is 01/07/2024. The evolution of generations is represented in Figure 5.49.

In this case, we decide to change the value of the defined tolerance to 1, due to the obtained solution is so similar, with a lower computational cost. The algorithm stops when it reaches 30 generations.

The solution that is obtained is:

$$v_{r_f} = 0.0705 \text{ UV} \quad v_{\theta_f} = 0.4000 \text{ UV} \quad r_P = 6.9577 R_{\oplus} \tag{5.21}$$

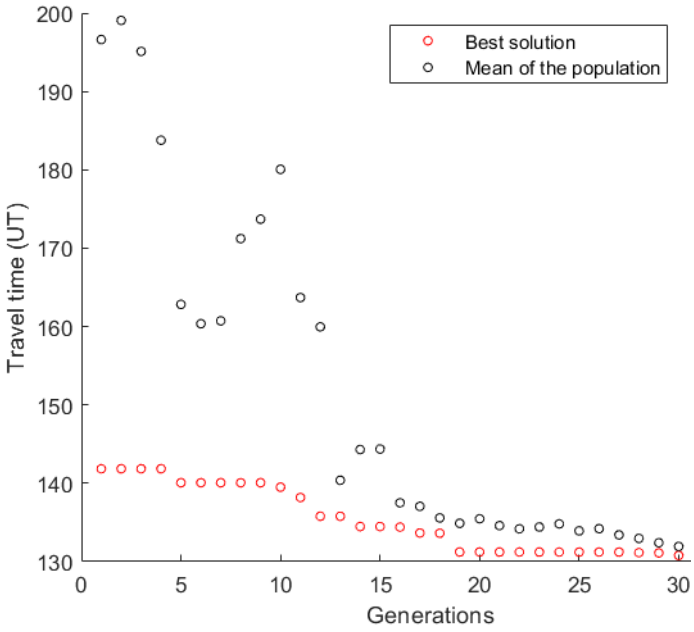


**Figure 5.49** Procedure of the genetic algorithm in Earth-Jupiter-Saturn on 01/07/2024.

We calculate the flight time for the first six months of 2024 with this arrival conditions to Jupiter, as shown in Figure 5.50.

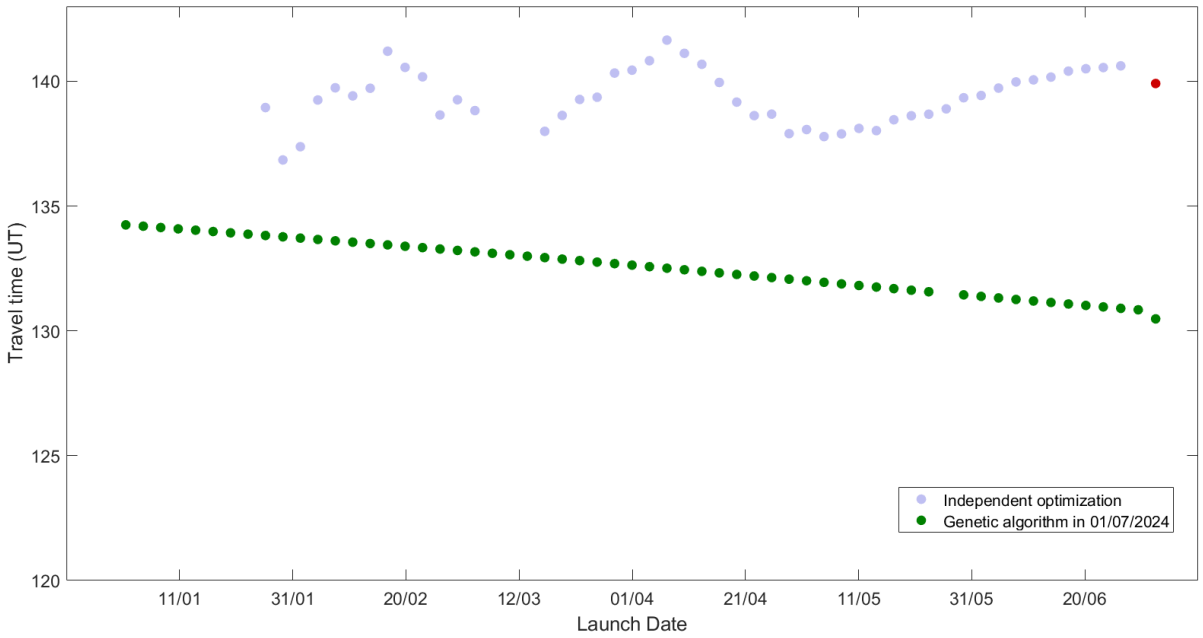


**Figure 5.50** Evolution of flight time of Earth-Jupiter-Saturn after applying genetic algorithm on 01/07/2024.

The improvement on 01/07/2024 is from a flight time of 139.912 UT to one of 130.48 UT. We can see that, with these arrival conditions, the flight time decreases as the launch is delayed.

As a summary, the different flight times in the analyzed dates are presented in Table 5.6.

**Table 5.6** Improvement in flight times of Earth-Jupiter-Saturn.

| Date | Independent optimization | Genetic algorithm |
|---|---|---|
| 29/01/2024 | 136.85 UT | 124.8 UT |
| 01/06/2024 | 139.43 UT | 134.57 UT |
| 01/07/2024 | 139.91 UT | 130.48 UT |

Lastly, superimposing all the results, we can present the minimum flight time in each date, as is shown in Figure 5.51.

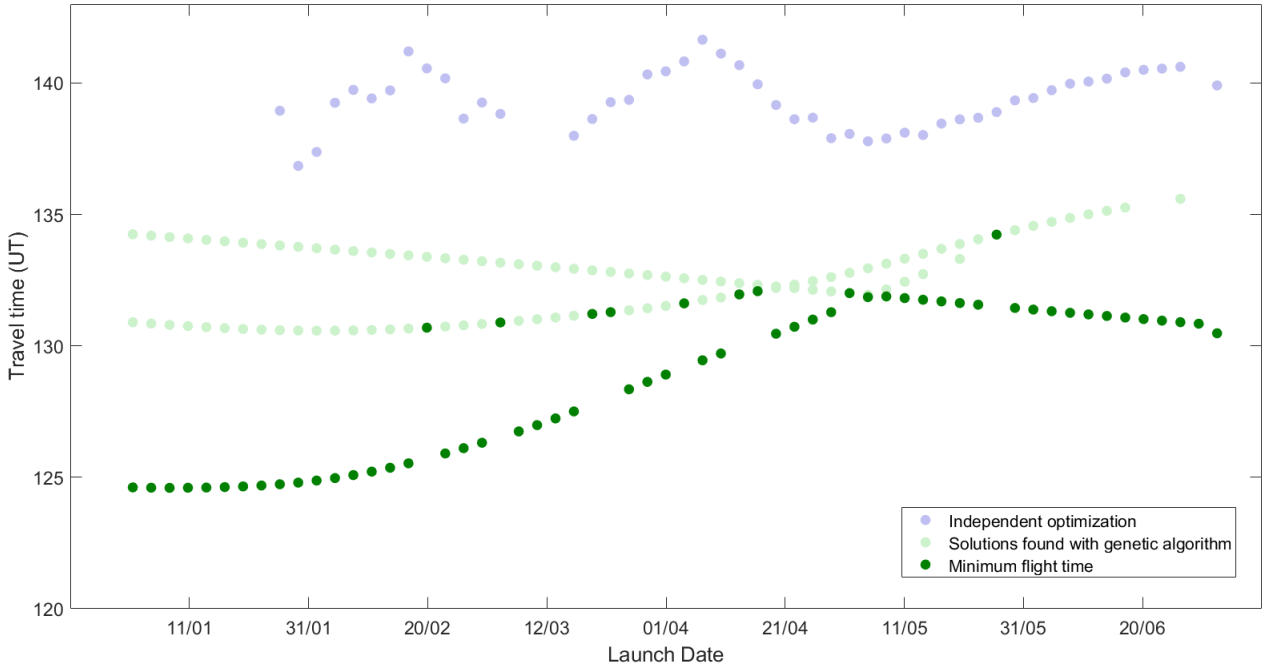


**Figure 5.51** Minimum flight time of Earth-Jupiter-Saturn in each date.

Again, we can see that the date with minimum flight time is the same before and after applying the genetic algorithm.

### 5.2.4 Earth-Venus-Saturn mission

The last analyzed mission has also Saturn as final planet, but Venus as intermediate planet. An example of trajectory of this mission is represented in Figure 5.52.

This trajectory has been calculated for a launch on 21/04/2024, with an approach radius in the gravity assist maneuver of $r_P = 4R_{\varphi}$.

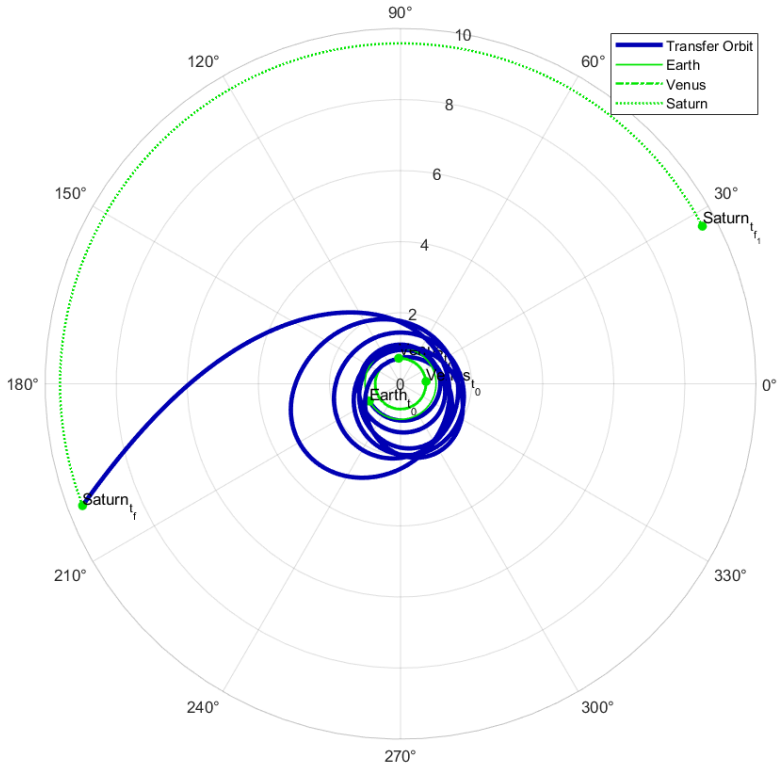


**Figure 5.52** Example of trajectory of the Earth-Venus-Saturn mission.

Next, in Figure 5.53, the results for the first six months of 2024 of the independent optimization, with $r_P = 4R_{\varphi}$ in the gravity assist maneuver, are presented.

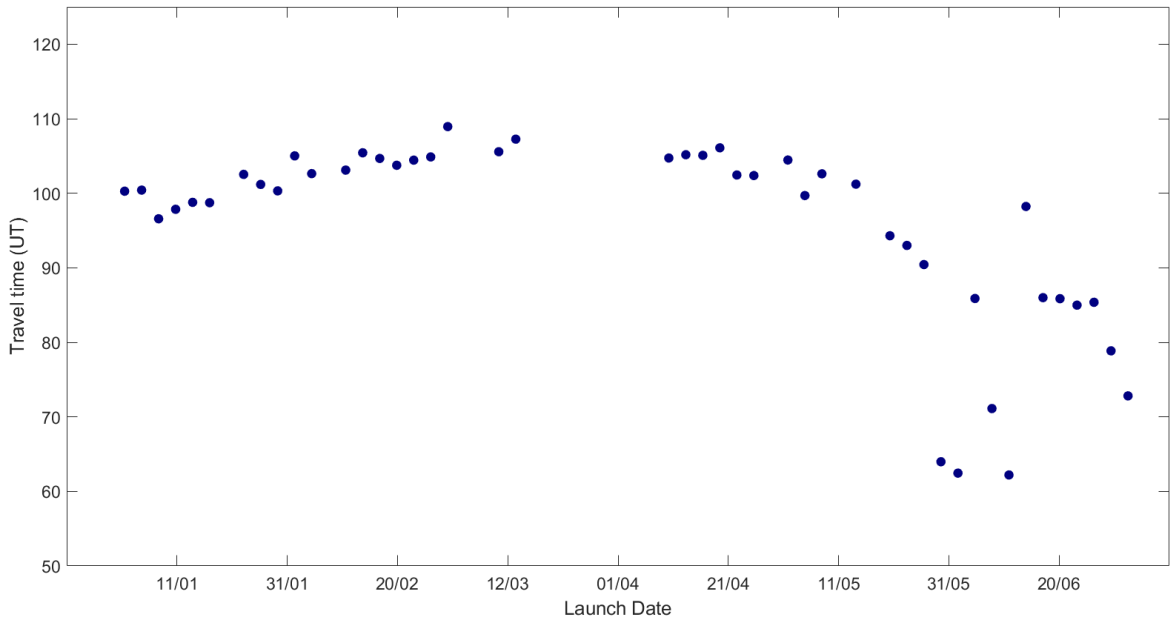


**Figure 5.53** Evolution of flight time in the independent optimization of Earth-Venus-Saturn.

In this case, the flight time decreases on launch dates that are close to June. In the rest of the launch dates, it is almost constant. In addition, there is an interval of launch dates without a solution for the independent optimization.

### Genetic algorithm in Earth-Venus-Saturn

Once we have analyzed the behaviour of the flight time according to the launch date, we discuss the appliance of the genetic algorithm in some points of the Figure 5.53. The value of the control parameters that we use in this section is:

$$[X,E,N,t,n_c,\eta_c,p_c,\sigma_c,p_{mut},p_m,TOL] = [15,6,50,6,2,3,0.4,20,0.15,0.35,0.01] \tag{5.22}$$

Regarding the lower and upper limits of the value of the optimization variables, they have been selected based on the results at the arrival to Venus, that are presented in (5.3). Thus, the limits are included in Table 5.7.

**Table 5.7** Lower and upper limits of the value of optimization variables in Earth-Venus-Saturn.

| | $v_{r_f}$ | $v_{\theta_f}$ | $r_P$ |
|---|---|---|---|
| LB | $-0.3$ | 1.21 | $2R_{\varphi}$ |
| UB | $-0.15$ | 1.34 | $5R_{\varphi}$ |

The first date on which we apply the genetic algorithm is 07/01/2024. The evolution of generations is shown in Figure 5.54.

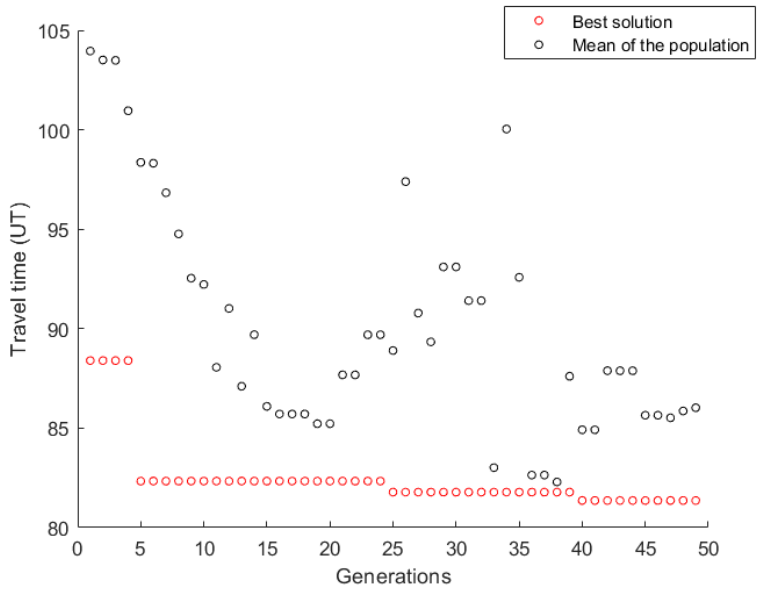


**Figure 5.54** Procedure of the genetic algorithm in Earth-Venus-Saturn on 07/01/2024.

The algorithm stops when it reaches the maximum allowed number of generations, that is, 50. In this case, it is not so clear that the black curve tends to the red one. In most cases, the mean increases due to there are more individuals of the population that converge to a solution in that generation.

The solution that is obtained is:

$$v_{r_f} = -0.2017 \text{ UV} \quad v_{\theta_f} = 1.2329 \text{ UV} \quad r_P = 3.9668R_{\varphi} \tag{5.23}$$

We calculate the flight time for the first six months of 2024 with these arrival conditions to Venus, as shown in Figure 5.55, where the date on which the genetic algorithm is applied is represented in red.

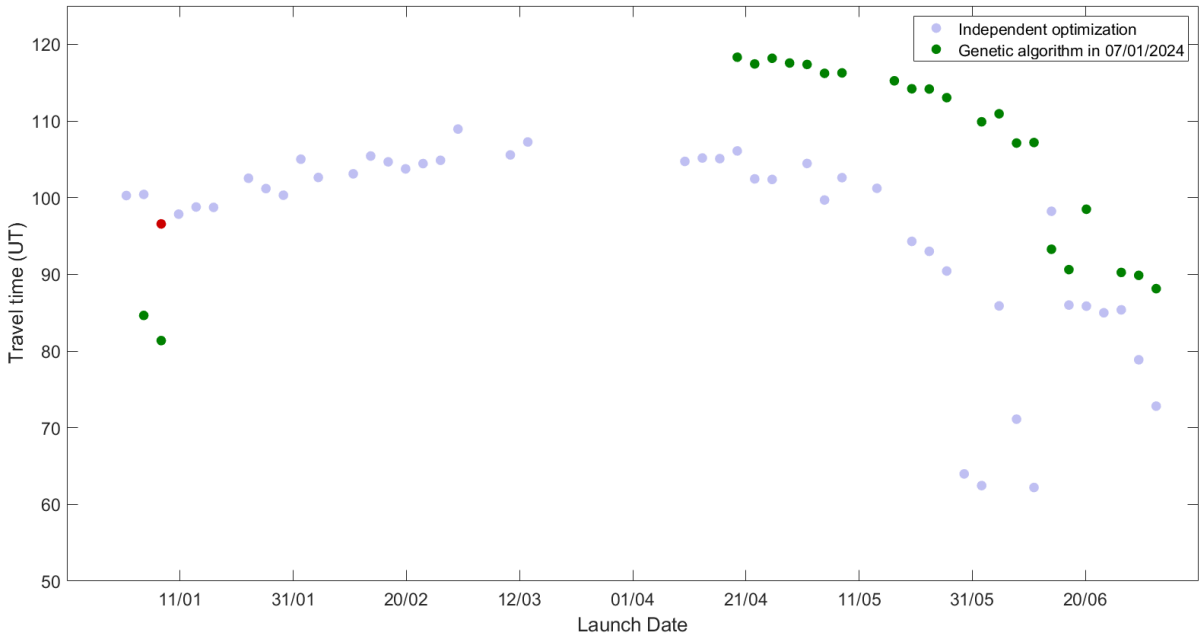


**Figure 5.55** Evolution of flight time of Earth-Venus-Saturn after applying genetic algorithm on 07/01/2024.

The improvement on 07/01/2024 is from a flight time of 96.57 UT to one of 81.36 UT. Not many solutions with these arrival conditions are found, and practically all the solutions that are found are worse than the solutions of the independent optimization.

The next date on which we apply the genetic algorithm is 10/04/2024. The evolution of generations is represented in Figure 5.56.

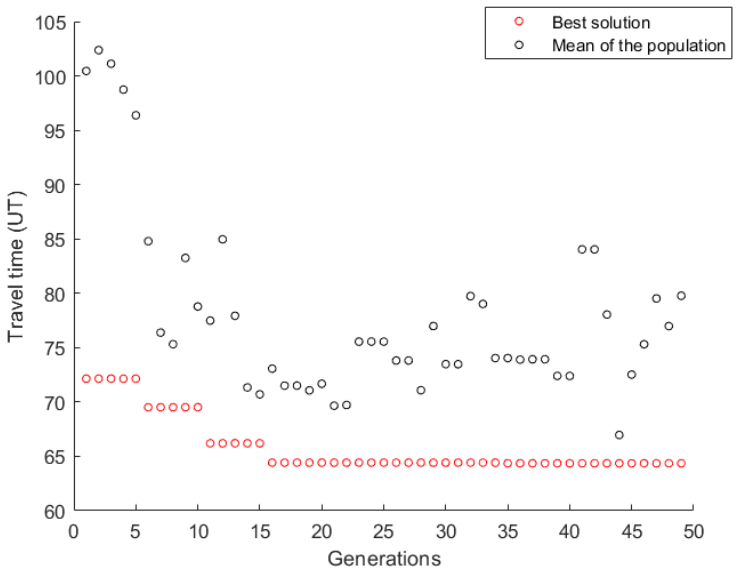


**Figure 5.56** Procedure of the genetic algorithm in Earth-Venus-Saturn on 10/04/2024.

In this case, the best individual is practically constant from the fifteenth generation, so the algorithm could stop earlier.

The solution that is obtained is:

$$v_{r_f} = -0.2858 \text{ UV} \quad v_{\theta_f} = 1.3043 \text{ UV} \quad r_P = 3.1429 R_{\varphi} \tag{5.24}$$

Again, we calculate the flight time for the first six months of 2024 with these arrival conditions to Venus, as shown in Figure 5.57, where the date on which the genetic algorithm is applied is represented in red.

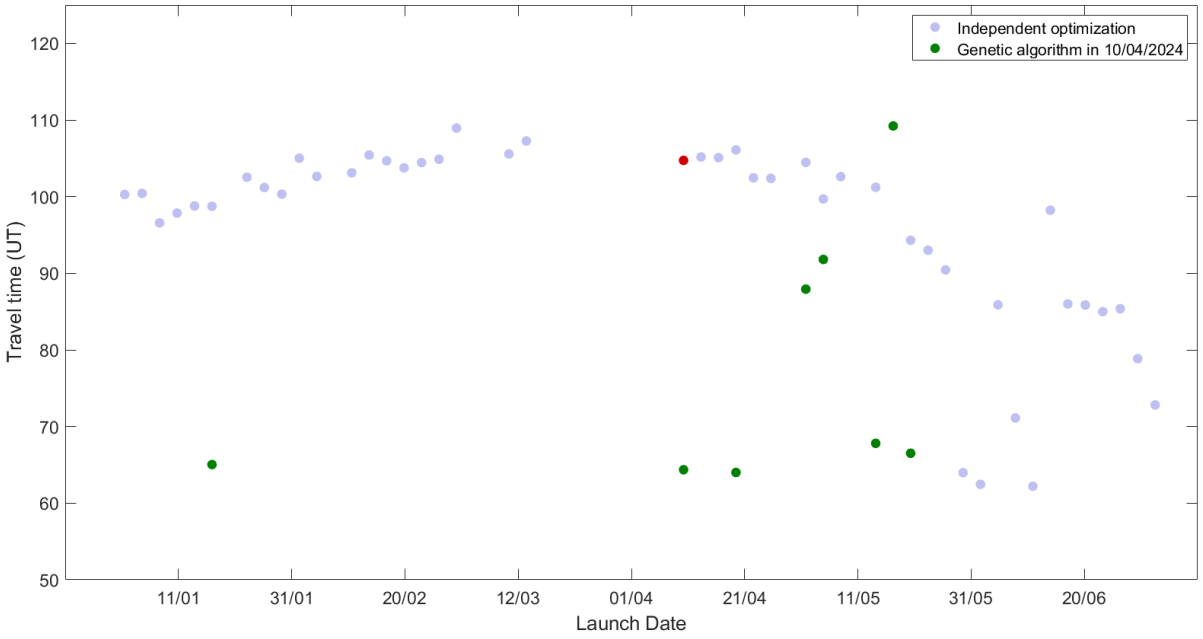


**Figure 5.57** Evolution of flight time of Earth-Venus-Saturn after applying genetic algorithm on 10/04/2024.

The improvement on 10/04/2024 is significant, from a flight time of 104.73 UT to one of 64.36 UT. A solution with these arrival conditions is found only on specific dates.

Next, we apply the genetic algorithm on 01/06/2024. The evolution of generations is represented in Figure 5.58. In this case, the algorithm stops when it reaches 50 generations.

The solution that is obtained is:

$$v_{r_f} = -0.2530 \text{ UV} \quad v_{\theta_f} = 1.3216 \text{ UV} \quad r_P = 3.4193 R_{\varphi} \tag{5.25}$$

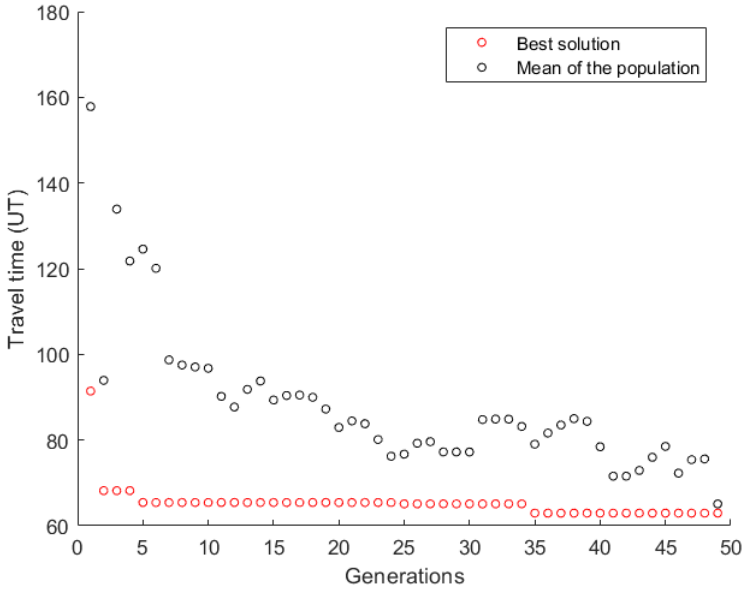


**Figure 5.58** Procedure of the genetic algorithm in Earth-Venus-Saturn on 01/06/2024.

We calculate the flight time for the first six months of 2024 with these arrival conditions to Venus, as shown in Figure 5.59.

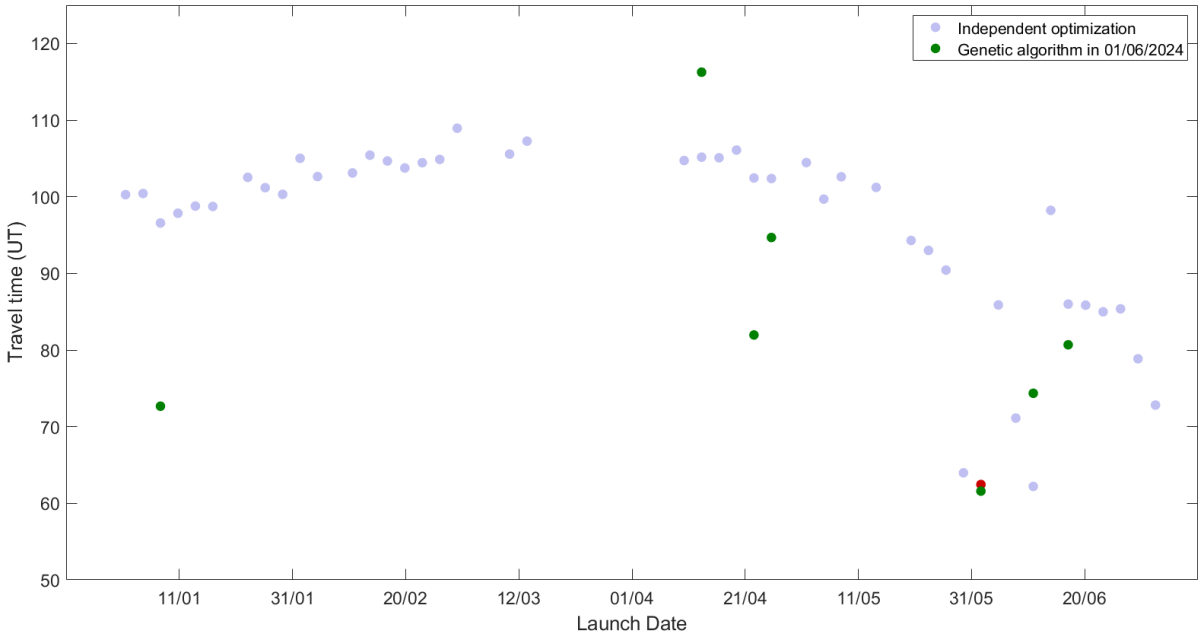


**Figure 5.59** Evolution of flight time of Earth-Venus-Saturn after applying genetic algorithm on 01/06/2024.

The improvement on 01/06/2024 is not very high, from a flight time of 62.45 UT to one of 61.59 UT. Again, we can see that, with these arrival conditions, solutions are found only on specific dates.

The last date on which we apply the genetic algorithm is 10/06/2024, when the flight time is minimum. The evolution of generations is represented in Figure 5.60.

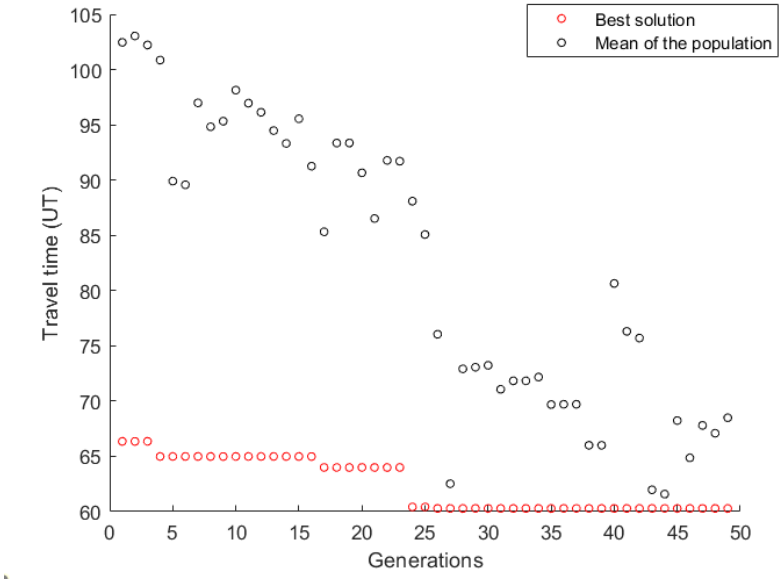


**Figure 5.60** Procedure of the genetic algorithm in Earth-Venus-Saturn on 10/06/2024.

In this case, the size of the base population, $X$, is increased to 25. The algorithm stops when it reaches 50 generations, although it could stop earlier because the best solution does not improve from the generation 24.

The solution that is obtained is:

$$v_{r_f} = -0.1813 \text{ UV} \quad v_{\theta_f} = 1.3270 \text{ UV} \quad r_P = 3.5737 R_{\varphi} \tag{5.26}$$

We calculate the flight time for the first six months of 2024 with these arrival conditions to Venus, as shown in Figure 5.61.

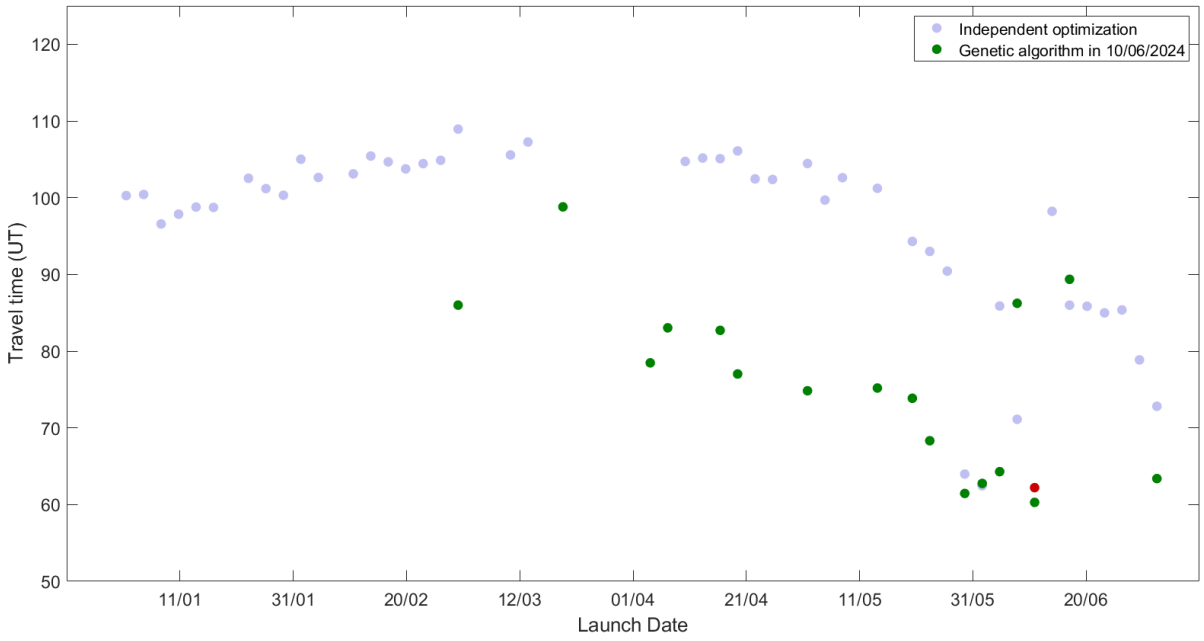


**Figure 5.61** Evolution of flight time of Earth-Venus-Saturn after applying genetic algorithm on 10/06/2024.

The improvement on 10/06/2024 is from a flight time of 62.21 UT to one of 60.29 UT. In addition, the flight time improves in some different dates around the selected one.

As a summary, the different flight times on the analyzed dates are presented in Table 5.8.

**Table 5.8** Improvement in flight times of Earth-Venus-Saturn.

| Date | Independent optimization | Genetic algorithm |
|---|---|---|
| 07/01/2024 | 96.57 UT | 81.36 UT |
| 10/04/2024 | 104.73 UT | 64.36 UT |
| 01/06/2024 | 62.45 UT | 61.59 UT |
| 10/06/2024 | 62.21 UT | 60.29 UT |

Lastly, superimposing all the results, we can present the minimum flight time in each date, as is shown in Figure 5.62.

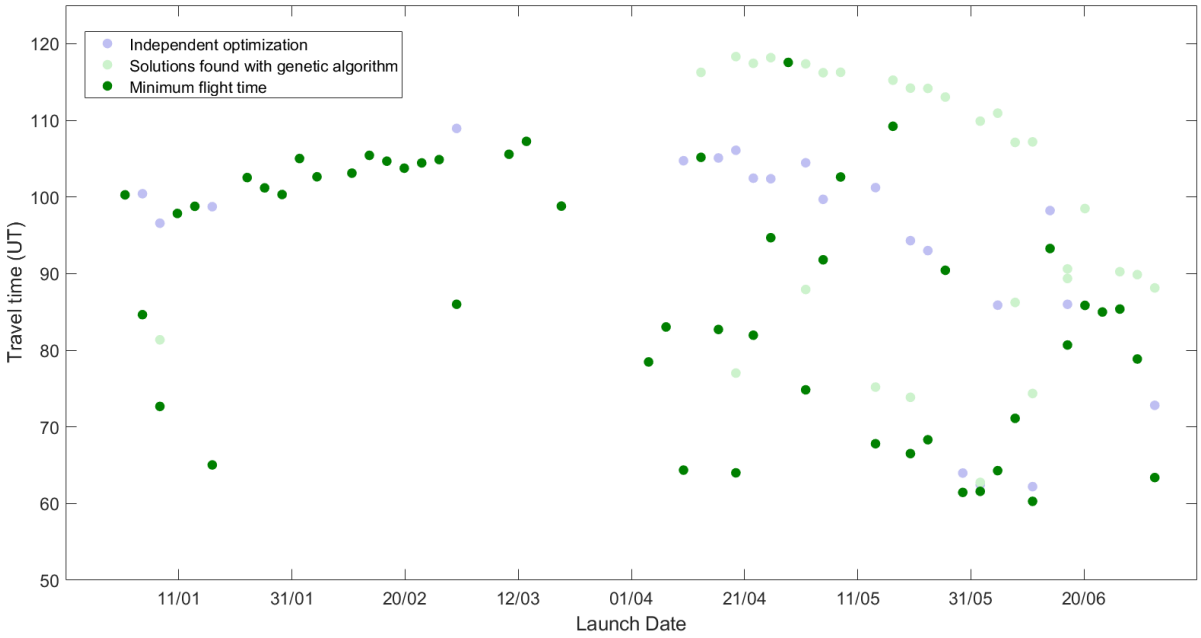


**Figure 5.62** Minimum flight time of Earth-Venus-Saturn in each date.

In this case, the distribution of minimum flight times is not so clear. The minimum flight time continues being on 10/06/2024.

### 5.2.5 Analysis of variations in the procedure

From now on, we center our focus on the case analyzed in Section 5.2.4, on the date of the minimum flight time, that is, on 10/06/2024. We analyze the effect of the size of the base population and slight modifications in mutation.

In order to analyze the effect of the size of the base population in the results, we study the number of individuals that converges to a solution in each generation. Based on this, we analyze the behaviour of the mean of the population. In Figure 5.63, a comparison between a base population of 15 individuals (left) and a base population of 25 individuals (right) is presented.

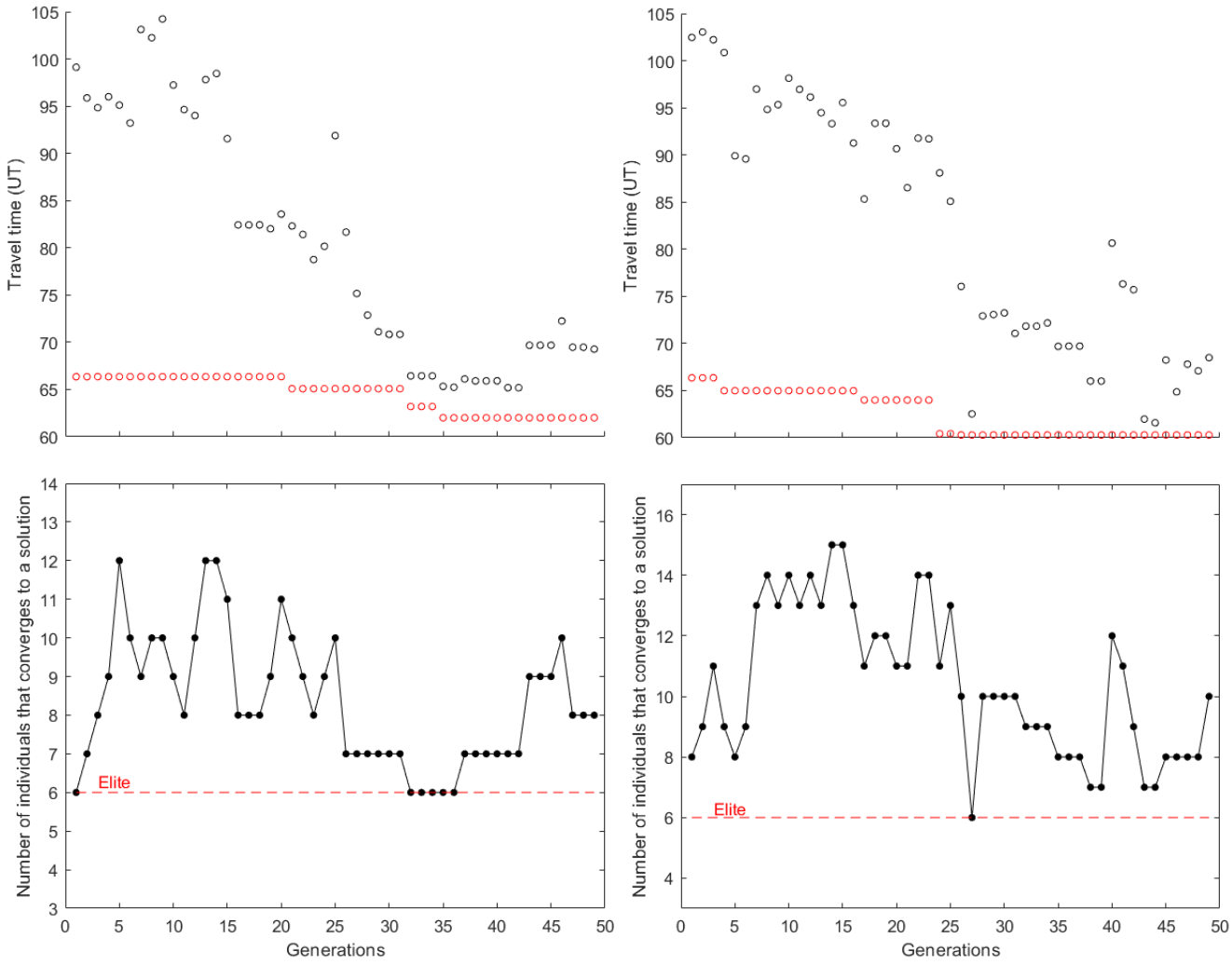


**(a)** Base population of 15.

**(b)** Base population of 25.

**Figure 5.63** Comparison between different base population sizes.

The following results are extracted:

**Table 5.9** Results of the comparison between sizes of the base population.

| Size of base population | Mean of number of individuals with solution | Maximum number of individuals with solution | Flight time (UT) | Computational time |
|---|---|---|---|---|
| 15 | 8.33 | 12 | 62.0019 | 15 h |
| 25 | 10.39 | 15 | 60.2863 | 26 h |

A size of 25 individuals in the base population presents a better solution, but with a higher computational cost. Even though the mean of number of individuals with a solution is higher in the second case, it is not higher enough to reduce the total computational time.

Comparing two different generations in the second case (for example), the generation in which there are more individuals that converge to a solution has a lower computational cost. However, the mean of individuals with a solution in a generation of the second case is not high enough to compensate the increment of computational time due to the higher size of the base population.

Ignoring the computational aspects, we can see that higher sizes of the base population offers better results.

Another important remark is the similarity between the mean of the objective values of the population and the number of individuals that converges to a solution. In both cases, we can see that the mean decreases when the number is close to the number of individuals of the elite (what means that most of individuals that participate in the average are close to the best one), and the mean increases when the number increases (which means that new individuals may appear far from the solution).

Next, in order to improve the number of individuals that converges to a solution in the case of a base population of 15 individuals, the strategy we follow is the next: we calculate an initial population of 50 individuals, and select the best 15. Then, we start the process that has been used in this project with this 15 individuals as initial population (a flowchart of the process is presented in Appendix A). In Figure 5.64, a comparison between the original process and the modified process is presented.

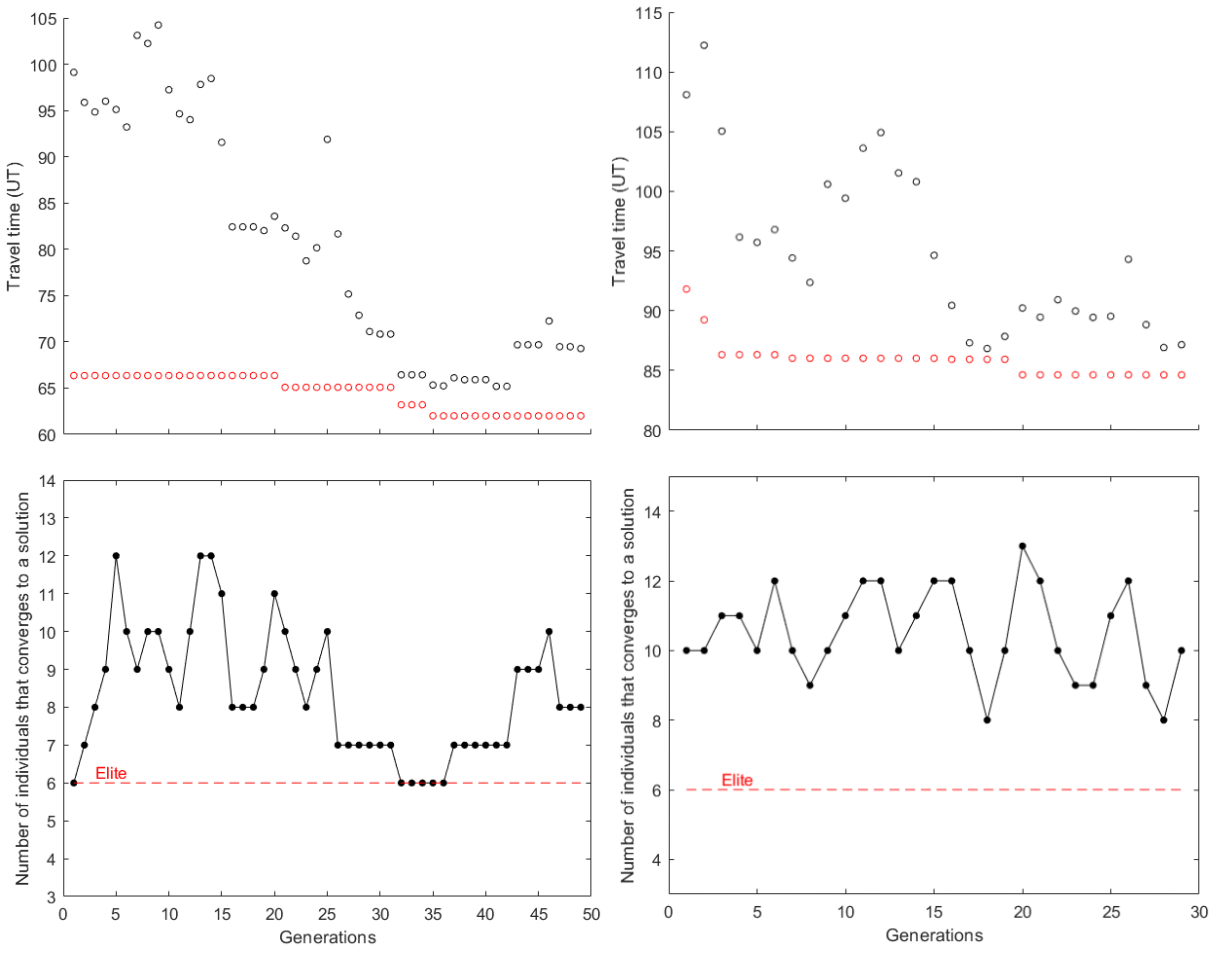


**(a)** Original process. **(b)** Modified process.

**Figure 5.64** Comparison between the original and the modified process.

In the modified process, the maximum allowed number of generations is changed to 30. The following results are extracted:

**Table 5.10** Results of the comparison between the original and the modified process.

| | Mean of number of individuals with solution | Maximum number of individuals with solution | Flight time (UT) |
|---|---|---|---|
| Original process | 8.33 | 12 | 62.0019 |
| Modified process | 10.48 | 13 | 84.6224 |

Even though the computational cost is lower, the flight time that we obtain is much higher. Selecting the 15 best individuals, it is possible that we select some individuals that are around the same local minimum, so we are reducing the exploration.

In order to avoid this, the denominator in the variance of the Normal distribution in mutation, $\sigma_c$, is reduced, adding more randomness to the mutation. We analyze the results for $\sigma_c = 5$ (left) and $\sigma_c = 3$ (right), as is shown in Figure 5.65.

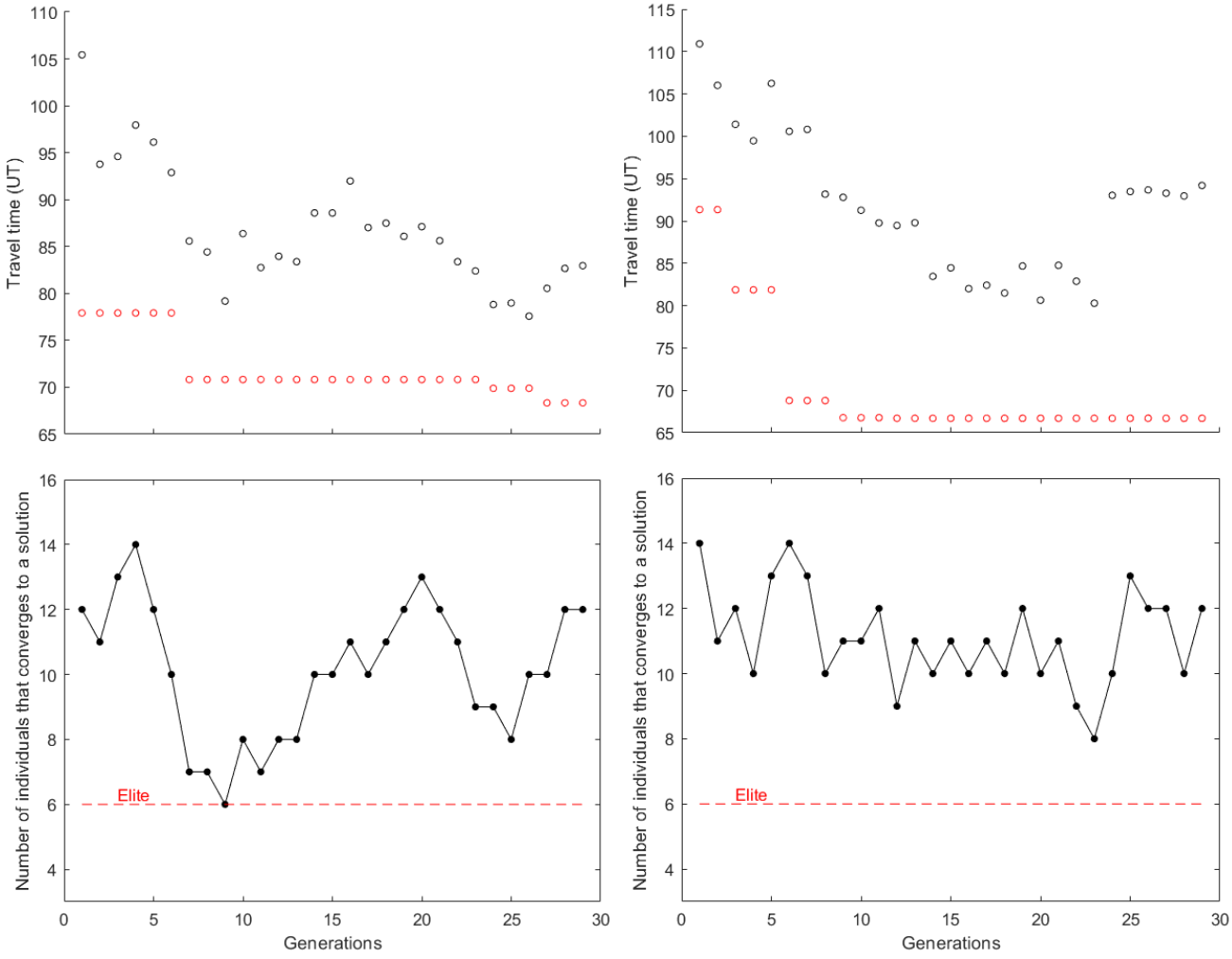


**(a)** Modified process with $\sigma_c = 5$.

**(b)** Modified process with $\sigma_c = 3$.

**Figure 5.65** Comparison of the modified process with different $\sigma_c$.

The following results are extracted:

**Table 5.11** Results of the comparison between the modified process with $\sigma_c = 5$ and $\sigma_c = 3$.

| $\sigma_c$ | Mean of number of individuals with solution | Maximum number of individuals with solution | Flight time (UT) |
|---|---|---|---|
| 5 | 10.10 | 14 | 68.3371 |
| 3 | 11.10 | 14 | 66.6973 |

We can see that reducing $\sigma_c$, the solution improves.

Lastly, we carry out another strategy, that consists in modifying the mutation. Until now, when an individual is subjected to mutation, we only keep the mutated individual. The modification consists in keeping both, that is, the individual before and after the mutation (a representation of the process is presented in Appendix B). In Figure 5.66, a comparison between the original process and the modified process is presented.

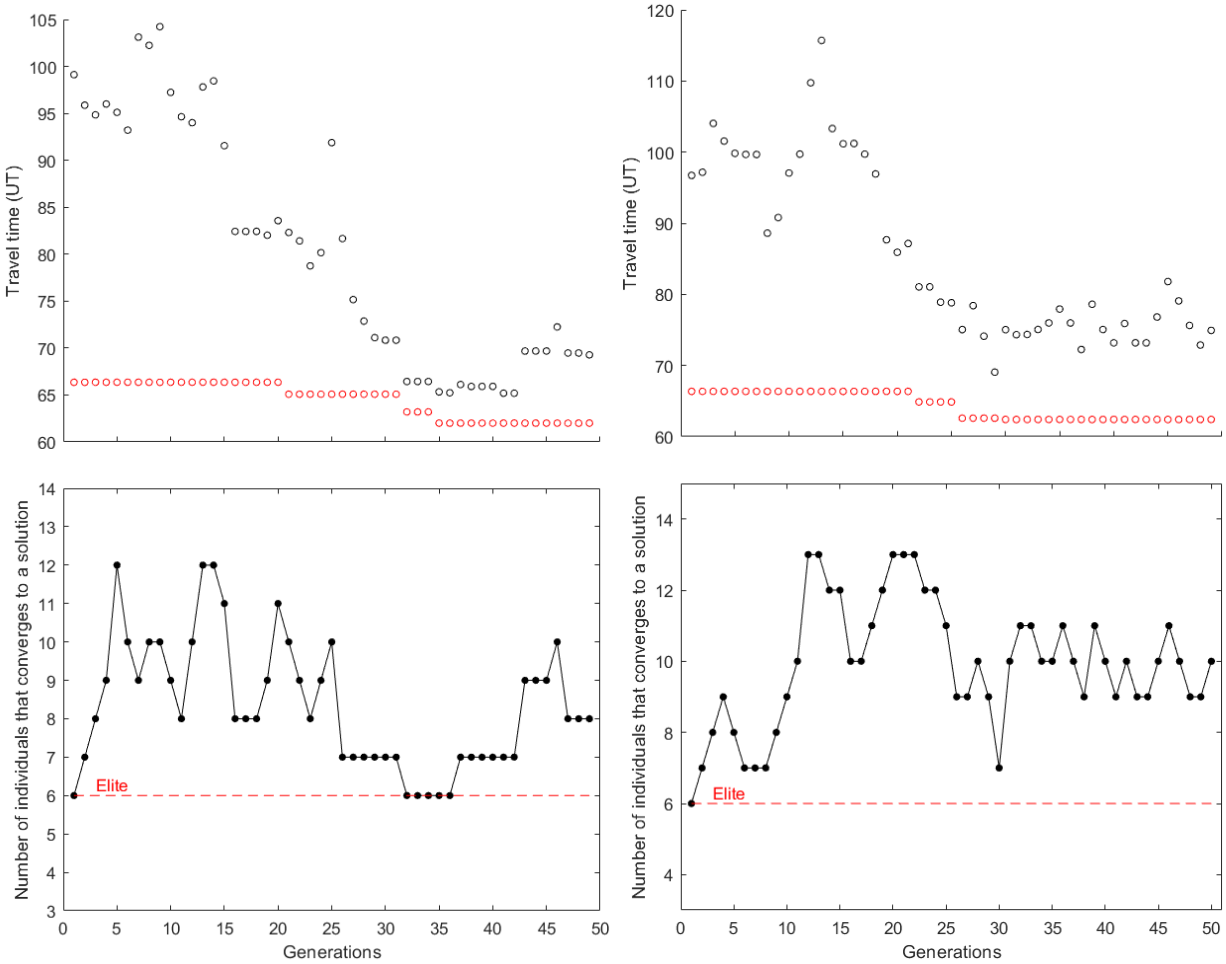


**(a)** Original mutation.

**(b)** Modified mutation.

**Figure 5.66** Comparison between the original and the modified mutation.

The following results are extracted:

**Table 5.12** Results of the comparison between the original and the modified mutation.

| | Mean of number of individuals with solution | Maximum number of individuals with solution | Flight time (UT) |
|---|---|---|---|
| Original mutation | 8.33 | 12 | 62.0019 |
| Modified mutation | 9.92 | 13 | 62.4097 |

In this case, the mean of number of individual with solution increases, what means a lower computational costs, and the flight time that we obtain is almost the same, so it could be a good upgrade.

# 6 Conclusions and future work

After the development of the project, we need to reflect on the applied procedure, on the utility of genetic algorithms in the applied case, and on the validity of the obtained results.

## 6.1 Conclusions

Commencing with the results of the optimization of transfer orbits between two planets, we observe that the flight times that we get for the different scenarios are remarkably similar to the ones in literature (comparing with the results for missions such as Earth-Mars or Earth-Jupiter, in [36] and [38]). Based on these outcomes, we assert that the optimization presents a high level of consistency.

Based on the various trajectories presented, we can affirm that the utilization of E-sails as a propellantless propulsion system represents a highly favorable option that enables efficient interplanetary travel.

By comparing the three different missions studied to Saturn, we can draw the following conclusions:

- In the case of the gravity assist maneuver in Jupiter, the flight time is more independent of the launch date, varying a maximum of 5 UT in six months. However, it is the case with the highest flight times.
- The minimum flight time is reached with a gravity assist maneuver in Venus. Nevertheless, the flight time is very sensitive to the launch date in this case and a possible launch window would be short.
- The flight times that we get with a gravity assist maneuver in Mars are not very high and they are more similar for different launch dates.

Therefore, continuing to improve the optimization of the Earth-Venus-Saturn mission is the most advantageous option.

We have learned about the heuristic behaviour of algorithms like IPOPT when it is used to solve highly non convex optimization problems, and its sensitivity to initial guesses. Despite this high sensitivity, we have obtained an initial guess that provides good solutions over a wide range of launch dates in various missions. However, this optimization can still be improved.

When considering the effectiveness of genetic algorithms, there is no doubt that their application in this case provides favorable results, improving the flight time across all tested launch dates. The optimal launch date remains unaltered both before and after the implementation of the algorithm. However, by analyzing the improvement in flight time for each tested date, it is evident that the solution significantly improves when the genetic algorithm is applied to launch dates that are far from optimal.

Regarding the various modifications analyzed to improve the results of the genetic algorithm, the best results are achieved by increasing the size of the base population. Additionally, incorporating the modification to the mutation process or initial population can help reduce the primary drawback, which is the computational cost, while offering similar results.

In this project, we use Parallel Computing Toolbox for MATLAB, that allows to make use of all the processing power of multi-core computers thanks to the execution of applications in workers (MATLAB calculation engines), which are executed locally. This extremely reduces the computational time. Even with that, each execution of the genetic algorithm has required more than 12 hours, with some cases exceeding 24 hours, performing the analysis in a computer with Windows 11 operating system, 16GB of RAM, and a 6-core processor at 2.2GHz.

It is true that the computational times are high and other methods can offer the same results more quickly. Nevertheless, it can be reduced with a more powerful computer and, of course, improving the non linear optimization.

In summary, we have developed a rigorous procedure that helps the identification of the most favorable launch date for a specific mission and reduces the flight time for all launch dates other than the optimal one.

## 6.2 Future work

There are many possibilities to add and take into consideration, that can be proposed as future work:

- The primary limitation of the process lies in the nonlinear optimizer, which is responsible for the high computational times associated with each solution obtained in the project. Therefore, there is a need for further improvement in the field of nonlinear optimization. The use of curve parametrizations can be employed to reduce the number of variables.
- The size of the base population can be increased, improving the results of the algorithm, but increasing the computational time.
- The maximum allowed number of generations can be increased too.
- The genetic algorithm can be applied to all dates instead of the selected dates for the analysis.
- The launch date can be added as a optimization variable of the genetic algorithm.
- Circular orbits hypothesis could be suppressed, considering real elliptic shapes by knowing the orbital elements $(a, e, \omega, \theta(t))$.
- 2D hypothesis can be suppressed too. By knowing all the set of orbital elements $(a, e, i, \omega, \Omega, \theta(t))$ we know where planet is going to be exactly at any instant of time. The problem can be extended into 3D by expressing the laws of motion in terms of orbital elements.
- Other perturbations that have been excluded, such as the gravitational force exerted by other planets, could be incorporated.
- New different missions with different intermediate and final planets or asteroids can be considered.

- Missions involving multiple gravity assist maneuvers can also be considered.

# Appendix A
# Modified Genetic Algorithm process

In this appendix, we present the flowchart of the modified genetic algorithm process that is used in Section 5.2.5 (see in Figure A.1).

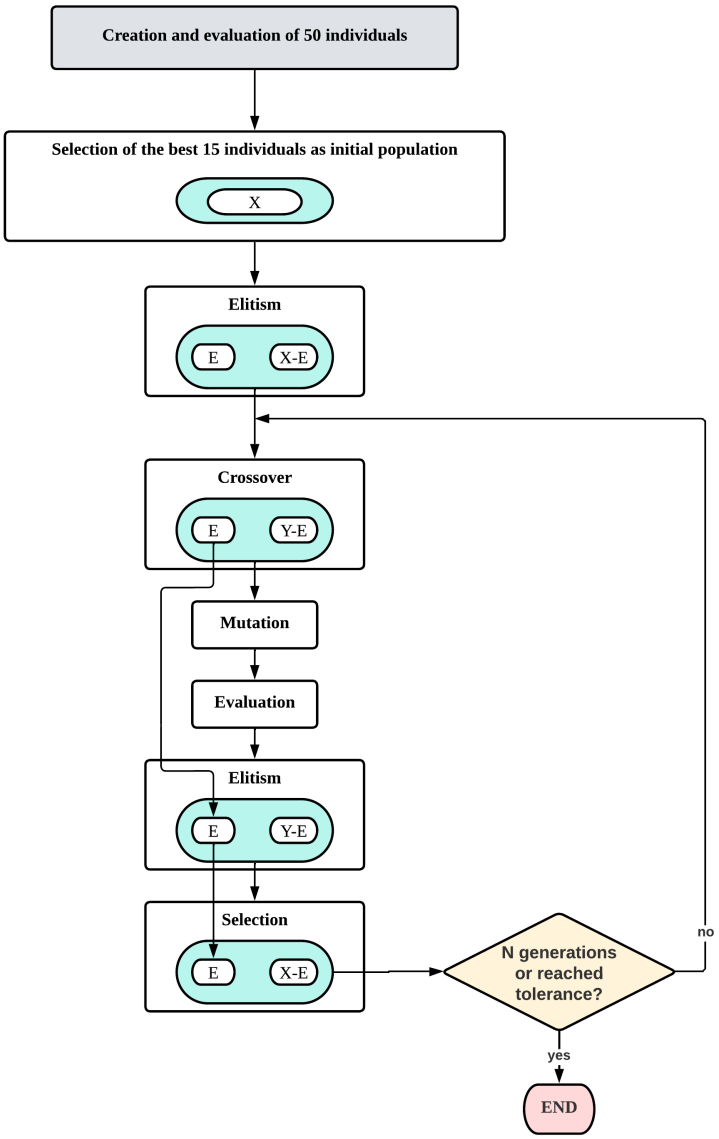


**Figure A.1** Flowchart of the modified Genetic Algorithm process.

# Appendix B
# Modified Mutation process

In this appendix, we present a representation of the modified mutation process that is used in Section 5.2.5 (see in Figure B.1).

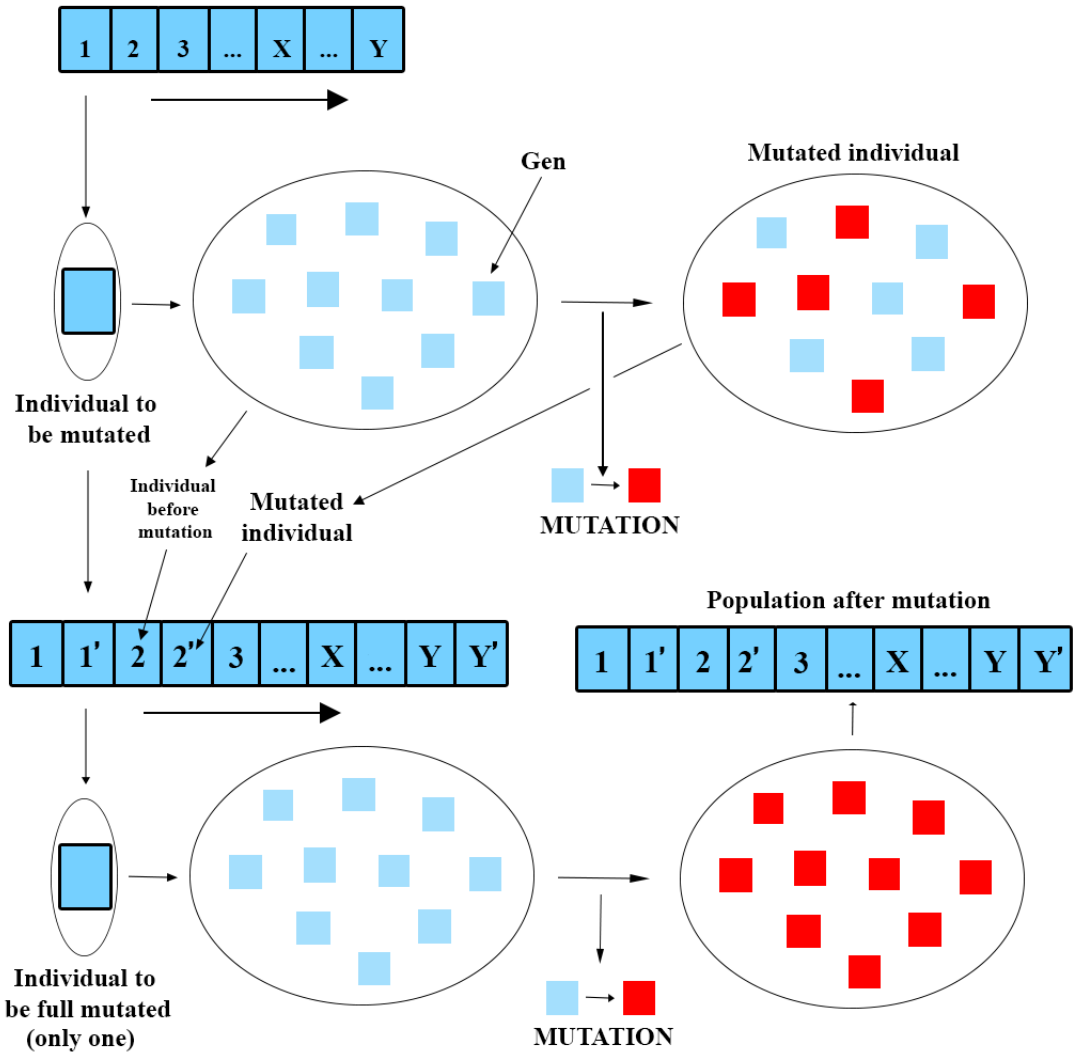


**Figure B.1** Representation of the modified Mutation.

In this case, the mutated individual is added to the population without replacing the non-mutated individual. Therefore, the size of the population increases after the mutation.

# List of Figures


2.1 *Voyager 1* and *Voyager 2* trajectories. (The “Grand Tour”) 6
2.2 *LightSail 2* deployed in space 7
2.3 E-sail concept scheme. Credit: [3] 7
2.4 E-sail typical configuration. Credit: [3] 8
2.5 Trip time to reach 100 AU using different propulsion systems. Credit: [13] 9

3.1 The two-body problem 12
3.2 Conceptual E-sail thrust model 14
3.3 Three-body problem. Center of mass is represented by CM 16
3.4 Patched conic method for Earth-Mars direct interplanetary transfer. Credit: [21] 17
3.5 Gravity assist maneuver. Triangles of velocities. Credit: [22] 18
3.6 Definition of the trajectory angle 19
3.7 Leading-side flyby and trailing-side flyby. Credit: [22] 20

4.1 Variation of $\alpha$ and $\gamma$ with respect to $\alpha_n$ 23
4.2 Visual scheme of the transcription of an Optimal Control Problem 26
4.3 Representation of exploration and exploitation 30
4.4 Representation of Crossover 32
4.5 Representation of Mutation 33
4.6 Representation of Tournament Selection 34
4.7 Flowchart of the Genetic Algorithm process 35
4.8 Flowchart of the objective function 37

5.1 Trajectory in a transfer orbit from Earth to Mars ignoring arrival velocity constraints 40
5.2 Evolution of variables in a transfer orbit from Earth to Mars 40
5.3 Evolution of flight time in transfer orbits from Earth to Mars 41
5.4 Trajectories from Earth to Mars before and after the discontinuity 42
5.5 Trajectory in a transfer orbit from Earth to Jupiter ignoring arrival velocity constraints 43
5.6 Evolution of variables in a transfer orbit from Earth to Jupiter 43
5.7 Evolution of flight time in transfer orbits from Earth to Jupiter 44
5.8 Trajectories from Earth to Jupiter before and after the discontinuity 45
5.9 Trajectory in a transfer orbit from Earth to Venus ignoring arrival velocity constraints 46
5.10 Evolution of variables in a transfer orbit from Earth to Venus 46
5.11 Comparison of flight times in transfer orbits to Mars and Venus 47
5.12 Trajectory in a transfer orbit from Mars to Jupiter ignoring arrival velocity constraints 48
5.13 Evolution of variables in a transfer orbit from Mars to Jupiter 48
5.14 Trajectory in a transfer orbit from Mars to Saturn ignoring arrival velocity constraints 49

5.15 Evolution of variables in a transfer orbit from Mars to Saturn 50
5.16 Trajectory in a transfer orbit from Jupiter to Saturn ignoring arrival velocity constraints 51
5.17 Evolution of variables in a transfer orbit from Jupiter to Saturn 51
5.18 Trajectory in a transfer orbit from Venus to Saturn ignoring arrival velocity constraints 52
5.19 Evolution of variables in a transfer orbit from Venus to Saturn 53
5.20 Example of trajectory of the Earth-Mars-Jupiter mission 54
5.21 Evolution of flight time in the independent optimization of Earth-Mars-Jupiter 54
5.22 Procedure of the genetic algorithm in Earth-Mars-Jupiter on 01/01/2024 56
5.23 Evolution of flight time of Earth-Mars-Jupiter after applying genetic algorithm on 01/01/2024 56
5.24 Procedure of the genetic algorithm in Earth-Mars-Jupiter on 01/02/2024 57
5.25 Evolution of flight time of Earth-Mars-Jupiter after applying genetic algorithm on 01/02/2024 58
5.26 Procedure of the genetic algorithm in Earth-Mars-Jupiter on 07/04/2024 58
5.27 Evolution of flight time of Earth-Mars-Jupiter after applying genetic algorithm on 07/04/2024 59
5.28 Procedure of the genetic algorithm in Earth-Mars-Jupiter on 02/07/2024 59
5.29 Evolution of flight time of Earth-Mars-Jupiter after applying genetic algorithm on 02/07/2024 60
5.30 Minimum flight time of Earth-Mars-Jupiter in each date 61
5.31 Procedure of the genetic algorithm in Earth-Mars-Jupiter on 01/01/2024 including a known solution in the initial population 61
5.32 Example of trajectory of the Earth-Mars-Saturn mission 62
5.33 Evolution of flight time in the independent optimization of Earth-Mars-Saturn 63
5.34 Procedure of the genetic algorithm in Earth-Mars-Saturn on 01/01/2024 64
5.35 Evolution of flight time of Earth-Mars-Saturn after applying genetic algorithm on 01/01/2024 64
5.36 Procedure of the genetic algorithm in Earth-Mars-Saturn on 28/03/2024 65
5.37 Evolution of flight time of Earth-Mars-Saturn after applying genetic algorithm on 28/03/2024 66
5.38 Procedure of the genetic algorithm in Earth-Mars-Saturn on 11/05/2024 66
5.39 Evolution of flight time of Earth-Mars-Saturn after applying genetic algorithm on 11/05/2024 67
5.40 Procedure of the genetic algorithm in Earth-Mars-Saturn on 30/06/2024 67
5.41 Evolution of flight time of Earth-Mars-Saturn after applying genetic algorithm on 30/06/2024 68
5.42 Minimum flight time of Earth-Mars-Saturn in each date 69
5.43 Example of trajectory of the Earth-Jupiter-Saturn mission 69
5.44 Evolution of flight time in the independent optimization of Earth-Jupiter-Saturn 70
5.45 Procedure of the genetic algorithm in Earth-Jupiter-Saturn on 29/01/2024 71
5.46 Evolution of flight time of Earth-Jupiter-Saturn after applying genetic algorithm on 29/01/2024 72
5.47 Procedure of the genetic algorithm in Earth-Jupiter-Saturn on 01/06/2024 72
5.48 Evolution of flight time of Earth-Jupiter-Saturn after applying genetic algorithm on 01/06/2024 73
5.49 Procedure of the genetic algorithm in Earth-Jupiter-Saturn on 01/07/2024 74
5.50 Evolution of flight time of Earth-Jupiter-Saturn after applying genetic algorithm on 01/07/2024 74
5.51 Minimum flight time of Earth-Jupiter-Saturn in each date 75
5.52 Example of trajectory of the Earth-Venus-Saturn mission 76
5.53 Evolution of flight time in the independent optimization of Earth-Venus-Saturn 76
5.54 Procedure of the genetic algorithm in Earth-Venus-Saturn on 07/01/2024 77
5.55 Evolution of flight time of Earth-Venus-Saturn after applying genetic algorithm on 07/01/2024 78
5.56 Procedure of the genetic algorithm in Earth-Venus-Saturn on 10/04/2024 78
5.57 Evolution of flight time of Earth-Venus-Saturn after applying genetic algorithm on 10/04/2024 79
5.58 Procedure of the genetic algorithm in Earth-Venus-Saturn on 01/06/2024 80
5.59 Evolution of flight time of Earth-Venus-Saturn after applying genetic algorithm on 01/06/2024 80
5.60 Procedure of the genetic algorithm in Earth-Venus-Saturn on 10/06/2024 81
5.61 Evolution of flight time of Earth-Venus-Saturn after applying genetic algorithm on 10/06/2024 81
5.62 Minimum flight time of Earth-Venus-Saturn in each date 82
5.63 Comparison between different base population sizes 83

(a) Base population of 15 83
(b) Base population of 25 83
5.64 Comparison between the original and the modified process 84
(a) Original process 84
(b) Modified process 84
5.65 Comparison of the modified process with different $\sigma_c$ 85
(a) Modified process with $\sigma_c = 5$ 85
(b) Modified process with $\sigma_c = 3$ 85
5.66 Comparison between the original and the modified mutation 86
(a) Original mutation 86
(b) Modified mutation 86

A.1 Flowchart of the modified Genetic Algorithm process 93

B.1 Representation of the modified Mutation 95

# List of Tables


| | | |
|---|---|---|
| 3.1 | Data of Solar System planets | 17 |
| 5.1 | Lower and upper limits of the value of optimization variables in Earth-Mars-Jupiter | 55 |
| 5.2 | Improvement in flight times of Earth-Mars-Jupiter | 60 |
| 5.3 | Lower and upper limits of the value of optimization variables in Earth-Mars-Saturn | 63 |
| 5.4 | Improvement in flight times of Earth-Mars-Saturn | 68 |
| 5.5 | Lower and upper limits of the value of optimization variables in Earth-Jupiter-Saturn | 70 |
| 5.6 | Improvement in flight times of Earth-Jupiter-Saturn | 75 |
| 5.7 | Lower and upper limits of the value of optimization variables in Earth-Venus-Saturn | 77 |
| 5.8 | Improvement in flight times of Earth-Venus-Saturn | 82 |
| 5.9 | Results of the comparison between sizes of the base population | 83 |
| 5.10 | Results of the comparison between the original and the modified process | 85 |
| 5.11 | Results of the comparison between the modified process with $\sigma_c = 5$ and $\sigma_c = 3$ | 86 |
| 5.12 | Results of the comparison between the original and the modified mutation | 87 |

# Bibliography


[1] B. V. Rauschenbakh, M. Y. Ovchinnikov, and S. McKenna-Lawlor, *Essential Spaceflight Dynamics and Magnetospherics*. Springer Netherlands, 2003.

[2] G. A. Flandro, "Fast reconnaissance missions to the outer solar system utilizing energy derived from the gravitational field of Jupiter," *Astronautica Acta*, vol. 12, pp. 329–337, 1966.

[3] M. Bassetto, L. Niccolai, A. Quarta, and G. Mengali, "A comprehensive review of electric solar wind sail concept and its applications," *Progress in Aerospace Sciences*, vol. 128, 2022.

[4] S. Gong and M. Macdonald, "Review on solar sail technology," *Astrodynamics*, vol. 3, pp. 93–125, 6 2019.

[5] D. A. Spencer, B. Betts, J. M. Bellardo, A. Diaz *et al.*, "The LightSail 2 solar sailing technology demonstration," *Advances in Space Research*, vol. 67, pp. 2878–2889, 5 2021.

[6] P. Janhunen, "Electric sail for spacecraft propulsion," *Journal of Propulsion and Power*, vol. 20, pp. 763–764, 7 2004.

[7] R. M. Zubrin and D. G. Andrews, "Magnetic sails and interplanetary travel," *Journal of Spacecraft and Rockets*, vol. 28, pp. 197–203, 3 1991.

[8] N. Perakis, "Maneuvering through solar wind using magnetic sails," *Acta Astronautica*, vol. 177, pp. 122–132, 12 2020.

[9] P. Janhunen, P. K. Toivanen, J. Polkko, S. Merikallio *et al.*, "Invited article: Electric solar wind sail: Toward test missions," *Review of Scientific Instruments*, vol. 81, p. 111301, 11 2010.

[10] P. Janhunen, "Increased electric sail thrust through removal of trapped shielding electrons by orbit chaotisation due to spacecraft body," *Annales Geophysicae*, vol. 27, pp. 3089–3100, 8 2009.

[11] J. Envall, P. Janhunen, P. Toivanen, M. Pajusalu *et al.*, "E-sail test payload of the ESTCube-1 nanosatellite," *Proceedings of the Estonian Academy of Sciences*, vol. 63, p. 210, 2014.

[12] A. Kestilä, T. Tikka, P. Peitso, J. Rantanen *et al.*, "Aalto-1 nanosatellite – technical description and mission objectives," *Geoscientific Instrumentation, Methods and Data Systems*, vol. 2, pp. 121–130, 2 2013.

[13] B. M. Wiegmann, "The heliopause electrostatic rapid transit system (HERTS) - design, trades, and analyses performed in a two year NASA investigation of electric sail propulsion systems." American Institute of Aeronautics and Astronautics, 7 2017.

[14] P. Janhunen, P. Toivanen, J. Envall, S. Merikallio *et al.*, "Overview of electric solar wind sail applications," *Proceedings of the Estonian Academy of Sciences*, vol. 63, pp. 4–11, 2014.

[15] P. K. Toivanen and P. Janhunen, "Spin plane control and thrust vectoring of electric solar wind sail," *Journal of Propulsion and Power*, vol. 29, pp. 178–185, 1 2013.

[16] P. Janhunen and A. Sandroos, "Simulation study of solar wind push on a charged wire: basis of solar wind electric sail propulsion," *Annales Geophysicae*, vol. 25, pp. 755–767, 3 2007.

[17] M. Bassetto, G. Mengali, and A. A. Quarta, "E-sail attitude control with tether voltage modulation," *Acta Astronautica*, vol. 166, pp. 350–357, 1 2020.

[18] G. Mengali, A. A. Quarta, and P. Janhunen, "Electric sail performance analysis," *Journal of Spacecraft and Rockets*, vol. 45, pp. 122–129, 1 2008.

[19] P. Janhunen, A. Quarta, and G. Mengali, "Electric solar wind sail mass budget model," *Geoscientific Instrumentation, Methods and Data Systems*, vol. 2, pp. 85–95, 2 2013.

[20] C. A. Kluever, *Spaceflight Mechanics*. Elsevier, 2003, pp. 507–520.

[21] B. Yang, H. Yang, and S. Li, "Hierarchical approach for fast searching optimal launch opportunity in a wide range," *Advances in Space Research*, vol. 63, pp. 572–588, 1 2019.

[22] R. V. Valenzuela, "Apuntes de Mecánica Orbital y Vehículos Espaciales," 2023. [Online]. Available: http://aero.us.es/move/desc.html

[23] B. Wie, *Space Vehicle Dynamics and Control, Second Edition*. American Institute of Aeronautics and Astronautics, 1 2008.

[24] O. Andrés-Martínez, O. Palma-Flores, and L. A. Ricardez-Sandoval, "Optimal control and the pontryagin's principle in chemical engineering: History, theory, and challenges," *AIChE Journal*, vol. 68, 8 2022.

[25] M. Huo, G. Mengali, and A. A. Quarta, "Electric sail thrust model from a geometrical perspective," *Journal of Guidance, Control, and Dynamics*, vol. 41, pp. 735–741, 3 2018.

[26] F. Topputo and C. Zhang, "Survey of direct transcription for low-thrust space trajectory optimization with applications," *Abstract and Applied Analysis*, vol. 2014, pp. 1–15, 2014.

[27] P. Williams, "Hermite-legendre-gauss-lobatto direct transcription in trajectory optimization," *Journal of Guidance, Control, and Dynamics*, vol. 32, pp. 1392–1395, 7 2009.

[28] J. A. E. Andersson, J. Gillis, G. Horn, J. B. Rawlings, and M. Diehl, "Casadi: a software framework for nonlinear optimization and optimal control," *Mathematical Programming Computation*, vol. 11, pp. 1–36, 3 2019.

[29] L. Bianchi, M. Dorigo, L. M. Gambardella, and W. J. Gutjahr, "A survey on metaheuristics for stochastic combinatorial optimization," *Natural Computing*, vol. 8, pp. 239–287, 6 2009.

[30] D. Stack, *Charles Darwin: Theory of Natural Selection*. Springer International Publishing, 2021.

[31] D. Beasley, D. R. Bull, and R. R. Martin, "An overview of genetic algorithms: Pt1, fundamentals," *University Computing archive*, vol. 15, pp. 58–69, 1993.

[32] S. Luke, *Essentials of Metaheuristics*, 2nd ed. Lulu, 2013, available for free at http://cs.gmu.edu/∼sean/book/metaheuristics/.

[33] K. Deb and A. Kumar, "Real-coded genetic algorithms with simulated binary crossover: Studies on multimodal and multiobjective problems," *Complex Syst.*, vol. 9, 1995.

[34] F. Cacciatore and C. Toglia, "Optimization of orbital trajectories using genetic algorithms," *Journal of Aerospace Engineering, Sciences and Applications*, vol. 1, pp. 58–69, 1 2008.

[35] B. L. Miller and D. E. Goldberg, "Genetic algorithms, tournament selection, and the effects of noise," *Complex Syst.*, vol. 9, 1995.

[36] F. J. U. Gómez, "Optimal planning and guidance strategies in coplanar circular interplanetary missions using electric solar wind sails," 2022.

[37] J. F. R. Sánchez, "Optimización de misiones interplanetarias mediante el uso de algoritmos genéticos," 2020.

[38] A. A. Quarta and G. Mengali, "Minimum-time trajectories of electric sail with advanced thrust model," *Aerospace Science and Technology*, vol. 55, pp. 419–430, 8 2016.